

CONSTRAINING THE IMPACT OF METALLICITY ON CEPHEID
DISTANCES USING A REFINED GALACTIC CALIBRATION

by

Daniel J. Majaess

A Thesis Submitted to Saint Mary's University, Halifax, Nova Scotia in Partial Fulfillment
of the Requirements for the Degree of

DOCTOR OF PHILOSOPHY

in

Astronomy

(Department of Physics and Astronomy)

SAINT MARY'S UNIVERSITY

July 2012, Halifax, Nova Scotia

© Daniel J. Majaess, 2012

Approved: D. G. Turner (Supervisor)

Approved: C. I. Short (Examiner)

Approved: P. D. Bennett (Examiner)

Approved: T. G. Barnes (Examiner)

Date: July 25, 2012



Library and Archives
Canada

Published Heritage
Branch

395 Wellington Street
Ottawa ON K1A 0N4
Canada

Bibliothèque et
Archives Canada

Direction du
Patrimoine de l'édition

395, rue Wellington
Ottawa ON K1A 0N4
Canada

Your file Votre référence

ISBN: 978-0-494-88940-4

Our file Notre référence

ISBN: 978-0-494-88940-4

NOTICE:

The author has granted a non-exclusive license allowing Library and Archives Canada to reproduce, publish, archive, preserve, conserve, communicate to the public by telecommunication or on the Internet, loan, distribute and sell theses worldwide, for commercial or non-commercial purposes, in microform, paper, electronic and/or any other formats.

The author retains copyright ownership and moral rights in this thesis. Neither the thesis nor substantial extracts from it may be printed or otherwise reproduced without the author's permission.

AVIS:

L'auteur a accordé une licence non exclusive permettant à la Bibliothèque et Archives Canada de reproduire, publier, archiver, sauvegarder, conserver, transmettre au public par télécommunication ou par l'Internet, prêter, distribuer et vendre des thèses partout dans le monde, à des fins commerciales ou autres, sur support microforme, papier, électronique et/ou autres formats.

L'auteur conserve la propriété du droit d'auteur et des droits moraux qui protègent cette thèse. Ni la thèse ni des extraits substantiels de celle-ci ne doivent être imprimés ou autrement reproduits sans son autorisation.

In compliance with the Canadian Privacy Act some supporting forms may have been removed from this thesis.

While these forms may be included in the document page count, their removal does not represent any loss of content from the thesis.

Conformément à la loi canadienne sur la protection de la vie privée, quelques formulaires secondaires ont été enlevés de cette thèse.

Bien que ces formulaires aient inclus dans la pagination, il n'y aura aucun contenu manquant.

Canada

CONTENTS

CONTENTS	1
LIST OF FIGURES	5
LIST OF TABLES	14
ABSTRACT	15
1 INTRODUCTION	16
REFERENCES	23
2 UNIVERSAL WESENHEIT TEMPLATE	24
2.1 INTRODUCTION	25
2.2 ANALYSIS	26
2.2.1 PHOTOMETRY (CALIBRATION)	26
2.2.2 PARALLAXES (CALIBRATION)	30
2.2.3 CALIBRATED WESENHEIT DIAGRAMS	33
2.3 SUMMARY AND FUTURE RESEARCH	40
REFERENCES	43
3 BENCHMARK OPEN CLUSTERS	47
3.1 INTRODUCTION	48

3.2	<i>JHK</i> , INTRINSIC RELATIONS	49
3.2.1	AGE AND METALLICITY DEPENDENCIES	52
3.3	CLUSTER δ SCUTIS	55
3.3.1	VI PHOTOMETRY	55
3.3.2	WESENHEIT MAGNITUDES	57
3.3.3	PULSATION MODE	61
3.3.4	δ SCT DISTANCE TO NGC 1817	65
3.4	SUMMARY AND FUTURE RESEARCH	66
	REFERENCES	69
4	δ CEP CLUSTER	73
4.1	INTRODUCTION	74
4.2	ANALYSIS	74
4.2.1	REVISED HIP OBSERVATIONS FOR CEP OB6	74
4.2.2	REDDENING	77
4.2.3	AGE	77
4.2.4	CLUSTER DISTANCE	78
4.2.5	MEAN DISTANCE TO δ CEP	81
4.3	CONCLUSION AND FUTURE RESEARCH	81
	REFERENCES	84
5	TW NOR/LYNGA 6	86
5.1	INTRODUCTION	86

5.2	VVV PHOTOMETRY	89
5.3	ANALYSIS	90
5.4	CONCLUSION	95
	REFERENCES	97
6	ζ GEM CLUSTER	99
6.1	INTRODUCTION	99
6.2	ANALYSIS	100
6.2.1	REDDENING AND AGE	101
6.2.2	LOWER-MASS CLUSTER MEMBERS	103
6.2.3	CLUSTER DISTANCE	105
6.3	CONCLUSION AND FUTURE RESEARCH	107
	REFERENCES	109
7	R CRU/NGC4349	111
7.1	INTRODUCTION	112
7.2	VVV PHOTOMETRY	113
7.2.1	THE ADVANTAGES OF <i>JHK_s</i> PHOTOMETRY	114
7.3	ANALYSIS	116
7.3.1	PISMIS 19	116
7.3.2	NGC 4349	119
7.4	CONCLUSION	122

REFERENCES	124
8 TYPE I/II CEPHEIDS IN NGC 5128	125
8.1 INTRODUCTION	126
8.2 TYPE II CEPHEIDS IN NGC 5128	127
8.3 THE CEPHEID DISTANCE TO NGC 5128	130
8.4 UNCERTAINTIES ASSOCIATED WITH THE CEPHEID DISTANCE TO NGC 5128	132
8.4.1 THE (NULL) ROLE OF METALLICITY	132
8.4.2 EXTRAGALACTIC CEPHEID PHOTOMETRY	138
8.5 SUMMARY & FUTURE RESEARCH	142
REFERENCES	146
9 METALLICITY EFFECTS	149
9.1 INTRODUCTION	150
9.2 EVIDENCE FOR THE ABSENCE OF A METALLICITY EFFECT IN V_C	153
9.3 EVALUATING THE VIABILITY OF $\gamma \simeq -0.8$ mag/dex	155
9.4 CONCLUSION AND FUTURE RESEARCH	159
REFERENCES	162
10 SUMMARY AND FUTURE RESEARCH	164
REFERENCES	170
11 ACKNOWLEDGEMENTS	171

LIST OF FIGURES

- 2.1 Light curves for a subsample of the objects studied here. Data for the type II Cepheid VY Pyx were obtained via the AAVSO's robotic telescope network. An analysis of that photometry yields the following mean parameters for VY Pyx: $\langle V \rangle = 7.25$ and $\langle V \rangle - \langle I \rangle = 0.67$. VZ Cnc and SX Phe are multiperiodic, and thus the scatter exhibited is only tied in part to photometric uncertainties (Fig. 2.2). 27
- 2.2 Several variables employed in the calibration (Table 2.1) are discernably multiperiodic and exhibit pronounced amplitude variations, as exemplified by observations of V703 Sco. Observations for V703 Sco were obtained via the AAVSO's robotic telescope network (red dots) and ASAS. No prewhitening was performed. 28
- 2.3 A *VI* Wesenheit diagram characterizing a subsample of the examined data. The distance to the LMC is secured by evaluating the offset from the calibration (*middle panel*, yellow dots, the size of the datapoints is representative of the uncertainties). The Wesenheit magnitudes of variable stars in globular clusters (e.g., M13, *bottom panel*, yellow dots) may be compared to the LMC template to derive the zero-point. The blue dashed line indicates the position of uncorrected δ Scuti stars pulsating in the overtone (see Poleski et al., 2010). A break in the classical Cepheid relation near $\log P_F \simeq -0.15$ may define the δ Sct / Cep boundary (see also Fig. 6 in Soszyński et al., 2008b, $\log P \simeq -0.3$). 33

2.4	Variables near the core of M15 suffer from photometric contamination. The surface brightness and stellar density increase rapidly toward the core, thereby increasing the likelihood of contamination. <i>Left</i> , the distance moduli and colour excess for RR Lyrae variables are computed via the calibrations of Majaess et al. 2009 and Majaess 2010b. <i>Right</i> , M15 imaged from the ARO (Lane, 2007). M15 is crucial because it is among the most metal-poor Galactic clusters and hosts a planetary nebula (Jacoby et al., 1997; Alves et al., 2000; Turner, 2010b).	37
3.1	Deep 2MASS JHK_s colour-magnitude and colour-colour diagrams for the calibration (red dots) and Praesepe star cluster (black dots). Likely members of Praesepe were selected on the basis of proper motions (NOMAD). The resulting parameters are $E(J - K_s) = 0.025 \pm 0.015$ and $d = 183 \pm 8$ pc.	51
3.2	Deep 2MASS JHK_s colour-magnitude diagrams for M67, Hyades, Praesepe, Pleiades, and α Persei star clusters. The clusters have a common ZAMS morphology in the infrared. The δ Scutis examined in §3.3 (red dots) may be evolved (Hyades/Praesepe), blue stragglers (M67), or occupy the binary/rapid rotator sequence (Pleiades). . .	53
3.3	Semi-empirical colour- T_e -[Fe/H] correlation for calibration stars (Fig. 3.1) in PASTEL. Red and black dots indicate metal-rich and metal-poor stars accordingly. $B - V$ and $U - B$ colour indices appear sensitive to metallicity, whereas $J - K_s$ is comparatively unaffected by changes in iron abundance (see text).	57

-
- 3.4 A calibrated universal VI Wesenheit template constructed from data found in Ma-
jaess et al. (2011a) and the latest OGLEIII observations (e.g., Poleski et al., 2010).
The cluster δ Scutis are displayed as black dots. Wesenheit magnitudes were com-
puted via Eqn. 3.1 using the JHK_s established cluster distances and VI photometry
presented in Tables 3.1 & 3.4 accordingly. First-order constraints on the inferred
pulsation modes (n) are listed in Tables 3.3 & 3.4. 59
- 3.5 Left, a *preliminary* VI colour-magnitude diagram for the open cluster NGC 1817
compiled from ARO observations. A subsample of the list of δ Scuti candidates from
Arentoft et al. 2005 are characterized by red dots. Right, the stars are displayed
in a Wesenheit diagram where green, red, and blue ridges correspond to $n = 0, 1, 3$
pulsators accordingly (right to left). The offset from the absolute Wesenheit magni-
tudes (Fig. 3.4) yields $d \simeq 1.7$ kpc, provided the variables define the $n \geq 1$ boundary
(see §3.3.3). The uncertainties are typically smaller than the symbol size. 63
- 4.1 Colour-colour diagram for stars in Table 4.1 with UBV photometry that are asso-
ciated with δ Cep. The sample is offset from the intrinsic relation (dotted line) by
 $E(B - V) = 0.077 \pm 0.016(\sigma)$ (solid line). The result confirms the reddening estab-
lished for δ Cep by Benedict et al. (2002a). The intrinsic relation and reddening law
for the region were adopted from Turner (1976, 1989). The uncertainties are smaller
than the symbol size. 76

-
- 4.2 Left to right, JH and BV colour-magnitude diagrams for the Table 4.1 and NO-MAD samples (panels 1, 2), and comparison fields (panels 3, 4). Small dots denote calibration stars from Majaess et al. (2011), which were employed to tie the cluster distance to a geometrically anchored scale (van Leeuwen, 2009; Majaess et al., 2011). Large dots characterize stars with $\mu_\alpha = 11 - 19$ mas/yr and $\mu_\delta = 2 - 7$ mas/yr. Open circles are likely field stars (Table 4.1). HIP 110459 (circled dot) was previously identified as a cluster member, yet $BVJHK_s$ photometry imply the object is a field star. In panel 2 a Padova $\log \tau = 7.9$ isochrone was applied. The brightest likely cluster members are the supergiants ζ Cep (K1.5Ib) and δ Cep (amplitude variation indicated). An early-type cluster sequence is absent from the comparison fields (HIP data for the cluster μ_α/μ_δ). 76
- 4.3 Top, J2000 RA/DEC positions for probable (squares) and non-members (open circles) presented in Table 4.1, and new potential members (filled circles) outlined in Table 4.2. Bottom, dotted open circles represent all HIP stars near the (approximate) cluster centre. The red circle represents the δ Cep cluster. 79

-
- 5.1 VVV colour-magnitude and colour-colour diagrams for Lyngå 6 stars and a comparison field. A population of mid-to-late B-type cluster stars is absent from the latter. Stars left of the cyan line are typically earlier than \simeq F5 (Straižys & Lazauskaitė, 2009; Turner, 2011). The isochrone and intrinsic fit were adjusted (reddened) to match the observed data. Ly6-4 (an evolved red star, Lyngå, 1977) and the classical Cepheid TW Nor (circled dots) share a common radial velocity (Mermilliod et al., 1987, 2008). Applying the intrinsic colour-colour relation of Turner (2011) and a $\log \tau = 7.9 \pm 0.1$ Padova isochrone to Lyngå 6 stars yields $E(J-H) = 0.38 \pm 0.02$ and $d = 1.91 \pm 0.10$ kpc. The extinction laws adopted are described in the text. 88
- 5.2 A map of local spiral structure as delineated by long period classical Cepheids (dots) and young clusters (circled dots) (see also Majaess et al., 2009). The Carina (A) and Centaurus (E) spiral arms are indicated on the diagram. TW Nor/Lyngå 6 (red dot) reside in the Centaurus spiral arm. 93
- 5.3 The hybrid Galactic VI_c Wesenheit function for 32 classical Cepheid calibrators (Benedict et al., 2007; Turner, 2010). The Wesenheit magnitude for TW Nor (red dot) is tied to the revised distance for Lyngå 6. 95
- 6.1 Colour-colour diagram for all stars $r \leq 4^\circ$ from ζ Gem with UBV photometry (Mermilliod, 1991). The field is comparatively unreddened. The intrinsic UBV relation and reddening law for the region were adopted from Turner (1976, 1989). Most objects in the diagram are not associated with ζ Gem. The uncertainties are smaller than the symbol size. 101

-
- 6.2 A subset of the new DAO spectra obtained for objects in the field of the classical Cepheid ζ Gem. From top to bottom the spectra correspond to HD 50767, HD 53588, HD 52474, and ζ Gem B. 102
- 6.3 Left to right, JH and BV colour-magnitude diagrams for HIP/Tycho stars with $r \leq 2.5^\circ$ of ζ Gem exhibiting $-10 < \mu_\alpha < -2$ mas/yr and $-7 < \mu_\delta < 2$ mas/yr. An early type cluster sequence is absent from the comparison fields (panels 3, 4, HIP/Tycho), which encompass $r \leq 4^\circ$. Small dots denote calibration stars from Majaess et al. (2011), which were employed to tie the cluster distance to a geometrically anchored scale (van Leeuwen, 2009; Majaess et al., 2011). Open circles are likely field stars. In panel 2 a Padova $\log \tau = 7.85$ isochrone is shown. ζ Gem (amplitude variation indicated) and its companion ζ Gem B (circled dot) is the brightest cluster member. 105
- 7.1 A comparison between 2MASS and VVV $J - H$ photometry for the regions encompassing Pismis 19 and NGC 4349. A 1:1 correlation (red line) exists to within the uncertainties. The data for Pismis 19 were deliberately offset from zero for presentation purposes. Pertinent details regarding the pipeline employed here to process the VVV data are described in Moni Bidin et al. (2011) and Mauro et al. (2012, in preparation.). 114
- 7.2 VVV colour-magnitude diagrams for Pismis 19 at varying radii. JHK_s Padova isochrones (Bonatto et al., 2004) were employed. Individual reddenings were determined via the approach outlined in §7.3.1. Photometric errors and binary contamination artificially broaden the breadth of the differential reddening. 116

-
- 7.3 Colour-magnitude diagrams constructed for NGC 4349 and an adjacent comparison field using VVV/2MASS JHK_s photometry. The circled dot near the tip of the giant branch is TYC 8975-2606-1, which hosts a substellar companion (Lovis & Mayor, 2007). To reduce contamination the CMDs contain stars within $r < 1.2'$. Seven evolved red stars beyond that radius were added to the CMD for NGC 4349. . . . 118
- 8.1 VI Wesenheit and period-colour diagrams confirm the Ferrarese et al. (2007) discovery of five Type II Cepheids in NGC 5128. Type II and classical Cepheids are indicated by red triangles and black dots respectively, and are distinctly separated by ~ 2 magnitudes in Wesenheit space. The Wesenheit magnitudes were evaluated using $W_{VI} = V - R_{VI} \times (V - I)$, where $R_{VI} = 2.55$ is the canonical extinction law. The slopes of the Wesenheit functions are variants of the LMC calibration (Majaess et al., 2009c, OGLE photometry). Long-period classical Cepheids in NGC 5128 exhibit a sizable colour excess. The error bars are suppressed for clarity. . . . 128
- 8.2 The slope of the VI classical Cepheid Wesenheit relation is relatively insensitive to metallicity. HST observations of classical Cepheids in NGC 5128, NGC 1309, and NGC 3021 (blue squares) follow a different metallicity dependence relative to the latest ground-based observations of variables in the Milky Way, LMC, NGC 6822, SMC, and IC 1613 (black dots, $\alpha = -3.34 \pm 0.08(2\sigma)$). The slope of the Sandage et al. (2004) Galactic calibration, based upon the best available data at the time of derivation and represented by the red triangle, disagrees with that inferred from the new HST parallaxes and (revised) cluster Cepheids ($\alpha \simeq -3.4$). 132

-
- 8.3 A comparison of the distances established to Galactic classical Cepheids via the *VI* Wesenheit calibrations of Sandage et al. (2004) (S04), Fouqué et al. (2007, F07), Majaess et al. (2008, M08), and Turner (2010, T10). The latter three calibrations include HST trigonometric parallaxes for 10 nearby classical Cepheids (Benedict et al., 2007). The Sandage et al. (2004) distance scale diverges from that of Fouqué et al. (2007) and Turner (2010) by $\geq +10\%$ at $P \simeq 25^d$ 133
- 8.4 Left, the abundance gradient for M106 (Riess et al., 2009) implies that initial estimates of the *VI* classical Cepheid metallicity effect ($\gamma_i \simeq -0.3 \text{ mag dex}^{-1}$) nearly double. The exclusion of two data points implies an even larger value (left, top panel). A sizable metallicity effect contradicts evidence presented by a direct comparison of classical Cepheids, Type II Cepheids, and RR Lyrae variables at common zero-points. Right, the distance offset between RR Lyrae variables and classical Cepheids in the SMC and IC 1613 is nearly negligible. The base set of equations employed to compute the distances are OGLE *VI* Wesenheit functions of LMC classical Cepheids and RR Lyrae variables. The comparison is independent of zero-point and uncertainties tied to extinction corrections. The results, in tandem with those of Fig. 8.2, imply that the primary source of uncertainty tied to the Cepheid distance to NGC 5128 is unrelated to variations in chemical composition among Cepheids. 135

-
- 8.5 The distances of classical Cepheids in NGC 5128 exhibit a colour and CCD chip dependence, owing partly to photometric contamination. A colour-limited sample that reduces the effects of contamination yields $D \simeq 3.5$ Mpc ($V-I \leq 1.3$, see Fig. 8.1). A VI Wesenheit relation based on new OGLEIII observations was applied to infer the distance (LMC, $\mu_0 = 18.5$). 138
- 8.6 Top panels, a comparison of the reddenings established for a sample of galaxies (including NGC 5128) from classical Cepheids and the NED extinction calculator. $E(V-I)$ is tabulated according to equations adopted by Freedman et al. (2001, F01) and Sandage et al. (2004, S04), whereas $E(B-V)$ is computed following Abrahamyan (2003, A03). Extragalactic classical Cepheid reddenings lie above the relation describing unity (dashed line). The bulk of the data are offset $A_V \simeq 0.^m3$ beyond the foreground estimate. Classical Cepheids in NGC 5128 (red square) display a sizable mean colour excess (see also Figs. 8.1, 8.5). By comparison, the Cepheid-SNe calibrating galaxies NGC 1309, NGC 3021, and IC 4182 (blue triangles) exhibit negative mean reddenings (see also Saha et al., 2006). 139
- 9.1 The slope of the VI_c Wesenheit function as inferred from ground-based photometry of classical Cepheids in the Milky Way (equation 9.2), LMC, NGC 6822, SMC, and IC 1613. The slope of the VI_c Wesenheit function is insensitive to metallicity over the range examined. 153

LIST OF TABLES

2.1	Potential Calibrators	29
3.1	Distances to Benchmark Open Clusters	52
3.2	New Photometry for Cluster δ Scuti Variables	57
3.3	A Comparison of δ Sct Pulsation Modes	61
3.4	δ Scuti Variables in Benchmark Open Clusters	62
4.1	Cep OB6 Member List (Z99)	75
4.2	Additional Potential Cluster Members	80
5.1	Intrinsic Parameters for Red Clump Stars	91
6.1	Stars Near ζ Gem	107
9.1	Distances to the Magellanic Clouds	157

ABSTRACT

Date: July 25, 2012

Dissertation Title: Constraining the Impact of Metallicity on Cepheid Distances Using a Refined Galactic Calibration

Author: Daniel Majaess

Evidence is presented implying that the classical Cepheid VI_c period-Wesenheit function is relatively insensitive to metallicity. The results indicate that variations in chemical composition among Cepheids are a comparatively negligible source of uncertainty for VI_c Wesenheit-based relations and extragalactic distances, for determinations of H_0 , and for the selection of a cosmological model. The conclusions rest in part on a Galactic classical Cepheid VI_c Wesenheit function that has been revised using near-infrared JHK_s photometry for new and existing clusters containing Cepheid variables.

CHAPTER 1

INTRODUCTION

Cepheid variables are integral to establishing the spiral structure of the Milky Way (Turner & Majaess, 2010), extragalactic distances (Gieren et al., 2009), the SN Ia scale (Freedman et al., 2001), and cosmological parameters such as the Hubble constant and the equation of state of dark energy (Macri & Riess, 2009). However, any application of Cepheids to establish extragalactic distances requires an assessment of whether the period-magnitude relation is metallicity dependent. In other words, are Cepheid distances to a target galaxy established from a calibration affected by metallicity differences between the two samples. Freedman & Madore (2010) noted that ambiguities tied to the impact of metallicity account for $> 30\%$ of the total uncertainty associated with H_0 , which subsequently hinders efforts to constrain dark energy because $\sigma_w \sim 2 \times \sigma_{H_0}$ ¹ (Macri & Riess, 2009). Recent studies in the literature assert that the Cepheid VI_c period-Wesenheit relation exhibits a metallicity dependence that is four times larger (Shappee & Stanek, 2011) than the modest value employed in the final results of the Hubble Space Telescope (HST) key project to measure H_0 (Freedman et al., 2001). The Wesenheit function is defined as:

$$W = V - R_{VI_c} \times (V - I_c) \quad (1.1)$$

¹ σ_w and σ_{H_0} correspond to the uncertainties associated with the equation of state of dark energy and the Hubble constant, respectively

where V and I_c are the mean Johnson-Cousins visual and infrared magnitudes, and R_{VI_c} represents the ratio of total to selective extinction $A_V/E(V - I_c)$. The Wesenheit function is reddening free, as shown below:

$$\begin{aligned}
 V - A_V &= V_0 \\
 V - R_{VI_c} \times E(V - I_c) &= V_0 \\
 V - R_{VI_c}((V - I_c) - (V - I_c)_0) &= V_0 \\
 V - R_{VI_c}(V - I_c) &= V_0 - R_{VI_c}(V - I_c)_0 \\
 W = V - R_{VI_c}(V - I_c) &= V_0 - R_{VI_c}(V - I_c)_0 \tag{1.2}
 \end{aligned}$$

where A_V is the extinction in the Johnson V -band, and V_0 is the extinction-corrected V -band magnitude. A principal aim of the Ph.D. research was to fashion a multi-faceted approach to evaluate whether the VI_c period-Wesenheit relation is sensitive to chemical composition. The HST key project result for H_0 relies on extragalactic Cepheids observed in VI passbands². Solid constraints on the (null) dependence of metallicity would effectively eliminate $> 30\%$ of the error budget associated with H_0 , and a sizable fraction of the uncertainty hindering the selection of a cosmological model.

A diverse range of interpretations exist concerning the impact of metallicity on Cepheid distances. Gould (1994) compared classical Cepheids in the LMC and three separate fields in M31, and concluded that a sizable metallicity-distance correlation exists whereby distance moduli for Cepheids should be corrected by upwards of 0.88 ± 0.16 mag/dex when relying on $BVRI$ photometry. The three fields in M31 exhibit different metal abundances because

²<http://www.ipac.caltech.edu/H0kp/>

of that galaxy's galactocentric metallicity gradient. Kochanek (1997) argued that the mean $V - I_c$ colours for classical Cepheids at a given period change by 0.13 ± 0.04 mag/dex. Kochanek (1997) noted that the metallicity correction profoundly impacts existing estimates of H_0 , and in a given case augments the value from 69 ± 8 km/s/Mpc to 80 ± 6 km/s/Mpc. Kennicutt et al. (1998) examined the offset between Cepheids near the central (metal-rich) and outer (metal-poor) regions of M101, and concluded that the distance moduli based on VI_c photometry exhibit a dependence of -0.24 ± 0.16 mag/dex. The Kennicutt et al. (1998) results were challenged by Macri et al. (2001), who noted that increased photometric contamination by neighbouring stars in the crowded central region of M101 may bias the Cepheid flux measurements. Sakai et al. (2004) compared the distances inferred to a series of galaxies from classical Cepheids and the tip of the red giant branch (TRGB), and asserted that the results implied that Cepheids exhibit a metallicity dependence of -0.24 ± 0.05 mag/dex. However, the Sakai et al. (2004) results were challenged by Rizzi et al. (2007). Macri et al. (2006) sampled classical Cepheids at varying galactocentric radii in M106, thereby exploiting the galaxy's metallicity gradient to determine the impact of metallicity on Cepheid distances. Macri et al. (2006) determined that distance moduli for classical Cepheids established from VI_c photometry exhibit a dependence of -0.29 ± 0.09 mag/dex. The results cited by Kennicutt et al. (1998), Sakai et al. (2004), and Macri et al. (2006) are consistent to within the uncertainties, and were most often adopted in the literature to correct Cepheid distances for variations in chemical abundance. Scowcroft et al. (2009) pursued the same methodology as Kennicutt et al. (1998) and Macri et al. (2006), and performed a differential test of classical Cepheids in M33 that are located at

varying galactocentric radii. Scowcroft et al. (2009) corroborated the Macri et al. (2006) determination, yielding a value of -0.29 ± 0.11 mag/dex. A similar test was performed by Shappee & Stanek (2011) and Gerke et al. (2011) using data from the HST and the Large Binocular Telescope for Cepheids in M101 and M81, respectively. Shappee & Stanek (2011) concluded that the metallicity effect is upwards of -0.80 ± 0.21 mag/dex, and Gerke et al. (2011) likewise support a large metallicity effect (i.e., -0.62 ± 0.33 mag/dex).

The results from the studies noted above generally imply that at a fixed pulsation period classical Cepheids in M33, M81, M101, and M106 brighten (W_{VI_c}) with decreasing galactocentric distance (e.g., Kennicutt et al., 1998). A debate persists as to whether the trend is tied to a metallicity gradient, or arises from photometric contamination (Majaess, 2010b; Majaess et al., 2009, 2011c; Kudritzki et al., 2012, and references therein). The degeneracy exists because the surface brightness, density, and metal abundance (Andrievsky et al., 2004, their Fig. 3) all increase with decreasing galactocentric distance. In other words, photometric contamination becomes more likely with decreasing galactocentric distance, and can explain the brightening of Cepheids lying near the galaxy cores. The following independent tests were performed to assess the impact of metallicity on Cepheid distances:

- i. The slopes of the period-magnitude (VI_c) relation inferred from Cepheids in galaxies spanning a sizable abundance baseline were compared, namely metal-rich to metal-poor Cepheids in the Milky Way, LMC, NGC 6822, SMC, and IC 1613. Consequently, establishing a reliable Galactic Cepheid calibration is of utmost importance for assessing the impact of metallicity (i.e., by way of a comparison of the slopes). A principal aim of the Ph.D. thesis was thus to refine the Galactic Cepheid calibration with cluster Cepheids

(Turner, 2010), while seeking to corroborate the inferred parameters by independent means (e.g., Baade-Wesselink Infrared Surface Brightness, BW/ISB, distances, Gieren et al., 2005; Barnes, 2009). Four studies related to the refinement of the Galactic Cepheid calibration by way of an analysis of cluster Cepheids (TW Nor, δ Cep, ζ Gem, R Cru) are included in this thesis (chapters 4, 5, 6, 7). An empirical JHK_s main-sequence calibration was established from deep 2MASS photometry and precise Hipparcos (HIP) parallaxes for nearby stars to secure (unbiased) distances to those Cepheid clusters (chapter 3). The infrared calibration is comparatively insensitive to stellar age and [Fe/H], and is anchored to seven benchmark open clusters that exhibit matching JHK_s and revised Hipparcos distances (van Leeuwen 2009). The objective was to avoid deriving distances to the Cepheid clusters using a single benchmark cluster (i.e., the Pleiades), and thus introduce a potentially large systematic uncertainty into the Cepheid calibration. By employing seven benchmark clusters, and shifting to the infrared where metallicity-effects are mitigated, that problem was avoided. The density of stellar lines is less in the infrared than the optical, thereby mitigating the impact of metallicity effects arising from line-blanketing. In addition, potential variations in the JHK_s reddening and extinction laws are predicted to be comparatively smaller than in the optical. Obscuration by dust is less significant in the infrared ($A_\lambda \propto \lambda^{-\beta}$), which consequently mitigates the impact of variations in R_λ ($J_0 = J - E_{J-H} \times R_J$). Moreover, the deep JHK_s calibration extends into the low mass regime ($\simeq 0.4M_\odot$) where $J - K_s$ remains constant with increasing magnitude ($M_J > 6$) for low mass M-type dwarfs, and $J - H$ exhibits an inversion. The trends ensure precise JHK_s main-sequence fits by providing distinct anchor points in colour-magnitude and colour-colour diagrams. The advantages

of complimenting optical observations with data from the infrared are discussed in chapter 7. The distances for the Cepheid clusters were typically established by first determining the colour-excess from a colour-colour diagram by adjusting the intrinsic relation along the reddening vector to match the target data. An estimate for the cluster age likewise resulted from an analysis of stars in the colour-colour diagram. Once the reddening and an estimate for the cluster age were determined, a Padova isochrone was applied to cluster stars in the colour-magnitude diagram until a best fit was established by eye. The isochrone was shifted in one dimension because the colour-excess was established, and metallicity effects in the infrared are minimal, particularly for cluster Cepheids that exhibit near solar abundances (Andrievsky et al., 2004, and references therein). Padova isochrones were chosen because they are readily available for a range of stellar ages on the 2MASS system (by contrast the Dartmouth isochrones are presently only for older clusters). The uncertainty determined for the cluster distances represents the value at which a difference from the best fit was clearly perceived.

ii. Magnitude offsets between differing classes of pulsating stars were compared to show that they are insensitive to the galaxy sampled (chapters 2, 8). That was evaluated by examining magnitude differences between standard candles such as RR Lyrae variables, δ Scuti variables, and Cepheids in the Galaxy, LMC, SMC, and IC 1613.

iii. Published metallicity corrections were evaluated by applying them to distances established for the Magellanic Clouds using a calibration consisting of nearby and more metal-rich Galactic Cepheids (chapter 9). The aim was to examine whether the metallicity corrected distances match expectations for the Magellanic Clouds as established from

independent published estimates, such as by means of a Universal Wesenheit template (described in chapter 2). In particular, a recently advocated sizable metallicity dependence may be evaluated by applying the proposed correction ($\gamma = -0.8$ mag/dex, Shappee & Stanek, 2011) to distances established for the Magellanic Clouds using a Galactic period-magnitude calibration (hence a motivation for refining the Galactic calibration).

In this thesis, the impact of metallicity on Cepheid distances is assessed. This work is organized as follows: in chapter 2 the Universal Wesenheit template is discussed, in chapter 3 the ZAMS calibration used to establish the distances to the cluster Cepheids is outlined, in chapters 4 and 5 new parameters are established for the clusters associated with δ Cep and TW Nor, in chapter 6 a previously overlooked cluster associated with ζ Gem is characterized, in chapter 7 the Cepheid R Cru is shown to be unassociated with the open cluster NGC 4349, in chapters 8, 9, 10 evidence supporting a negligible impact of metallicity on VI_c -based distances is summarized, future work is described in chapter 10, and finally in chapter 11 coauthors who provided observations and pertinent advice on the various studies are acknowledged.

REFERENCES

- Andrievsky, S. M., Luck, R. E., Martin, P., & Lépine, J. R. D. 2004, *A&A*, 413, 159
- Barnes, T. G. 2009, *American Institute of Physics Conference Series*, 1170, 3
- Benedict, G. F., McArthur, B. E., Feast, M. W., et al. 2007, *AJ*, 133, 1810
- Evans, N. R. 2011, *IAU Symposium*, 272, 537
- Freedman, W. L., Madore, B. F., Gibson, B. K., et al. 2001, *ApJ*, 553, 47
- Freedman, W. L., & Madore, B. F. 2010, *ARA&A*, 48, 673
- Gerke, J. R., Kochanek, C. S., Prieto, J. L., Stanek, K. Z., & Macri, L. M. 2011, *ApJ*, 743, 176
- Gieren, W., Storm, J., Barnes, T. G., III, et al. 2005, *ApJ*, 627, 224
- Gieren, W., Pietrzyński, G., Soszyński, I., et al. 2009, *ApJ*, 700, 1141
- Gould, A. 1994, *ApJ*, 426, 542
- Kennicutt, R. C., Jr., Stetson, P. B., Saha, A., et al. 1998, *ApJ*, 498, 181
- Kochanek, C. S. 1997, *ApJ*, 491, 13
- Kudritzki, R.-P., Urbaneja, M. A., Gazak, Z., et al. 2012, *ApJ*, 747, 15
- Macri, L. M., Calzetti, D., Freedman, W. L., et al. 2001, *ApJ*, 549, 721
- Macri, L. M., & Riess, A. G. 2009, *American Institute of Physics Conference Series*, 1170, 23
- Macri, L. M., Stanek, K. Z., Bersier, D., Greenhill, L. J., & Reid, M. J. 2006, *ApJ*, 652, 1133
- Majaess, D., Turner, D., & Lane, D. 2009, *Acta A*, 59, 403
- Majaess, D., Turner, D., Moni Bidin, C., et al. 2011, *ApJ*, 741, L27
- Riess, A. G., Macri, L., Casertano, S., et al. 2009, *ApJ*, 699, 539
- Rizzi, L., Tully, R. B., Makarov, D., et al. 2007, *ApJ*, 661, 815
- Sakai, S., Ferrarese, L., Kennicutt, R. C., Jr., & Saha, A. 2004, *ApJ*, 608, 42
- Sandage, A., Tammann, G. A., & Reindl, B. 2004, *A&A*, 424, 43
- Scowcroft, V., Bersier, D., Mould, J. R., & Wood, P. R. 2009, *MNRAS*, 396, 1287
- Shappee, B. J., & Stanek, K. Z. 2011, *ApJ*, 733, 124
- Soderblom, D. R., Nelan, E., Benedict, G. F., et al. 2005, *AJ*, 129, 1616
- Turner, D. G. 1996, *JRASC*, 90, 82
- Turner, D. G. 2010, *Ap&SS*, 326, 219
- Turner, D. G., & Majaess, D. J. 2010, *Bulletin of the American Astronomical Society*, 42, 929
- van Leeuwen, F. 2009, *A&A*, 497, 209

CHAPTER 2

UNIVERSAL WESENHEIT TEMPLATE

Anchoring the Universal Distance Scale through a Wesenheit Template

Abstract: A *VI* Wesenheit diagram with SX Phoenicis, δ Scuti, RR Lyrae, type II, and classical Cepheid variables is calibrated by means of geometric-based distances inferred from HST, Hipparcos, and VLBA observations ($n = 30$). The distance to a target population follows from the offset between the observed Wesenheit magnitudes and the calibrated template. The method is evaluated by ascertaining the distance moduli for the LMC ($\mu_0 = 18.43 \pm 0.03(\sigma_{\bar{x}})$) and the globular clusters ω Cen, M54, M13, M3, and M15. The results agree with estimates cited in the literature, although a nearer distance to M13 is favoured (pending confirmation of the data's photometric zero-point) and observations of variables near the core of M15 suffer from photometric contamination. The calibrated LMC data are subsequently added to the Wesenheit template, because that galaxy exhibits precise OGLE photometry for innumerable variables of differing classes that includes recent observations for δ Scuti variables indicating the stars follow a steeper *VI* Wesenheit function than classical Cepheids pulsating in the fundamental mode. *VI* photometry for the calibrators is tabulated to facilitate further research, and includes new observations acquired via the AAVSO's robotic telescope network (e.g., VY Pyx: $\langle V \rangle = 7.25$ and $\langle V \rangle - \langle I \rangle = 0.67$). The approach

outlined here supercedes the lead author’s prior first-order effort to unify variables of the instability strip in order to establish reliable distances.

2.1 INTRODUCTION

SX Phoenicis, δ Scuti, RR Lyrae, type II, and classical Cepheid variables are useful for establishing distances to globular clusters, the Galactic centre, and galaxies (McNamara et al., 2000, 2007; Kubiak & Udalski, 2003; Pritzl et al., 2003; Matsunaga et al., 2006, 2009; Majaess et al., 2009,c; Majaess, 2010a,b,c). However, there is an absence of precise trigonometric parallaxes for nearby type II Cepheids and RR Lyrae variables. RR Lyrae is the single member of its class exhibiting a parallax uncertainty $\leq 30\%$ (Table 2.1). Likewise, κ Pav and VY Pyx are unique among type II Cepheids that have small parallax uncertainties (Table 2.1). The meager statistics presently hamper efforts to establish individual zero-points for each variable type, particularly given that individual calibrators may exhibit peculiarities or multiplicity, or may sample the edge of the instability strip. Variables on the hot edge of the instability strip are brighter relative to objects on the cool edge that share a common pulsation period. Ignoring the distribution of calibrators within the instability strip may subsequently result in biased period- M_V and period-colour relations, especially in the absence of large statistics (Turner, 2010).

These problems may be mitigated by calibrating a *VI* Wesenheit diagram with SX Phe, δ Scuti, RR Lyrae, type II, and classical Cepheid variables. Wesenheit magnitudes are reddening-free and relatively insensitive to the width of the instability strip. The Wesenheit function is defined and discussed by Madore (1982), Opolski (1983, 1988), Madore &

Freedman (1991, 2009), Kovács & Jurcsik (1997), Kovács & Walker (2001), Di Criscienzo et al. (2004, 2007), and Turner (2010).

In this study, a *VI* Wesenheit template characterizing differing variables of the instability strip is calibrated by means of geometric-based distances (§2.2.2) and the pertinent photometry (§2.2.1). The calibration is evaluated by establishing distances to the LMC, ω Cen, M54, M13, M3, and M15 (§2.2.3).

2.2 ANALYSIS

2.2.1 PHOTOMETRY (CALIBRATION)

The author has advocated that RR Lyrae variables and Cepheids obey *VI*-based Wesenheit and period-colour relations that are comparatively insensitive to metallicity (Udalski et al., 2001; Bono, 2003; Pietrzyński et al., 2004; Majaess et al., 2008, 2009,c; Bono et al., 2008; Majaess, 2010a,b,c), hence the advantage of constructing such a relation. That conclusion is based in part upon a direct comparison of RR Lyrae variables, type II Cepheids, and classical Cepheids at common zero-points, which offers an opportunity to constrain the effects of chemical composition on their luminosities and intrinsic colours (Udalski et al., 2001; Majaess et al., 2009c). For example, the distances inferred for the LMC, SMC, IC 1613, and several globular clusters from those standard candles agree to within the uncertainties (Majaess et al., 2009c; Majaess, 2010a,c), despite the neglect of metallicity corrections for variable types sampling different temperature, radius, and density regimes. Admittedly, the subject is actively debated (Smith, 2004; Romaniello et al., 2008; Catelan, 2009, and references therein). By contrast there appears to be a consensus that relationships

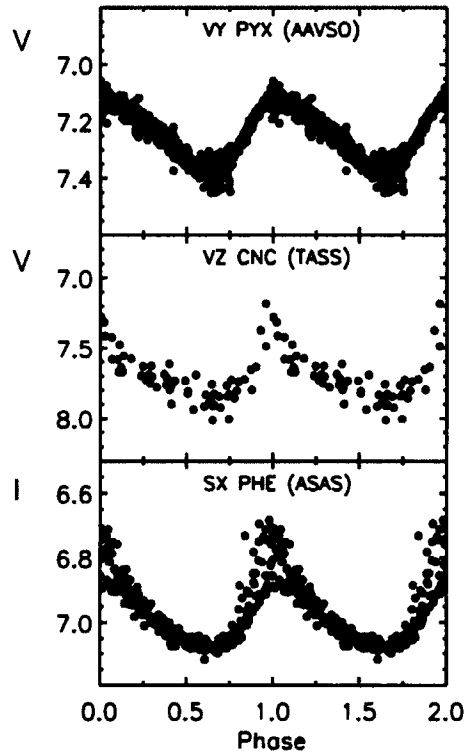


Figure 2.1 Light curves for a subsample of the objects studied here. Data for the type II Cepheid VY Pyx were obtained via the AAVSO’s robotic telescope network. An analysis of that photometry yields the following mean parameters for VY Pyx: $\langle V \rangle = 7.25$ and $\langle V \rangle - \langle I \rangle = 0.67$. VZ Cnc and SX Phe are multiperiodic, and thus the scatter exhibited is only tied in part to photometric uncertainties (Fig. 2.2).

which rely on BV photometry are sensitive to variations in chemical abundance, and a significant break in the period-magnitude relation is apparent (Majaess et al., 2009c, and references therein). Consequently, a VI -based Wesenheit calibration is developed here.

A notable success of the Hipparcos mission was the establishment of time-series and standardized photometry for bright stars. Hipparcos surveyed the sky in $B_T V_T$ while follow-up surveys such as ASAS and TASS obtained VI photometry (Pojmański, 2002; Droege et al., 2006). Observations from a series of studies by Balona & Stobie (1980a), in addition to

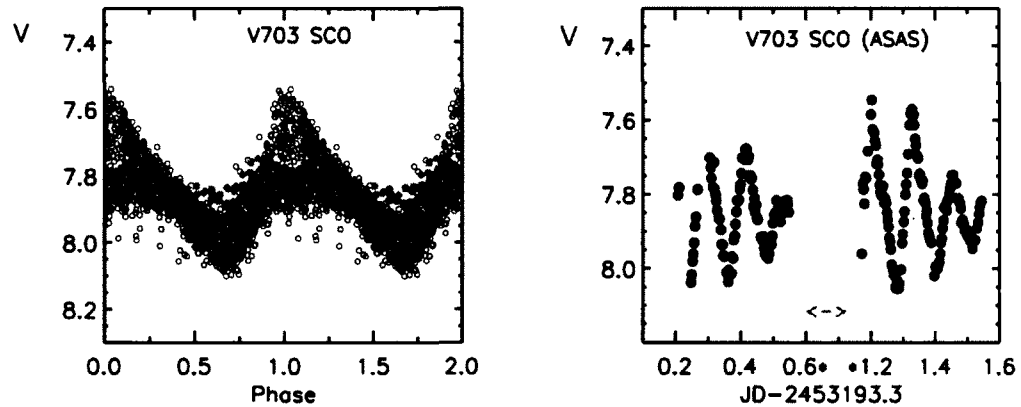


Figure 2.2 Several variables employed in the calibration (Table 2.1) are discernably multiperiodic and exhibit pronounced amplitude variations, as exemplified by observations of V703 Sco. Observations for V703 Sco were obtained via the AAVSO's robotic telescope network (red dots) and ASAS. No prewhitening was performed.

data from those sources, provide the photometry for the shorter period calibrators examined (Table 2.1). Additional observations for VY Pyx and V703 Sco were obtained via the AAVSO's Sonoita (SRO) and Bright Star Monitor (BSM) telescopes.¹ The SRO (Sonoita, Arizona) has an SBIG STL-1001E CCD detector (fov: 20'x20') mounted upon a 35-cm telescope. The BSM has an SBIG ST8XME CCD detector (fov: 127'x84') mounted upon a 6-cm wide-field telescope located at the Astrokolhoz telescope facility near Cloudcroft, New Mexico. The AAVSO observations are tied to Landolt (1983, 1992) photometric standards according to precepts outlined in Henden & Kaitchuck (1990) (see also Henden & Munari, 2008). The data for VZ Cnc were supplemented by observations taken at the Abbey Ridge Observatory (Lane, 2007). *VI* photometry for the Benedict et al. (2007) Galactic classical Cepheid calibrators was obtained from the catalogue of Berdnikov et al. (2000).

The phased light curves for several variables are presented in Fig. 2.1. The relevant

¹<http://www.aavso.org/aavsonet>

Table 2.1. Potential Calibrators

Object	Variable Type	σ_{π}/π	Source	VI Photometry
SX Phe	SX Phe	0.04	van Leeuwen et al. 2007	ASAS
V703 Sco	δ Scuti:	0.12	van Leeuwen et al. 2007	Balona & Stobie 1983, AAVSO
AI Vel	δ Scuti:	0.03	van Leeuwen et al. 2007	Balona & Stobie 1980b, ASAS
VW Ari	SX Phe:	0.07	van Leeuwen et al. 2007	TASS
AD CMi	δ Scuti	0.24	van Leeuwen et al. 2007	Balona & Stobie 1983, TASS
VZ Cnc	δ Scuti	0.10	van Leeuwen et al. 2007	Balona & Stobie 1983, TASS, ARO
RS Gru	δ Scuti:	0.29	van Leeuwen et al. 2007	Balona & Martin 1978
V474 Mon	δ Scuti:	0.04	van Leeuwen et al. 2007	Balona & Stobie 1980a
RR Lyrae	RR Lyr	0.05	Benedict et al. 2002a	TASS
UV Oct	RR Lyr	0.33	van Leeuwen et al. 2007	ASAS
XZ Cyg	RR Lyr	0.37	van Leeuwen et al. 2007	TASS
BN Vul	RR Lyr	0.37	van Leeuwen et al. 2007	TASS
VY Pyx	TII Cep	0.09	van Leeuwen et al. 2007	AAVSO (this study)
κ Pav	TII Cep	0.12	van Leeuwen et al. 2007	Shobbrook 1992, Berdnikov et al. 2008
MSB2006 O-38462	TII Cep	0.05	Herrnstein et al. 1999	Macri et al. 2006
MSB2006 O-07822	TII Cep	0.05	Herrnstein et al. 1999	Macri et al. 2006
MSB2006 O-11134	TII Cep	0.05	Herrnstein et al. 1999	Macri et al. 2006
MSB2006 O-28609	TII Cep	0.05	Herrnstein et al. 1999	Macri et al. 2006
MSB2006 O-29582	TII Cep	0.05	Herrnstein et al. 1999	Macri et al. 2006
MSB2006 O-31291	TII Cep	0.05	Herrnstein et al. 1999	Macri et al. 2006
RT Aur	TI Cep	0.08	Benedict et al. 2007	Berdnikov et al. 2000
T Vul	TI Cep	0.12	Benedict et al. 2007	Berdnikov et al. 2000
FF Aql	TI Cep	0.06	Benedict et al. 2007	Berdnikov et al. 2000
δ Cep	TI Cep	0.04	Benedict et al. 2002b, 2007	Berdnikov et al. 2000
Y Sgr	TI Cep	0.14	Benedict et al. 2007	Berdnikov et al. 2000
X Sgr	TI Cep	0.06	Benedict et al. 2007	Berdnikov et al. 2000
W Sgr	TI Cep	0.09	Benedict et al. 2007	Berdnikov et al. 2000
β Dor	TI Cep	0.05	Benedict et al. 2007	Berdnikov et al. 2000
ζ Gem	TI Cep	0.06	Benedict et al. 2007	Berdnikov et al. 2000
ℓ Car	TI Cep	0.10	Benedict et al. 2007	Berdnikov et al. 2000

Note. — Unpublished *I*-band ASAS observations for several calibrators were kindly provided by G. Pojmański. There are concerns regarding the photometric zero-point for bright stars sampled in the all-sky surveys (Henden & Sallman, 2007; Pojmański, 2009). Colons next to the variable types indicate cases where contradictory designations were assigned in the literature. Distinguishing between Population II SX Phe variables and Population I δ Scuti variables on the basis of metallicity alone may be inexact given there are innumerable metal-rich RR Lyrae variables exhibiting $[\text{Fe}/\text{H}] \geq -0.5$ (e.g., Feast, 2008).

photometry (is) will be available online via databases maintained by CDS, ASAS, TASS, and the AAVSO. The pulsation periods employed to phase the data were adopted from the GCVS (Samus et al., 2009a), the AAVSO's VSX archive² (Watson, Henden & Price, 2010), and the GEOS RR Lyr survey (Le Borgne et al., 2007). Several pulsators display pronounced amplitude variations and are discernably multiperiodic (e.g., AI Vel, V703 Sco, SX Phe, Figs. 2.1 and 2.2), topics that will be elaborated upon elsewhere.

2.2.2 PARALLAXES (CALIBRATION)

A total of 24 variables with parallaxes measured by Hipparcos and HST are employed to calibrate the *VI* Wesenheit diagram (Table 2.1). The sample consists of 8 SX Phoenicis and δ Scuti variables, 4 RR Lyrae variables, 2 type II Cepheids, and 10 classical Cepheids. That sample is supplemented by 6 type II Cepheids detected by Macri et al. (2006) in their comprehensive survey of the galaxy M106 (Majaess et al., 2009c), which has a precise geometric-based distance estimate (Herrnstein et al., 1999). It is perhaps ironic that stars 7.2 Mpc distant may be enlisted as calibrators because of an absence of accurate parallaxes for nearby objects. Type II Cepheids within the inner region of M106 were not employed in the calibration because of the likelihood of photometric contamination via crowding and blending (Fig. 2.4, see also Mochejska et al., 2001; Majaess, 2010c). The stars employed were observed in the outer regions of M106 where the stellar density and surface brightness are diminished by comparison. Extragalactic type II Cepheids are often detected fortuitously near the limiting magnitude of surveys originally aimed at discovering more luminous classical Cepheids, hence the preference toward detecting the longer period (brighter) RV Tau

²<http://www.aavso.org/vsx/>

subclass (Majaess et al., 2009c).

Parallaxes for several calibrators were sought from the van Leeuwen (2007) catalogue of revised Hipparcos data (Table 2.1). The parallaxes cited in the study differ from those published by van Leeuwen et al. (2007). The reliability of Hipparcos parallaxes has been questioned because of disagreements over the distances to Polaris and the Pleiades cluster (Turner & Burke, 2002; Soderblom et al., 2005; Turner et al., 2005; van Leeuwen et al., 2007; van Leeuwen, 2009,b; Turner, 2009, 2010). The Hipparcos parallax for the Pleiades corresponds to a distance of $d = 120.2 \pm 1.9$ pc (van Leeuwen, 2009), whereas HST observations imply $d = 134.6 \pm 3.1$ pc (Soderblom et al., 2005). A comparison of stars with both Hipparcos and HST parallaxes indicates that there may be a marginal systemic offset ($\sim 5\%$). However, the statistics are presently too poor. van Leeuwen (2009,b) argues in favor of the Hipparcos scale and the reader is referred to that comprehensive study.

Tammann et al. (2008) questioned the reliability of HST parallaxes for nearby classical Cepheids because the resulting period-magnitude relations inferred from that sample do not match their own functions (Tammann et al., 2003; Sandage et al., 2004), which were constructed from the best available data at the time³ and prior to the publication of the HST parallaxes (Benedict et al., 2007). The viability of the HST parallaxes is supported by the results of Turner (2010) and Majaess (2010c). A central conclusion of the Turner (2010) study was that the classical Cepheid period-luminosity relation tied to the HST sample is in agreement with that inferred from cluster Cepheids. Majaess (2010c) confirmed that the slope of the *VI* Wesenheit function inferred from the Benedict et al. (2007) HST data matches that of precise ground-based observations of classical Cepheids in the LMC, NGC

³Turner (2010) has revised the parameters for longer-period classical Cepheid calibrators.

6822, SMC, and IC 1613 (see Fig. 2 in Majaess, 2010c). Classical Cepheids in those galaxies span a sizable abundance baseline and adhere to a common *VI* Wesenheit slope to within the uncertainties, thereby precluding a dependence on metallicity (see Fig. 2 in Majaess, 2010c).

The uncertainty tied to the Wesenheit magnitude for a given calibrator is presently dominated by the parallax and distance uncertainties. Those uncertainties are converted into magnitude space (σ_w) via:

$$\begin{aligned}\sigma_w &\simeq |5 \log(d + \sigma_d) - 5 - (5 \log(d - \sigma_d) - 5)|/2 \\ &\simeq \left| 2.5 \log \left(\frac{d + \sigma_d}{d - \sigma_d} \right) \right| \\ &\simeq \left| 2.5 \log \left(\frac{\pi - \sigma_\pi}{\pi + \sigma_\pi} \right) \right|\end{aligned}$$

The uncertainty associated with Wesenheit magnitudes for type II Cepheids in M106 (σ'_w) is estimated as:

$$\sigma'_w \simeq \sqrt{\sigma_{TII}^2 + \sigma_w^2}$$

where σ_{TII} is the average photometric deviation of type II Cepheids occupying the outer region of M106 from the mean *VI* Wesenheit function.

The calibration derived here will be bolstered by additional and precise parallax measurements. F. Benedict and coauthors are presently acquiring HST parallaxes for important stars such as κ Pav, XZ Cyg, UV Oct, and VY Pyx (Table 2.1).

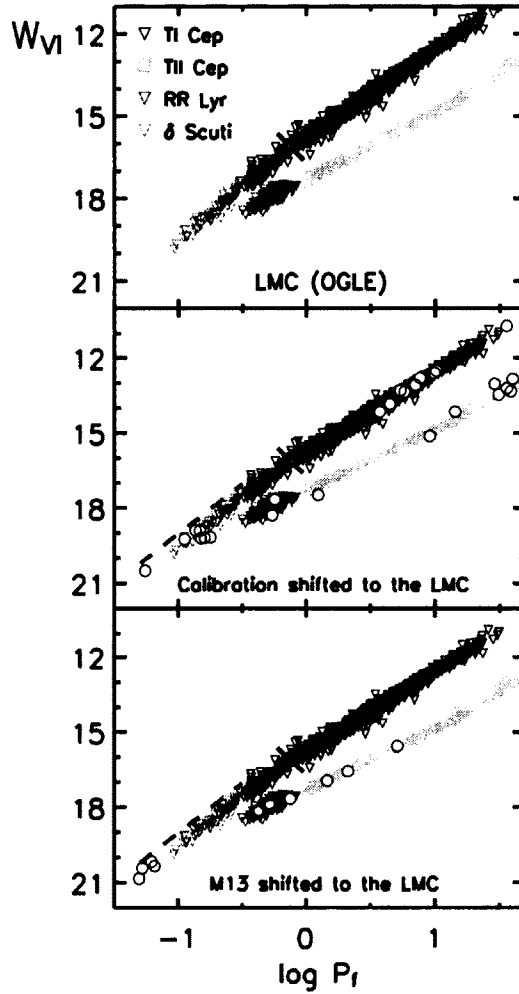


Figure 2.3 A VI Wesenheit diagram characterizing a subsample of the examined data. The distance to the LMC is secured by evaluating the offset from the calibration (*middle panel*, yellow dots, the size of the datapoints is representative of the uncertainties). The Wesenheit magnitudes of variable stars in globular clusters (e.g., M13, *bottom panel*, yellow dots) may be compared to the LMC template to derive the zero-point. The blue dashed line indicates the position of uncorrected δ Scuti stars pulsating in the overtone (see Poleski et al., 2010). A break in the classical Cepheid relation near $\log P_F \simeq -0.15$ may define the δ Sct / Cep boundary (see also Fig. 6 in Soszyński et al., 2008b, $\log P \simeq -0.3$).

2.2.3 CALIBRATED WESENHEIT DIAGRAMS

The calibrating and LMC VI Wesenheit diagrams are displayed in Fig. 2.3. The Wesenheit magnitudes were computed as follows:

$$W_{VI,0} = \langle V \rangle - R_{VI}(\langle V \rangle - \langle I \rangle) - \mu_0$$

$$W_{VI} = \langle V \rangle - R_{VI}(\langle V \rangle - \langle I \rangle)$$

where $R_{VI} = 2.55$ is the canonical extinction law, although there are concerns about adopting a colour-independent extinction law. The Wesenheit magnitudes tied to BN Vul and AD CMi are anomalous so the stars were omitted from Fig. 2.3. The cases may be similar to RT Aur, Y Sgr, or perhaps FF Aql (see Table 1 in van Leeuwen et al., 2007), where the parallaxes are problematic. RR Lyrae variables pulsating in the overtone were shifted by $\log P_f \simeq \log P_o + 0.13$ to obtain the equivalent fundamental mode period (Walker & Nemeč, 1996; Hurdis & Krajci, 2010). Fig. 2.3 was plotted with the equivalent fundamental mode periods to illustrate the general continuity across the variable types. Plotting the uncorrected principal period is preferred, however, to permit a direct assessment of the pulsation mode.

The distance to a target population follows from the offset between the observed Wesenheit magnitudes and the calibration.

LMC

The resulting distance modulus for the LMC is $\mu_0 = 18.43 \pm 0.03(\sigma_{\bar{x}}) \pm 0.17(\sigma)$. That agrees with the value obtained by Majaess et al. (2008) and Majaess (2010a), and has smaller uncertainties. Likewise, the estimate is consistent with a mean derived from the NASA/IPAC Extragalactic Database (NED-D) master list of galaxy distances, which has over 300 distance estimates for the LMC (Madore & Steer, 2007; Steer & Madore, 2010).^{4,5}

The author's prior estimates were inferred by applying a *VI* Galactic classical Cepheid

⁴<http://nedwww.ipac.caltech.edu/level5/NED1D/intro.html>

⁵<http://nedwww.ipac.caltech.edu/Library/Distances/>

calibration (Majaess et al., 2008) to the LMC photometry of Udalski et al. (1999) and Sebo et al. (2002). The Majaess et al. (2008) calibration is based primarily on the efforts of fellow researchers who established classical Cepheids as members of Galactic open clusters (e.g., Sandage, 1958; Madore & van den Bergh, 1975; Turner, 2010) or secured precise trigonometric parallaxes (HST, Benedict et al., 2002b, 2007).

The latest OGLE LMC observations indicate that δ Scuti stars exhibit a steeper *VI* Wesenheit slope than classical Cepheids pulsating in the fundamental mode (Fig. 2.3, see also Soszyński et al., 2008b; Poleski et al., 2010). The pulsation modes of δ Scuti variables may be constrained by overlaying a target demographic — along with RR Lyrae and type II Cepheid variables that are often detected together — upon the calibrated LMC Wesenheit template. SX Phe variables appear toward the shorter-period extension of the δ Scuti regime on the Wesenheit diagram (Fig. 2.3).

M3

The distance to variable stars in globular clusters may be established by comparing the observed Wesenheit magnitudes to the calibrated LMC template, which exhibits extensive statistics and period coverage for innumerable variable types. The distance modulus for M3 from the analysis is: $\mu_0 = 15.12 \pm 0.01(\sigma_{\bar{x}}) \pm 0.20(\sigma)$. That agrees with the estimate of $\mu_0 \simeq 15.08$ by Harris (1996), which was established from the magnitude of the horizontal branch.⁶

⁶<http://physwww.mcmaster.ca/~harris/mwgc.ref>

ω Cen

The distance modulus for ω Cen from the Wesenheit approach is: $\mu_0 = 13.49 \pm 0.01(\sigma_{\bar{x}}) \pm 0.09(\sigma)$. Estimates in the literature for ω Cen span a range: $\mu_0 \simeq 13.41 \rightarrow 13.76$ (van de Ven et al., 2006; Del Principe et al., 2006). The *VI* photometry characterizing variables in ω Cen was obtained somewhat indirectly (see Weldrake et al., 2007). Securing multiepoch *I*-band observations is therefore desirable to permit a more confident determination of the zero-point and enable further constraints on the effects of chemical composition on the luminosities of RR Lyrae variables. Stars in ω Cen exhibit a sizable spread in metallicity at a common zero-point because of the presence of multiple populations ($-1.0 \geq [Fe/H] \geq -2.4$, Rey et al. 2000). Evaluating the correlation between the distance modulus computed for a given RR Lyrae variable and its abundance yields direct constraints on the effects of metallicity (e.g., Majaess, 2010a).

M13

An analysis of the variable stars in M13 yields: $\mu_0 = 14.09 \pm 0.02(\sigma_{\bar{x}}) \pm 0.06(\sigma)$ (caution warranted, see below). That may agree with the infrared weighted solution of $\mu_0 = 14.25$ by Buckley & Longmore (1992), but the estimate is significantly smaller than the distance modulus for M13 cited by Harris (1996) ($\mu_0 \simeq 14.43$). The observations of M13 are from a series of studies that detected at least 4 SX Phe variables, 5 RR Lyrae variables (4 RRc and 1 RRab), and 3 type II Cepheids (Kopacki et al., 2003; Pietrukowicz & Kaluzny, 2004; Kopacki, 2005). The surveys were conducted as part of renewed efforts to secure multiband photometric parameters for variable stars in globular clusters (Pietrukowicz & Kaluzny,

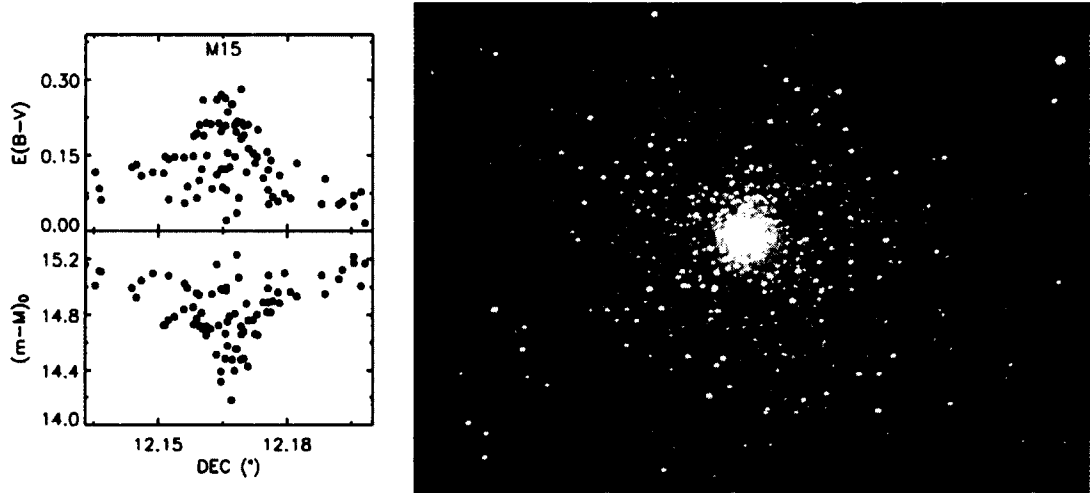


Figure 2.4 Variables near the core of M15 suffer from photometric contamination. The surface brightness and stellar density increase rapidly toward the core, thereby increasing the likelihood of contamination. *Left*, the distance moduli and colour excess for RR Lyrae variables are computed via the calibrations of Majaess et al. 2009 and Majaess 2010b. *Right*, M15 imaged from the ARO (Lane, 2007). M15 is crucial because it is among the most metal-poor Galactic clusters and hosts a planetary nebula (Jacoby et al., 1997; Alves et al., 2000; Turner, 2010b).

2003; Pietrukowicz et al., 2008, see also Sawyer 1939, Clement et al. 2001, Samus et al. 2009b).

Applying the *VI* RR Lyrae variable period-reddening calibration of Majaess (2010b) to the M13 data yields a mean colour excess of: $E_{B-V} = 0.06 \pm 0.02(\sigma)$ (caution warranted, see below). The *VI* RR Lyrae variable period-colour relation derived by Pejcha & Stanek (2009) yields $E_{V-I} = 0.05 \pm 0.02(\sigma)$ ($E_{B-V} \simeq 0.04$). The estimates are larger than the reddening inferred from the NED extinction calculator for the direction toward M13 ($E_{B-V} \simeq 0.02$). The consensus position is that the line of sight toward M13 is unobscured, however the Wesenheit approach is extinction free and independent of that assertion (for the canonical extinction law). Applying the new reddening to previous optical estimates of the cluster's distance modulus would result in a correction of $\Delta\mu_0 \simeq -E_{B-V} \times R_V \simeq -0.15$ (R_V , Turner,

1976), thereby bringing the estimates into closer agreement.

The data for M13 are ground-based and HST photometry, which are challenging to standardize and may therefore be susceptible to a host of concerns related to photometric contamination and floating photometric zero-points (e.g., see Saha et al., 2006). If the photometry is trustworthy, then the distance and reddening estimates obtained for M13 are reliable. Additional observations are presently being acquired to facilitate that assessment.

M54

The distance modulus derived for M54 is $\mu_0 = 17.04 \pm 0.01(\sigma_{\bar{x}}) \pm 0.05(\sigma)$. That agrees with the Harris (1996) estimate of $\mu_0 \simeq 17.14$.

M15

The distance modulus for M15 from the analysis is $\mu_0 \geq 14.82$. Estimates in the literature for M15 span the range $\mu_0 \simeq 14.69 \rightarrow 14.99$ (Arellano Ferro et al., 2006; McNamara et al., 2004). Applying the *VI* RR Lyrae variable period-reddening calibration of Majaess (2010b) yields a mean colour excess of $E_{B-V} < 0.12$, matching that cited by Harris (1996). However, the observations suffer from photometric contamination, particularly for stars near the cluster core where the surface brightness and stellar density increase rapidly (Fig. 2.4). Blending may introduce spurious flux and cause variables to appear brighter (often redder) and hence nearer (Fig. 2.4). Photometric contamination provides an explanation for the discrepancy noted in the Bailey diagram that describes variables in M15 (see Corwin et al., 2008).

That contamination was overlooked by the author when previously investigating the

cluster (Majaess, 2010a). Other globular cluster photometry should be examined in similar fashion, pending the availability of published positional data beyond pixel coordinates. Photometric contamination may bias efforts to construct a RR Lyrae variable period-amplitude-metallicity relation, and may exaggerate the perceived spread of the cluster's main-sequence and red giant branch, thereby mimicking the signature of multiple populations (in certain instances). A trend similar to that displayed in Fig. 2.4 is observed in data for extragalactic Cepheids (Majaess et al., 2009c). In an effort to constrain the effect of chemical composition on the luminosities of classical Cepheids, researchers have endeavored to compare the distance offset between classical Cepheids located in the central (metal-rich) and outer (metal-poor) regions of a particular galaxy (e.g., M101, M106, M33). A degeneracy (photometric contamination) complicates the analysis because the stellar density and surface brightness often increase toward the central region. Depending on the circumstances, the effects of metallicity and blending/crowding may act in the same sense and be of similar magnitude (e.g., compare Figs. 17 and 18 in Macri et al., 2006, see also Macri et al. 2001). Furthermore, R (the ratio of total to selective extinction) may also vary as a function of radial distance from the centres of galaxies in conjunction with the metallicity gradient. For example, the extinction law characterizing dust properties near the centre of the Milky Way is possibly anomalous (Udalski, 2003, see Kunder et al. 2008 for the dissenting view). As stated earlier, the author has advocated that VI -based Cepheid and RR Lyrae variable Wesenheit and period-colour relations are comparatively insensitive to metallicity, and thus the offset arises from photometric contamination or another source.

The uncertainties associated with the derived distance modulus and mean colour excess

for M15 cited above are exacerbated systemically and statistically by the aforementioned bias (Fig. 2.4). The distance modulus and colour excess representing stars near the periphery of the cluster, where the effects of photometric contamination are mitigated, are: $\mu_0 \simeq 15$ and $E_{B-V} \simeq 0.06$ (Fig. 2.4). The analysis reaffirms the advantage of adopting a period-magnitude-colour approach to investigating RR Lyrae variables, in addition to the approach outlined in Fig. 2.3 or the canonical $[\text{Fe}/\text{H}] - M_V$ relation. The slope of the Wesenheit function is also an important diagnostic for assessing photometric irregularities (Majaess et al., 2009c; Majaess, 2010c), and should be assessed in conjunction with the establishment of distances via the Wesenheit template (Fig. 2.3).

2.3 SUMMARY AND FUTURE RESEARCH

A *VI* Wesenheit diagram unifying variables of the instability strip is calibrated by means of geometric-based distances inferred from HST, Hipparcos, and VLBA observations (Table 2.1, Fig. 2.3). The distance modulus for a target population is determined by evaluating the offset between the observed Wesenheit magnitudes and the calibrating template. The approach reduces the uncertainties tied to establishing a distance scale based on type II Cepheids or RR Lyrae variables individually, because presently there is an absence of reliable parallaxes. F. Benedict and coauthors are engaged in ongoing efforts to secure precise parallaxes for a host of variables employed in the calibration (Table 2.1).

To first order the distance moduli established for the LMC, ω Cen, M54, M13, M3, and M15 via the calibration agree with estimates in the literature (§2.2.3). *VI* photometry for variable stars in the globular clusters examined (and LMC) were sought from innumerable

sources (Udalski et al., 1999; Layden & Sarajedini, 2000; Soszyński et al., 2003; Soszyński et al., 2008; Soszyński et al., 2008b, 2009a; Kopacki et al., 2003; Pietrukowicz & Kaluzny, 2004; Kopacki, 2005; Benkő et al., 2006; Weldrake et al., 2007; Corwin et al., 2008; Poleski et al., 2010).

VI photometry for the calibrating set was acquired from the AAVSO's robotic telescope network and other sources (Table 2.1, §2.2.1). This study reaffirms the importance of modest telescopes in conducting pertinent research (Percy, 1986, 2007; Welch et al., 1995; Szabados, 2003; Henden, 2006; Paczyński, 2006; Genet et al., 2009; Pojmański, 2009; Udalski, 2009; Turner et al., 2009a), whether that is facilitating an understanding of terrestrial mass extinction events, discovering distant supernovae, aiding the search for life by detecting exoplanets, or anchoring the universal distance scale (e.g., Price et al., 2005; Lane & Gray, 2005; Charbonneau et al., 2009; Majaess et al., 2009c).

Lastly, the present holistic approach supercedes the lead author's prior first order and somewhat erroneous effort (Majaess, 2010a).⁷ Yet it is envisioned that the universal distance scale could be further constrained via the current approach by relying on an additional suite of calibrators, namely variables in globular clusters that possess dynamically-established distances (e.g., ω Cen and M15, McNamara et al., 2004; van de Ven et al., 2006), δ Scuti stars in nearby open clusters (e.g., Pleiades, Praespaes, Hyades; Li & Michel, 1999), variable stars in clusters with distances secured by means of eclipsing binaries (e.g., Cluster AgeS Experiment), and variables in the Galactic bulge that are tied to a precise geometric-based distance (Eisenhauer et al., 2005; Reid et al., 2009, bolstered by observations from the up-

⁷SX Phe, RR Lyrae, and type II Cepheid variables may be characterized by a common *VI* Wesenheit function to first order, as noted by Majaess (2010a,b), but not to second order (Fig. 2.3).

coming *VVV* survey; Minniti et al. 2010). The resulting *VI* Wesenheit calibration (Fig. 2.3) could be applied to galaxies beyond the LMC that have *VI* observations for Population I and II variables, such as the SMC (Udalski et al., 1999; Soszyński et al., 2002), IC 1613 (Udalski et al., 2001; Dolphin et al., 2001), and M33 (Sarajedini et al., 2006; Scowcroft et al., 2009). The results of such an analysis would support ongoing efforts to constrain the Hubble constant (e.g., Ngeow & Kanbur, 2006; Macri & Riess, 2009). However, a successful outcome is contingent upon the admittedly challenging task of obtaining precise, commonly standardized, multi-epoch, multi-band, comparatively uncontaminated photometry.

REFERENCES

- Alves, D. R., Bond, H. E., & Livio, M. 2000, *AJ*, 120, 2044
- Arellano Ferro, A., García Lugo, G., & Rosenzweig, P. 2006, *Revista Mexicana de Astronomía y Astrofísica*, 42, 75
- Artigau, E., Doyon, R., Lamontagne, R., & Malo, L. 2010, *Proc. SPIE*, 7737, 63
- Balona, L. A., & Martin, W. L. 1978, *MNRAS*, 184, 1
- Balona, L. A., & Stobie, R. S. 1980 (a), *MNRAS*, 190, 931
- Balona, L. A., & Stobie, R. S. 1980 (b), *MNRAS*, 192, 625
- Balona, L. A., & Stobie, R. S. 1983, *South African Astronomical Observatory Circular*, 7, 19
- Benedict, G. F., et al. 2002 (b), *AJ*, 124, 1695
- Benedict G. F. et al., 2002 (a), *AJ*, 123, 473
- Benedict G. F. et al., 2007, *AJ*, 133, 1810
- Benkő, J. M., Bakos, G. Á., & Nuspl, J. 2006, *MNRAS*, 372, 1657
- Berdnikov, L. N., Dambis, A. K., & Vozyakova, O. V. 2000, *A&AS*, 143, 211
- Berdnikov, L. N. 2008, *VizieR Online Data Catalog*, 2285, 0
- Bono, G. 2003, *Stellar Candles for the Extragalactic Distance Scale*, 635, 85
- Bono, G., Caputo, F., Fiorentino, G., Marconi, M., & Musella, I. 2008, *ApJ*, 684, 102
- Buckley, D. R. V., & Longmore, A. J. 1992, *MNRAS*, 257, 731
- Catelan, M. 2009, *Ap&SS*, 320, 261
- Charbonneau, D., et al. 2009, *Nature*, 462, 891
- Clement, C. M., et al. 2001, *AJ*, 122, 2587
- Corwin, T. M., Borissova, J., Stetson, P. B., Catelan, M., Smith, H. A., Kurtev, R., & Stephens, A. W. 2008, *AJ*, 135, 1459
- Del Principe, M., et al. 2006, *ApJ*, 652, 362
- Di Criscienzo, M., Marconi, M., & Caputo, F. 2004, *ApJ*, 612, 1092
- Di Criscienzo, M., Caputo, F., Marconi, M., & Cassisi, S. 2007, *A&A*, 471, 893
- Dolphin, A. E., et al. 2001, *ApJ*, 550, 554
- Droege T. F., Richmond M. W., Sallman M. P., Creager R. P., 2006, *PASP*, 118, 1666
- Eisenhauer, F., et al. 2005, *ApJ*, 628, 246
- Feast M. W., Laney C. D., Kinman T. D., van Leeuwen F., Whitelock P. A., 2008, *MNRAS*, 386, 2115
- Feast, M. W. 2010, *Variable Stars, the Galactic halo and Galaxy Formation*, 45
- Freedman, W. L., & Madore, B. F. 1996, *Clusters, Lensing, and the Future of the Universe*, 88, 9
- Genet, R. M., Johnson, J. M., Wallen, V., 2009, *Small Telescopes and Astronomical Research*, Collins Foundation Press.
- Harris, W. E. 1996, *AJ*, 112, 1487
- Henden, A. A., & Kaitchuck, R. H. 1990, *Richmond, Va. : Willmann-Bell, c1990.*

- Henden, A. 2006, *Astrophysics of Variable Stars*, 349, 165
- Henden, A. A., & Sallman, M. P. 2007, *The Future of Photometric, Spectrophotometric and Polarimetric Standardization*, 364, 139
- Henden, A., & Munari, U. 2008, *Information Bulletin on Variable Stars*, 5822, 1
- Herrnstein, J. R., et al. 1999, *Nature*, 400, 539
- Hurdis, D. A., & Krajci, T. 2010, *JAAVSO*, 116
- Jacoby, G. H., Morse, J. A., Fullton, L. K., Kwitter, K. B., & Henry, R. B. C. 1997, *AJ*, 114, 2611
- Kopacki, G., Kołaczowski, Z., & Pigulski, A. 2003, *A&A*, 398, 541
- Kopacki, G. 2005, *Acta Astronomica*, 55, 85
- Kovács, G., & Jurcsik, J. 1997, *A&A*, 322, 218
- Kovács, G., & Walker, A. R. 2001, *A&A*, 371, 579
- Kubiak M., Udalski A., 2003, *Acta Astr.*, 53, 117
- Kunder, A., Popowski, P., Cook, K. H., & Chaboyer, B. 2008, *AJ*, 135, 631
- Landolt, A. U. 1983, *AJ*, 88, 439
- Landolt, A. U. 1992, *AJ*, 104, 340
- Lane, D., & Gray, P. 2005, *Central Bureau Electronic Telegrams*, 224, 1
- Lane D. J., 2007, 96th Spring Meeting of the AAVSO, <http://www.aavso.org/aavso/meetings/spring07present/Lane.ppt>
- Layden, A. C., & Sarajedini, A. 2000, *AJ*, 119, 1760
- Le Borgne, J. F., et al. 2007, *A&A*, 476, 307
- Li, Z. P., & Michel, E. 1999, *A&A*, 344, L41
- Macri, L. M., et al. 2001, *ApJ*, 549, 721
- Macri, L. M., Stanek, K. Z., Bersier, D., Greenhill, L. J., & Reid, M. J. 2006, *ApJ*, 652, 1133
- Macri, L. M., & Riess, A. G. 2009, *American Institute of Physics Conference Series*, 1170, 23
- Madore, B. F., & van den Bergh, S. 1975, *ApJ*, 197, 55
- Madore B. F., 1982, *ApJ*, 253, 575
- Madore, B. F., & Freedman, W. L. 1991, *PASP*, 103, 933
- Madore, B. F., & Steer, I. 2007, *NASA/IPAC Extragalactic Database Master List of Galaxy Distances* (<http://nedwww.ipac.caltech.edu/level5/NED1D/intro.html>)
- Madore, B. F., & Freedman, W. L. 2009, *ApJ*, 696, 1498
- Majaess D. J., Turner D. G., Lane D. J., 2008, *MNRAS*, 390, 1539
- Majaess, D. J., Turner, D. G., & Lane, D. J. 2009 (a), *MNRAS*, 398, 263
- Majaess, D., Turner, D., & Lane, D. 2009 (b), *Acta Astronomica*, 59, 403
- Majaess, D. J., Higgins, D., Molnar, L. A., Haegert, M. J., Lane, D. J., Turner, D. G., & Nielsen, I. 2009 (c), *JRASC*, 103, 7
- Majaess, D. J. 2009, *arXiv:0912.2928*
- Majaess, D. 2010 (a), *Acta Astronomica*, 60, 55
- Majaess, D. J. 2010 (b), Majaess, D. 2010, *Acta A*, 60, 121
- Matsunaga, N., et al. 2006, *MNRAS*, 370, 1979
- Matsunaga, N., Kawadu, T., Nishiyama, S., Nagayama, T., Hatano, H., Tamura, M., Glass, I. S., & Nagata, T. 2009, *MNRAS*, 399, 1709

- McNamara, D. H., Madsen, J. B., Barnes, J., & Ericksen, B. F. 2000, *PASP*, 112, 202
- McNamara, B. J., Harrison, T. E., & Baumgardt, H. 2004, *ApJ*, 602, 264
- McNamara, D. H., Clementini, G., & Marconi, M. 2007, *AJ*, 133, 2752
- Minniti, D., et al. 2010, *New Astronomy*, 15, 433
- Mochejska, B. J., Macri, L. M., Sasselov, D. D., & Stanek, K. Z. 2000, *AJ*, 120, 810
- Mochejska, B. J., Macri, L. M., Sasselov, D. D., & Stanek, K. Z. 2001, arXiv:astro-ph/0103440
- Ngeow, C., & Kanbur, S. M. 2006, *ApJ*, 642, L29
- Opolski A., 1983, *IBVS*, 2425, 1
- Opolski, A. 1988, *Acta Astronomica*, 38, 375
- Paczyński, B. 2006, *PASP*, 118, 1621
- Pejcha, O., & Stanek, K. Z. 2009, *ApJ*, 704, 1730
- Percy, J. R. 1986, *Study of Variable Stars using Small Telescopes*
- Percy, J. R. 2007, *Understanding variable stars / Cambridge University Press*
- Pietrukowicz, P., & Kaluzny, J. 2003, *Acta Astronomica*, 53, 371
- Pietrukowicz, P., & Kaluzny, J. 2004, *Acta Astronomica*, 54, 19
- Pietrukowicz, P., Olech, A., Kedzierski, P., Zloczewski, K., Wisniewski, M., & Mularczyk, K. 2008, *Acta Astronomica*, 58, 121
- Pietrzyński, G., Gieren, W., Udalski, A., Bresolin, F., Kudritzki, R.-P., Soszyński, I., Szymański, M., & Kubiak, M. 2004, *AJ*, 128, 2815
- Pojmański, G. 2002, *Acta Astronomica*, 52, 397
- Pojmański, G. 2009, *Astronomical Society of the Pacific Conference Series*, 403, 52
- Poleski, R., et al. 2010, *Acta Astronomica*, 60, 1
- Price, A., et al. 2005, *JAAVSO*, 34, 17
- Pritzl B. J., Smith H. A., Stetson P. B., Catelan M., Sweigart A. V., Layden A. C., Rich R. M., 2003, *AJ*, 126, 1381
- Rey, S.-C., Lee, Y.-W., Joo, J.-M., Walker, A., & Baird, S. 2000, *AJ*, 119, 1824
- Reid, M. J., Menten, K. M., Zheng, X. W., Brunthaler, A., & Xu, Y. 2009, *ApJ*, 705, 1548
- Romaniello, M., et al. 2008, *A&A*, 488, 731
- Saha, A., Thim, F., Tammann, G. A., Reindl, B., & Sandage, A. 2006, *ApJS*, 165, 108
- Samus, N. N., Durlevich, O. V., & et al. 2009, *VizieR Online Data Catalog*, 1, 2025
- Samus, N. N., Kazarovets, E. V., Pastukhova, E. N., Tsvetkova, T. M., & Durlevich, O. V. 2009, *PASP*, 121, 1378
- Sandage, A. 1958, *ApJ*, 128, 150
- Sandage, A., Tammann, G. A., & Reindl, B. 2004, *A&A*, 424, 43
- Sarajedini, A., Barker, M. K., Geisler, D., Harding, P., & Schommer, R. 2006, *AJ*, 132, 1361
- Sawyer, H. B. 1939, *Publications of the David Dunlap Observatory*, 1, 125
- Scowcroft, V., Bersier, D., Mould, J. R., & Wood, P. R. 2009, *MNRAS*, 396, 1287
- Sebo, K. M., et al. 2002, *ApJS*, 142, 71
- Shobbrook, R. R. 1992, *MNRAS*, 255, 486
- Smith, H. A. 2004, *RR Lyrae Stars*, by Horace A. Smith, pp. 166. ISBN 0521548179. Cambridge, UK: Cambridge University Press, September 2004
- Smith, M. C., Woźniak, P., Mao, S., & Sumi, T. 2007, *MNRAS*, 380, 805

- Soderblom, D. R., Nelan, E., Benedict, G. F., McArthur, B., Ramirez, I., Spiesman, W., & Jones, B. F. 2005, *AJ*, 129, 1616
- Soszyński, I., et al. 2002, *Acta Astronomica*, 52, 369
- Soszyński, I., et al. 2003, *Acta Astronomica*, 53, 93
- Soszyński, I., et al. 2008, *Acta Astronomica*, 58, 293
- Soszyński, I., et al. 2008 (b), *Acta Astronomica*, 58, 163
- Soszyński, I., et al. 2009, *Acta Astronomica*, 59, 1
- Stanek, K. Z., & Udalski, A. 1999, arXiv:astro-ph/9909346
- Steer, I. & Madore, B. F. 2010, NED-D: A Master List of Redshift-Independent Extragalactic Distances (<http://nedwww.ipac.caltech.edu/Library/Distances/>)
- Szabados, L. 2003, *Astrophysics and Space Science Library*, 289, 207
- Tammann, G. A., Sandage, A., & Reindl, B. 2003, *A&A*, 404, 423
- Tammann, G. A., Sandage, A., & Reindl, B. 2008, *ApJ*, 679, 52
- Turner, D. G. 1976, *AJ*, 81, 1125
- Turner, D. G. 2001, *Odessa Astronomical Publications*, 14, 166
- Turner D. G., Burke J. F., 2002, *AJ*, 124, 2931
- Turner, D. G., Savoy, J., Derrah, J., Abdel-Sabour Abdel-Latif, M., & Berdnikov, L. N. 2005, *PASP*, 117, 207
- Turner, D. G., Majaess, D. J., Lane, D. J., Szabados, L., Kovtyukh, V. V., Usenko, I. A., & Berdnikov, L. N. 2009, *American Institute of Physics Conference Series*, 1170, 108
- Turner, D. G. 2009, *American Institute of Physics Conference Series*, 1170, 59
- Turner, D. G. 2010, *Ap&SS*, 326, 219
- Turner, D. G. et al. 2010, *submitted*.
- Udalski A. et al., 1999, *Acta Astr.*, 49, 223
- Udalski, A., Wyrzykowski, L., Pietrzynski, G., Szewczyk, O., Szymanski, M., Kubiak, M., Soszyński, I., & Zebrun, K. 2001, *Acta Astronomica*, 51, 221
- Udalski, A. 2003, *ApJ*, 590, 284
- Udalski, A. 2009, *Astronomical Society of the Pacific Conference Series*, 403, 110
- van de Ven, G., van den Bosch, R. C. E., Verolme, E. K., & de Zeeuw, P. T. 2006, *A&A*, 445, 513
- van Leeuwen, F., Feast, M. W., Whitelock, P. A., & Laney, C. D. 2007, *MNRAS*, 379, 723
- van Leeuwen, F. 2007, *A&A*, 474, 653
- van Leeuwen, F. 2009 (a), *A&A*, 497, 209
- van Leeuwen, F. 2009 (b), *A&A*, 500, 505
- Vilardell, F., Jordi, C., & Ribas, I. 2007, *A&A*, 473, 847
- Walker, A. R., & Nemec, J. M. 1996, *AJ*, 112, 2026
- Watson, C., Henden, A. A., & Price, A. 2010, *VizieR Online Data Catalog*, 1, 2027
- Welch, D. L., et al. 1995, *IAU Colloq. 155: Astrophysical Applications of Stellar Pulsation*, 83, 232
- Weldrake, D. T. F., Sackett, P. D., & Bridges, T. J. 2007, *AJ*, 133, 1447

CHAPTER 3

BENCHMARK OPEN CLUSTERS

Deep Infrared ZAMS Fits to Benchmark Open Clusters Hosting δ Scuti Stars

Abstract: This research aims to secure precise distances for cluster δ Scuti variables in order to investigate their properties via a *VI* Wesenheit framework. Deep JHK_s colour-colour and ZAMS relations derived from ~ 700 unreddened stars having 2MASS photometry and precise Hipparcos parallaxes ($d \leq 25$ pc) are applied to establish distances to several benchmark open clusters that host δ Scuti variables: Hyades, Pleiades, Praesepe, α Persei, and M67 ($d = 47 \pm 2, 138 \pm 6, 183 \pm 8, 171 \pm 8, 815 \pm 40$ pc, respectively). The analysis provided constraints on the δ Sct sample's absolute Wesenheit magnitudes ($W_{VI,0}$), evolutionary status, and pulsation modes (order, n). The reliability of JHK_s -established cluster parameters is demonstrated via a comparison with van Leeuwen (2009) revised Hipparcos results. Distances to 7 of 9 nearby ($d \leq 250$ pc) clusters agree, and the discrepant cases (Pleiades and Blanco 1) are unrelated to variations in cluster age or iron abundance. JHK_s photometry is tabulated for $\sim 3 \times 10^3$ probable cluster members on the basis of proper motions (NOMAD). The deep JHK_s photometry extends into the low mass regime ($\sim 0.4M_\odot$) and ensures precise ($\leq 5\%$) ZAMS fits. Pulsation modes inferred for cluster δ Scuti variables from *VI* Wesenheit and independent analyses are comparable, and the methods are consistent in identifying higher order pulsators. Most small-amplitude cluster δ Scutis lie on

VI Wesenheit loci characterizing $n \geq 1$ pulsators. A distance ($d \simeq 1.7$ kpc) established to NGC 1817 from δ Scutis via a universal *VI* Wesenheit template agrees with estimates in the literature, provided the variables delineate the $n \geq 1$ boundary. Small statistics in conjunction with other factors presently encumber the use of mmag δ Scuti variables as solid distance indicators for intermediate-age open clusters, yet a *VI* Wesenheit approach is a pertinent means for studying δ Scutis in conjunction with other methods.

3.1 INTRODUCTION

δ Sct variables are unique among standard candles of the classical instability strip in permitting the determination of distances to Population I and II groups from a single *VI* Wesenheit calibration. SX Phe variables and other metal-poor Population II δ Scutis lie toward the short-period extension of the Wesenheit ridge characterizing Population I δ Scutis (Fig. 3 in Majaess et al., 2011a, see also Petersen & Høg 1998). That presents an opportunity to bridge and strengthen distance scales tied to globular clusters, open clusters, nearby galaxies, and the Galactic centre, where such variables are observed (McNamara et al., 2000, 2007; Poleski et al., 2010; Majaess et al., 2011a). To that end the present research examines via a *VI* Wesenheit framework δ Sct calibrators associated with benchmark open clusters, an analysis that relies on the establishment of precise cluster distances and multiband photometry (*VIJHK_s*).

In this study, infrared colour-colour and ZAMS relations are constructed from unreddened stars in close proximity to the Sun with precise Hipparcos parallaxes (§3.2). The relations are subsequently employed to establish parameters for five benchmark open clus-

ters that host δ Scuti variables, namely the Hyades, Pleiades, Praesepe, α Persei, and M67 (§3.2). Cluster membership provides constraints on absolute Wesenheit magnitudes ($W_{VI,0}$), evolutionary status, and pulsation modes (order, n) for the δ Scutis (§3.3). An independent determination of the cluster parameters is pursued because the objects form the foundation of the open cluster scale and yet their distances are uncertain. Most notably the Hipparcos distance to stars in the Pleiades is $d = 120.2 \pm 1.9$ pc (van Leeuwen, 2009), whereas HST observations imply $d = 134.6 \pm 3.1$ pc (Soderblom et al., 2005). Likewise, four Hipparcos-based distances cited in the literature for α Persei disagree (Table 3.1). In §3.3, a Wesenheit analysis (VI) is shown to be a useful means for investigating δ Scutis. Lastly, the distance to NGC 1817 is evaluated via a universal Wesenheit template using new VI photometry acquired from the Abbey Ridge Observatory (ARO, Lane, 2007; Turner et al., 2009a) for the cluster's numerous δ Scutis (§3.3.4).

3.2 JHK_s INTRINSIC RELATIONS

Intrinsic colour-colour and ZAMS relations are derived from JHK_s photometry for A, F, G, K, and M-type stars that have precise parallaxes ($d \leq 25$ pc). The infrared photometry and parallaxes are provided via the 2MASS and Hipparcos surveys (Perryman & ESA, 1997; Cutri et al., 2003; Skrutskie et al., 2006). 2MASS photometry may be saturated for nearby stars, yet reliable data are available for fainter stars of late spectral types. The photometric uncertainties thus increase for bright early-type stars (Fig. 3.1), which are already undersampled because of the nature of the initial mass function. Spurious data deviating from the evident intrinsic functions were excluded.

M_J vs. $(J - H)_0$ and M_J vs. $(J - K_s)_0$ colour-magnitude diagrams for the calibration are presented in Fig. 3.1 (red dots). The latter passband combination exhibits less scatter (compare the top panels in Fig. 3.1). $(J - H)_0$ vs. $(H - K_s)_0$ and $(J - K_s)_0$ vs. $(H - K_s)_0$ colour-colour diagrams are likewise shown in Fig. 3.1 (red dots). Infrared relations offer advantages over those tied to *UBV* photometry because they are less affected by chemical composition (§3.2.1, Fig. 3.3), differential reddening, and total extinction.

Colour-magnitude and colour-colour diagrams were assembled for the target clusters (Figs. 3.1, 3.2) by obtaining 2MASS photometry for members on the basis of proper motions. The Naval Observatory Merged Astrometric Dataset (NOMAD, Zacharias et al., 2004) contains proper motion data for the fields inspected. JHK_s photometry for $\sim 3 \times 10^3$ probable clusters members were tabulated, and the list includes several previously unidentified members. That sample will be made available online via the *Centre de Données astronomiques de Strasbourg*. Photometry for the brighter stars may be saturated, as noted earlier, while lower mass members are catalogued despite being near the faint-limit of the 2MASS survey. High-precision multi-epoch JHK_s data for M67 are available from Nikolaev et al. (2000, see also Sarajedini et al. 2009).

Reddenings for the target clusters were secured by shifting the intrinsic colour-colour relations to the observed data. JHK_s extinction laws were adopted from Bonatto et al. (2008) and references therein. The distance to a cluster follows by matching the ZAMS to the observed data for the reddening established by the intrinsic colour-colour relation. Precise results were obtained because the trends for late-type stars in JHK_s colour-magnitude and colour-colour diagrams provide excellent anchor points for fitting ZAMS and intrinsic

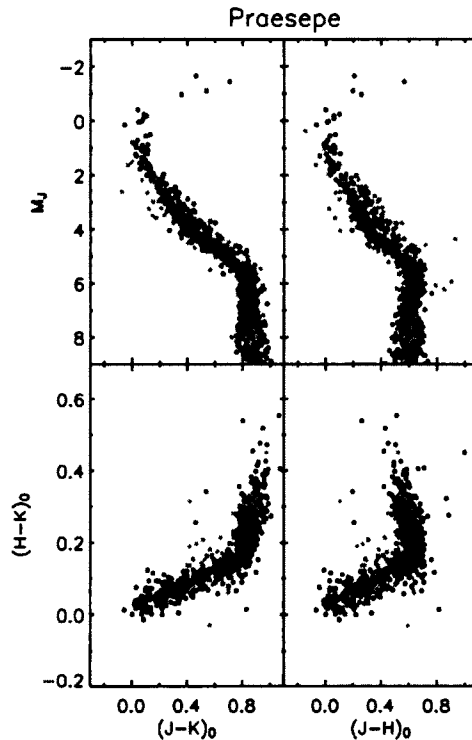


Figure 3.1 Deep 2MASS JHK_s colour-magnitude and colour-colour diagrams for the calibration (red dots) and Praesepe star cluster (black dots). Likely members of Praesepe were selected on the basis of proper motions (NOMAD). The resulting parameters are $E(J - K_s) = 0.025 \pm 0.015$ and $d = 183 \pm 8$ pc.

relations (Figs. 3.1, 3.2). The $J - K_s$ and $J - H$ colours were found to remain nearly constant and become bluer with increasing magnitude ($M_J \geq 6$) for low mass main-sequence stars beginning near spectral type M (Figs. 3.1, 3.2, see also Samus et al. 2009a and references therein). A sizable separation exists between main-sequence and evolved M-type stars in the JHK_s colour-colour diagram (see also Straižys & Lazauskaitė, 2009). Turner (2011) developed intrinsic JHK_s functions to describe early-type stars ($\leq K0$) via an alternate approach.

Distances obtained for the benchmark clusters examined are summarized in Table 3.1.

Table 3.1. Distances to Benchmark Open Clusters

Cluster	HIP (M97)	HIP (R99)	HIP (V99)	HIP (V09)	JHK_s	HST
M67	815 ± 40 pc	...
Hyades	46.45 ± 0.50 pc	47 ± 2 pc	48.3 ± 2.0 pc
Praesepe	177.0 ± 10.3 pc	180.5 ± 10.7 pc	180 pc	181.6 ± 6.0 pc	183 ± 8 pc	...
Pleiades	116.3 ± 3.3 pc	118.2 ± 3.2 pc	125 pc	120.2 ± 1.9 pc	138 ± 6 pc	134.6 ± 3.1 pc
α Persei	184.2 ± 7.8 pc	190.5 ± 7.2 pc	170 pc	172.4 ± 2.7 pc	171 ± 8 pc	...
Coma Ber*	88.2 ± 1.7 pc	87.0 ± 1.6 pc	86 pc	86.7 ± 0.9 pc	85 ± 6 pc	...
Blanco 1	252.5 ± 31.1 pc	263 ± 31 pc	190 pc	207 ± 12 pc	240 ± 10 pc	...
IC 2391*	147.5 ± 5.4 pc	146.0 ± 4.7 pc	140 pc	144.9 ± 2.5 pc	134 ± 13 pc	...
IC 2602*	146.8 ± 4.7 pc	152 ± 3.7 pc	155 pc	148.6 ± 2.0 pc	147 ± 14 pc	...
NGC 2451*	...	188.7 ± 6.8 pc	220 pc	183.5 ± 3.7 pc	189 ± 15 pc	...

Note. Hipparcos (HIP) distances are from Mermilliod et al. (1997, M97), Robichon et al. (1999a, R99), van Leeuwen (1999, V99), and van Leeuwen (2009, V09). HST distances to the Hyades and Pleiades are from van Altena et al. (1997) and Soderblom et al. (2005). JHK_s results are from this study. Clusters with an asterisk were more difficult to assess (JHK_s). Iron abundances and age estimates for the clusters are tabulated in Mermilliod et al. (1997) and van Leeuwen (1999). The clusters are comparatively unreddened.

3.2.1 AGE AND METALLICITY DEPENDENCIES

The JHK_s distances agree with the van Leeuwen (2009) Hipparcos results for 7 of 9 star clusters lying within 250 pc (Table 3.1). The distance to the Pleiades determined here agrees with the HST estimate rather than that established by Hipparcos (Table 3.1).¹ Soderblom et al. (2005) (and others) argue that the Hipparcos distance to the Pleiades is erroneous. Conversely, the reliability of the ZAMS distance to the Pleiades has been questioned because of the possible neglect of colour- T_e variations with stellar age and chemical composition. The matter is now investigated.

An age-luminosity effect has been proposed as a possible source of the disagreement between the ZAMS and Hipparcos distance estimates for the Pleiades. That hypothesis is not supported by the infrared distances established here. The Hyades, Praesepe, and α Persei clusters bracket the discrepant cases of the Pleiades and Blanco 1 in age (Table 3.1).

¹The HST and Hipparcos Pleiades surveys lack overlap, and the former surveyed fewer stars.

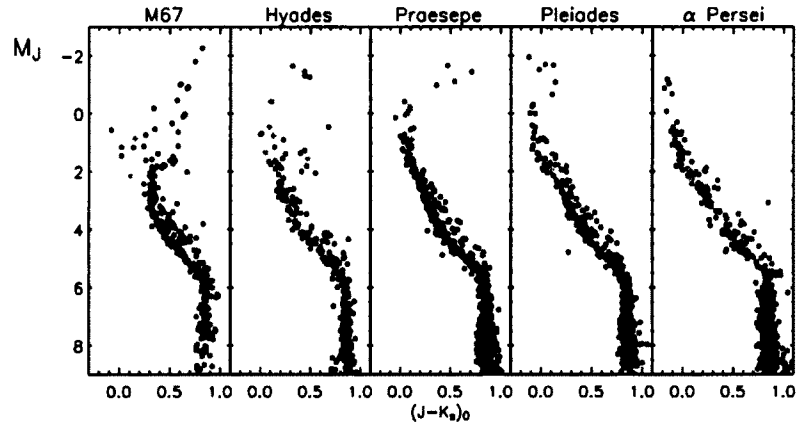


Figure 3.2 Deep 2MASS JHK_s colour-magnitude diagrams for M67, Hyades, Praesepe, Pleiades, and α Persei star clusters. The clusters have a common ZAMS morphology in the infrared. The δ Scutis examined in §3.3 (red dots) may be evolved (Hyades/Praesepe), blue stragglers (M67), or occupy the binary/rapid rotator sequence (Pleiades).

JHK_s and van Leeuwen (2009) Hipparcos distances to the former clusters are in broad agreement (Table 3.1). The comparatively nearby ($d \leq 250$ pc) open clusters IC 2602, NGC 2451, IC 2391, and Coma Ber were investigated to bolster the case, but proved more difficult to assess. The Hipparcos distance to the Pleiades implies that the cluster's ZAMS is a sizable ($\sim 0^m.4$) amount below the faintest calibration stars (Fig. 3.1, where the photometric uncertainties are minimized). The Hipparcos zero-point for the Pleiades is inconsistent with a M_J vs. $(J - K_s)_0$ ZAMS calibration (Fig. 3.1) containing stars of differing age, chemical composition, and peculiarities.

Clusters in Table 3.1 exhibiting discrepant distances are not correlated with iron abundance. That supports conclusions by Alonso et al. (1996) and Percival et al. (2005) that $J - K_s$ colours are relatively insensitive to metallicity over the baseline examined. Percival et al. (2005) suggested that $J - K_s$ colour may exhibit a marginal dependence on metallicity, but cautioned that the errors are sizable and the correlation coefficient is consistent with

zero. The impact of a marginal $T_e - [\text{Fe}/\text{H}] - (J - K_s)$ dependence appears insignificant because stars belonging to the clusters examined display near solar iron abundances (Mermilliod et al., 1997; van Leeuwen, 1999, their Table 1). A collection of 270 calibration stars (Fig. 3.1) in the Soubiran et al. (2010) PASTEL catalogue of stellar atmospheric parameters exhibit a peak distribution near $[\text{Fe}/\text{H}] \simeq -0.05$, which is similar to or inappreciably less than found for members of the Pleiades ($[\text{Fe}/\text{H}] = -0.039 \pm 0.014, +0.03 \pm 0.05, +0.06 \pm 0.01$, Taylor 2008; Soderblom et al. 2009; Paunzen et al. 2010). Colours for calibrating stars (Fig. 3.1) in PASTEL were plotted as a function of effective temperature and metallicity (Fig. 3.3, optical photometry from Mermilliod 1991). $B - V$ and $U - B$ colour indices appear sensitive to iron abundance, where metal-rich stars are hotter at a given colour (Fig. 3.3), as noted previously (Turner, 1979, and references therein). Conversely, $J - K_s$ colour appears comparatively insensitive to iron abundance over the restricted baseline examined (Fig. 3.3).

The clusters exhibit a similar ZAMS morphology in the infrared (M_J vs. $(J - K_s)_0$, Figs. 3.1, 3.2). The Hyades, Praesepe, Pleiades, and M67 zero-age main sequences (un-evolved members) are nearly indistinguishable (Fig. 3.2). Stauffer et al. (2003) likewise noted that the Praesepe and Pleiades clusters share a ZAMS (M_V vs. $(V - I)_0$) that is essentially coincident with colour. By contrast, the apparent sensitivity of optical photometry to metallicity may explain (in part) certain anomalies that distinguish individual clusters in optical colour-magnitude and colour-colour diagrams (Fig. 3.3, see also Turner, 1979; Mermilliod et al., 1997; Stauffer et al., 2003; van Leeuwen, 2009). Compounded uncertainties prevent a direct assessment of the infrared colour-colour function's universality ($(J - K_s)_0$ vs. $(H - K_s)_0$). Minimizing uncertainties associated with the JHK_s photometry and ex-

tending the restricted temperature baseline are desirable. Fainter JHK_s observations could be acquired from Observatoire du Mont-Mégantic or the forthcoming VVV survey (Artigau et al., 2009, 2010; Minniti et al., 2010), whereas brighter stars could be observed as part of the AAVSO's IR photoelectric photometry program (Henden, 2002; Templeton, 2009).

In summary, neither variations in iron abundance nor stellar age readily explain the discrepancies between the JHK_s ZAMS, and Hipparcos distances (Table 3.1). It is emphasized that the problematic cases (the Pleiades and Blanco 1) constitute a minority (Table 3.1). Note that the four published Hipparcos distances for Blanco 1 exhibit a 20% spread (Table 3.1, see also α Persei).

3.3 CLUSTER δ SCUTIS

3.3.1 VI PHOTOMETRY

The cluster δ Scuti variables examined are summarized in Table 3.4, along with references to their VI photometry. Certain sources have I -band photometry not standardized to the Cousins system (e.g., Mendoza, 1967). Additional observations for the δ Scutis were obtained via the AAVSO's Bright Star Monitor (BSM)² and the U. S. Naval Observatory's Flagstaff Station (NOFS) (Table 3.2). The BSM has an SBIG ST8XME CCD detector (fov: $127' \times 84'$) mounted upon a 6-cm wide-field telescope located at the Astrokolkhoz telescope facility near Cloudcroft, New Mexico. The AAVSO observations are tied to Landolt (1983, 1992) photometric standards according to precepts outlined by Henden & Kaitchuck (1990) (see also Henden & Munari, 2008).

²<http://www.aavso.org/aavsonet>

VI photometry is used because LMC and Galactic δ Scutis follow *VI* Wesenheit relations that vary as a function of the pulsation order n (Fig. 3.4, Poleski et al., 2010; Majaess et al., 2011a), thereby enabling constraints on that parameter for target δ Scutis at common or known distances (see §3.3.3). Furthermore, the author has advocated that RR Lyrae variables and Cepheids — that partly form the basis for the calibration used in §3.3.2 — obey *VI* Wesenheit and period-colour relations that are comparatively insensitive to metallicity (Udalski et al., 2001; Majaess, 2010c). For example, Majaess (2010c) confirmed that the slope of the *VI* Wesenheit function for Milky Way classical Cepheids (Benedict et al., 2007; Turner, 2010) characterizes classical Cepheids in the LMC, NGC 6822, SMC, and IC 1613 (see Fig. 2 in Majaess, 2010c). Classical Cepheids in those galaxies possess precise ground-based photometry, span a sizable abundance baseline, and adhere to a common *VI* Wesenheit slope to within the uncertainties ($\alpha = -3.34 \pm 0.08(2\sigma)$, $\Delta[\text{Fe}/\text{H}] \simeq 1$). More importantly, Majaess (2010c) noted that a negligible distance offset exists between OGLE classical Cepheids and RR Lyrae variables in the LMC, SMC, and IC 1613, as established via a *VI* Wesenheit function, thereby precluding a dependence on metallicity. Admittedly, the impact of a reputed metallicity effect is actively debated in the literature (Smith, 2004; Romaniello et al., 2008; Catelan, 2009, and references therein). By contrast, there appears to be a consensus that relations that rely on *BV* photometry are sensitive to variations in chemical abundance, and a significant break in the period-magnitude relation is apparent (Majaess et al. 2008, 2009c and references therein).

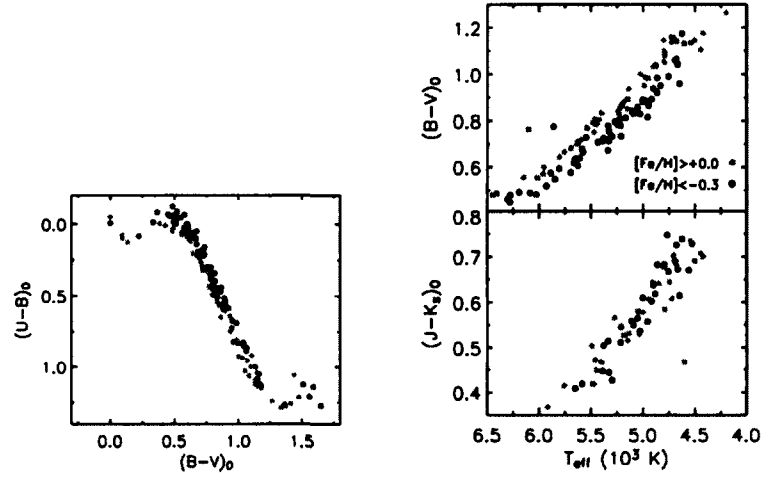


Figure 3.3 Semi-empirical colour- T_e - $[\text{Fe}/\text{H}]$ correlation for calibration stars (Fig. 3.1) in PASTEL. Red and black dots indicate metal-rich and metal-poor stars accordingly. $B - V$ and $U - B$ colour indices appear sensitive to metallicity, whereas $J - K_s$ is comparatively unaffected by changes in iron abundance (see text).

Table 3.2 New Photometry for Cluster δ Scuti Variables

Star	Cluster	CMD position (Fig. 3.2)	V	$V - I_c$
EX Cnc	M67	BS	10.90	0.30
EW Cnc	M67	BS	12.24	0.30
HD 23156	Pleiades	MS	8.23	0.28
HD 23194	Pleiades	MS	8.08	0.20
HD 23567	Pleiades	MS	8.29	0.41
HD 23607	Pleiades	MS	8.25	0.27
HD 23628	Pleiades	MS, BR	7.69	0.24
HD 23643	Pleiades	MS, BR	7.79	0.16

Notes: magnitudes are means of observations acquired from the AAVSO's BSM, NOFS, and TASS (Droege et al., 2006), and Mendoza (1967). The identifiers are: stars occupying the blue straggler region (BS), binary/rapid rotator sequence (BR), and main-sequence (MS) of the colour-magnitude diagram (Fig. 3.2).

3.3.2 WESENHEIT MAGNITUDES

A Wesenheit diagram segregates variables into distinct classes (Fig. 3.4). Wesenheit magnitudes for cluster δ Scutis were computed as follows:

$$W_{VI,0} = \langle V \rangle - R_{VI}(\langle V \rangle - \langle I \rangle) - \mu_0 \quad (3.1)$$

where μ_0 is the distance modulus from Table 3.1, $\langle V \rangle$ and $\langle I \rangle$ are mean Johnson-Cousins visual and infrared magnitudes, respectively, from the light curves, and the value for the ratio of total to selective extinction is $R_{VI} = 2.55$, although there are concerns about adopting a colour-independent extinction law. *VI* Wesenheit magnitudes are reddening-free and comparatively insensitive to chemical composition variations and the width of the instability strip. The Wesenheit function is defined and discussed by Madore (1982), Opoliski (1983, 1988), Madore & Freedman (1991, 2009), Kovács & Jurcsik (1997), Kovács & Walker (2001), Di Criscienzo et al. (2004, 2007), and Turner (2010). The Wesenheit function can be derived as follows:

$$\begin{aligned} V - R_{VI}E(V - I) &= V_0 \\ V - R_{VI}((V - I) - (V - I)_0) &= V_0 \\ V - R_{VI}(V - I) &= V_0 - R_{VI}(V - I)_0 \end{aligned} \quad (3.2)$$

Cluster δ Scuti variables in Tables 3.3 and 3.4 are plotted on a universal *VI* Wesenheit template (Fig. 3.4, see also Majaess et al., 2011a). Some 30 variables with distances measured by geometric means formed the calibration (Majaess et al., 2011a, their Table 1). The sample consists of 8 SX Phe and δ Sct variables (HIP, van Leeuwen, 2007), 4 RR Lyrae variables (HIP and HST, Benedict et al., 2002b; van Leeuwen, 2007), 2 Type II Cepheids (HIP, van Leeuwen, 2007), and 10 classical Cepheids (HST, Benedict et al., 2002a, 2007).

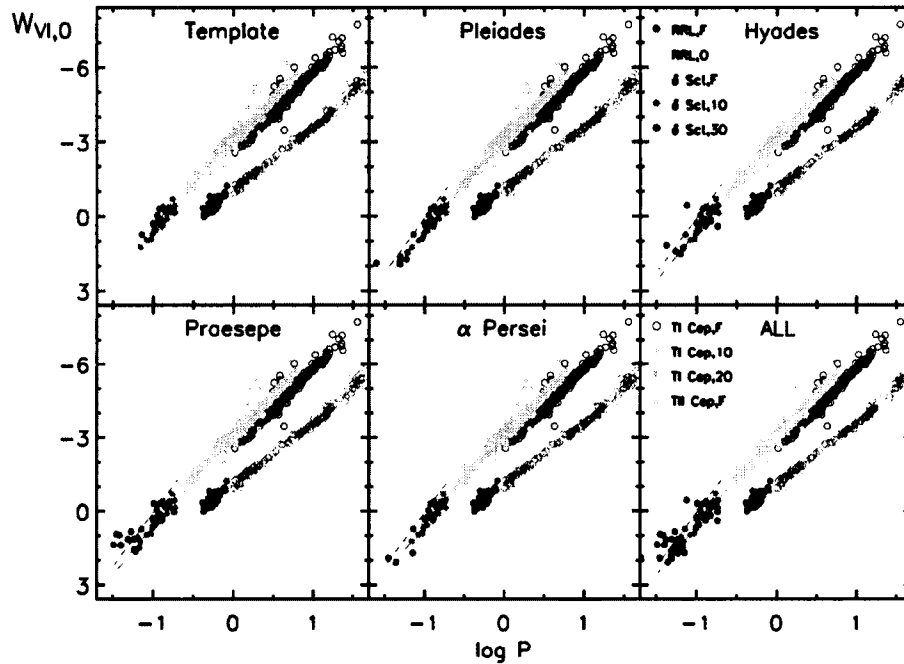


Figure 3.4 A calibrated universal VI Wesenheit template constructed from data found in Majaess et al. (2011a) and the latest *OGLEIII* observations (e.g., Poleski et al., 2010). The cluster δ Scutis are displayed as black dots. Wesenheit magnitudes were computed via Eqn. 3.1 using the JHK_s established cluster distances and VI photometry presented in Tables 3.1 & 3.4 accordingly. First-order constraints on the inferred pulsation modes (n) are listed in Tables 3.3 & 3.4.

The sample was supplemented by 6 Type II Cepheids detected by Macri et al. (2006) in their comprehensive survey of the galaxy M106 (Majaess et al., 2009c), which has a precise geometric-based distance estimate (VLBA, Herrnstein et al., 1999). Type II Cepheids within the inner region of M106 were not incorporated into the calibration because of the likelihood of photometric contamination from crowding and blending (Mochejska et al., 2001; Majaess, 2010c). The stars employed were observed in the outer regions of M106, where the stellar density and surface brightness are diminished by comparison. It is perhaps ironic that stars 7.2 Mpc distant may be enlisted as calibrators because of an absence of precise parallaxes for nearby objects. Additional observations of new variables in M106

are forthcoming (Macri & Riess, 2009).

LMC variables catalogued by OGLE, including the latest sample of δ Scutis (Poleski et al., 2010), were added to the Wesenheit template (Udalski et al., 1999, Fig. 3.4, OGLE data: e.g.,). The LMC data were calibrated with a distance established via the geometric-anchored universal Wesenheit template ($\mu_0 = 18.43 \pm 0.03(\sigma_{\bar{x}})$, Majaess et al., 2011a). That distance agrees with a mean derived from 300+ results tabulated for the LMC in the NASA/IPAC Extragalactic Database (NED) (Madore & Steer, 2007; Steer & Madore, 2010). Adding the Turner (2010) list of classical Cepheids in Galactic clusters to the universal VI Wesenheit calibration yields the same LMC distance with reduced uncertainties.

The universal Wesenheit template (Fig. 3.4) unifies variables of the instability strip to mitigate uncertainties tied to establishing a distance scale based on Cepheids, RR Lyrae, or δ Sct variables individually. Anchoring the distance scale via the universal Wesenheit template (Fig. 3.4) mobilizes the statistical weight of the entire variable star demographic to ensure a precise distance determination. Moreover, the universal Wesenheit template may be calibrated directly via parallaxes and apparent magnitudes, mitigating the propagation of uncertainties tied to extinction corrections. Further calibration could likewise ensue via variables in clusters with distances secured by dynamical means or from eclipsing binaries (Cluster AgeS Experiment, Pietrukowicz & Kaluzny, 2004; Guinan & Engle, 2006; Kaluzny et al., 2007), and variables in the Galactic bulge that are tied to a precise geometric-based distance (Kubiak & Udalski, 2003; Eisenhauer et al., 2005; Reid et al., 2009, supported by observations from the upcoming *VVV* survey; Minniti et al. 2010).

Lastly, Majaess et al. (2011a) plotted the universal Wesenheit template (Fig. 3.4) as a

Table 3.3 A Comparison of δ Sct Pulsation Modes

Star	Cluster	$n(W_{VI})$	n	Source
EX Cnc	M67	>3	3	Z05
EW Cnc	M67	1 or 0	0	Z05
HD 23156	Pleiades	1	0	F06
HD 23194	Pleiades	>3	4	F06
HD 23567	Pleiades	1 or 2	0	F06
HD 23607	Pleiades	1	0	F06
HD 23628	Pleiades	1	0	F06
HD 23643	Pleiades	1 or 0	0	F06
HD 73175	Praesepe	>3	3	P98
HD 73450	Praesepe	1	1	P98
HD 73575	Praesepe	≥ 3	3/?	P98
HD 73576	Praesepe	≥ 3	3	P98
HD 73763	Praesepe	>3	3/?	P98
HD 74028	Praesepe	≥ 3	3	P98

Notes: pulsation modes (primary signal, order n) inferred for M67, Pleiades, and Praesepe δ Scutis from the Wesenheit template (Fig. 3.4, $n(W_{VI})$) and sources in the literature (n). Sources are Zhang et al. (2005, Z05), Fox Machado et al. (2006, F06), and Pena et al. (1998, P98).

function of the inferred fundamental mode period to highlight the first-order VI period-magnitude continuity between RR Lyrae and Type II Cepheid variables (Matsunaga et al., 2006; Majaess, 2010a, see also Marconi & Di Criscienzo 2007 and references therein). The Wesenheit template presented here as Fig. 3.4 is plotted as a function of the dominant period, so pulsation modes may be inferred directly from the diagram.

3.3.3 PULSATION MODE

Wesenheit ridges in Fig. 3.4 that define δ Scutis pulsating in the fundamental, first, second, and third overtone modes were constructed from data presented in Poleski et al. (2010, LMC) and Majaess et al. (2011a, Galactic). LMC and Galactic δ Scutis pulsating in overtone

Table 3.4 δ Scuti Variables in Benchmark Open Clusters

Star	Cluster	CMD position (Fig. 3.2)	$n(W_{VI})$	VI Photometry
SAO 38754	α Persei	MS	1	TASS, S85
HD 20919	α Persei	MS,BR:	2 or 3	TASS
HD 21553	α Persei	MS	0	TASS
HD 23156	Pleiades	MS	1	Table 3.2
HD 23194	Pleiades	MS	>3	Table 3.2
HD 23567	Pleiades	MS	1 or 2	Table 3.2
HD 23607	Pleiades	MS	1	Table 3.2
HD 23628	Pleiades	MS,BR	1	Table 3.2
HD 23643	Pleiades	MS,BR	1 or 0	Table 3.2
HD 27397	Hyades	EV	1 or 2	T85
HD 27459	Hyades	EV	1	J06
HD 27628	Hyades	sat./EV:	1	J06
HD 28024	Hyades	sat./EV:	1 or 0	J06
HD 28052	Hyades	sat./EV:	0	J06
HD 28319	Hyades	sat./EV:	>3	J06
HD 30780	Hyades	sat.	>3	J06
HD 73175	Praesepe	MS/EV	>3	TASS, ME67
HD 73345	Praesepe	MS/EV	>3	TASS, ME67
HD 73450	Praesepe	MS	1	TASS, ME67
HD 73575	Praesepe	EV	≥ 3	TASS, ME67
HD 73576	Praesepe	MS/EV,BR	≥ 3	TASS, ME67
HD 73712	Praesepe	EV	1 or 2	TASS, ME67
HD 73729	Praesepe	MS/EV,BR	2 or 3	TASS, ME67
HD 73746	Praesepe	MS	1	TASS, ME67
HD 73763	Praesepe	MS/EV	>3	TASS, ME67
HD 73798	Praesepe	MS/EV	1	TASS, ME67
HD 73819	Praesepe	EV	0	TASS, ME67
HD 73890	Praesepe	MS/EV,BR	>3	TASS, ME67
HD 74028	Praesepe	MS/EV	≥ 3	TASS, ME67
HD 74050	Praesepe	MS/EV	3	TASS, ME67
EX Cnc	M67	BS	>3	Table 3.2
EW Cnc	M67	BS	1 or 0	Table 3.2

Notes: δ Sct cluster list compiled primarily from Li & Michel (1999) and references therein. The identifiers are as follows: stars occupying the blue straggler region (BS), binary/rapid rotator sequence (BR), evolved region (EV), and main-sequence (MS) of the colour-magnitude diagram (Fig. 3.2); Pulsation modes (primary signal, order n) inferred for the δ Scutis from the VI Wesenheit template (Fig. 3.4). Hyades members may have saturated (sat.) 2MASS photometry because of their proximity (Table 3.1). There are concerns regarding the photometric zero-point for bright δ Scutis sampled in all-sky surveys (Henden & Sallman, 2007). References for the photometry are Mendoza (1967, ME67), Taylor & Joner (1985, T85), Stauffer et al. (1985, S85), and Joner et al. (2006, J06).

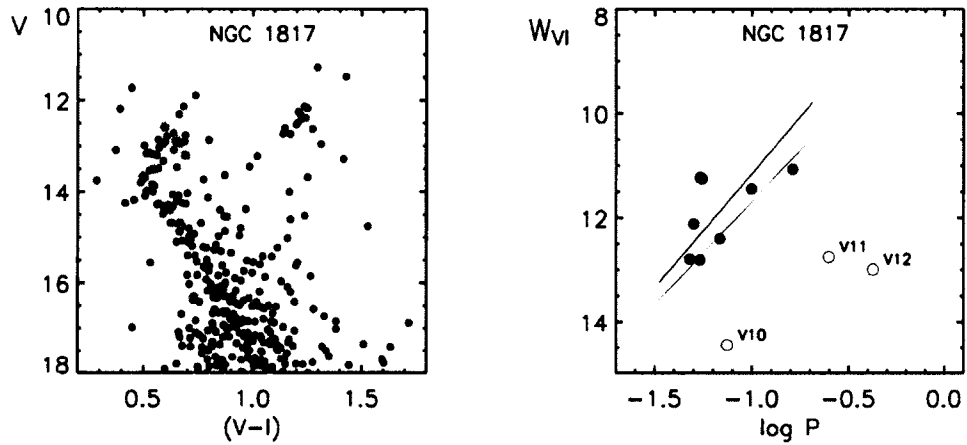


Figure 3.5 Left, a *preliminary VI* colour-magnitude diagram for the open cluster NGC 1817 compiled from ARO observations. A subsample of the list of δ Scuti candidates from Arentoft et al. 2005 are characterized by red dots. Right, the stars are displayed in a Wesenheit diagram where green, red, and blue ridges correspond to $n = 0, 1, 3$ pulsators accordingly (right to left). The offset from the absolute Wesenheit magnitudes (Fig. 3.4) yields $d \simeq 1.7$ kpc, provided the variables define the $n \geq 1$ boundary (see §3.3.3). The uncertainties are typically smaller than the symbol size.

modes exhibit brighter *VI* Wesenheit magnitudes (W_{VI}) than their fundamental mode counterparts at a given period (Fig. 3.4, or bottom panel of Fig. 4 in Poleski et al. 2010). However, a clear separation was less evident in the Garg et al. (2010) shorter-wavelength (*VR*) observations of LMC δ Scutis (their Fig. 3), thereby motivating those authors to adopt an alternate conclusion. The present research relies on *VI* observations of δ Scutis.

Estimates of the pulsation modes (order, n) for cluster δ Scutis were inferred from the Wesenheit template (Fig. 3.4) and are summarized in Table 3.4. Pulsation modes established from Wesenheit and seismological analyses for δ Scutis in the Pleiades, Praesepe, and M67 are consistent within the mutually expected (albeit large) uncertainties ($\pm n$) (Table 3.3). The methods identify high and low order pulsators in consistent fashion (e.g., HD 23194 and HD 73450, Table 3.3). Most small-amplitude cluster δ Scutis lie on Wesenheit loci

characterizing $n \geq 1$ pulsators (non-fundamental mode, Fig. 3.4 and Table 3.4), and a sizable fraction are associated with $n = 1$ (Table 3.4). The results are consistent with the findings of Poleski et al. (2010) and past predictions (Breger, 2000; McNamara et al., 2007, and references therein).

A primary source of uncertainty associated with the analysis rests with the pulsation periods adopted. Periods for the cluster δ Scutis were taken from Rodríguez et al. (2000), the GCVS (Samus et al., 2009a), and the AAVSO's VSX archive³ (Watson, Henden & Price, 2010). In several instances discrepant periods are cited and newer estimates were favoured (SAO 38754, Li, 2005). Efforts to extract the primary pulsation period (high SNR) for mmag δ Scutis in α Persei from ARO observations were unsuccessful, likely because of increased humidity tied to summertime observations in Nova Scotia. That underscores the challenge such mmag pulsators present to low altitude observatories near sea-level. An additional source of uncertainty arises from a companion's influence on the observed Wesenheit magnitudes. The pulsation mode assigned to HD 28052, which is a spectroscopic binary and bright X-ray source, should therefore be interpreted cautiously (Table 3.4). A star's non-radial and multi-mode pulsation, and rotation/inclination along the line of sight likewise complicate a determination of n solely from pulsation period and Wesenheit magnitude. Constraints established by Wesenheit analyses are admittedly limited in comparison with those inferred from uninterrupted space-based μ mag time-series photometry (MOST, COROT, Kepler), yet the Wesenheit approach is a useful first-order tool that can be applied to δ Scutis in any field and concurrently with other methods.

³<http://www.aavso.org/vsx/>

3.3.4 δ Sct DISTANCE TO NGC 1817

A potential role for mmag δ Scutis as distance indicators for intermediate-age open clusters is now explored using the aforementioned framework.

The observations of Arentoft et al. (2005) for NGC 1817 indicate that the open cluster hosts a statistically meaningful sample of 11 δ Scutis. The proper motions of Balaguer-Núñez et al. (2004) imply that five of those stars are not cluster members (V1, V6, V8, V10, V12, see Arentoft et al., 2005). Yet Arentoft et al. (2005) concluded that 11 variables (V1→V12, excluding V10) exhibit positions in V vs. $B-V$ and V vs. $b-y$ colour-magnitude diagrams consistent with δ Sct pulsation and cluster membership. A preliminary V vs. $V-I$ colour-magnitude diagram for NGC 1817 (Fig. 3.5) confirms that most variables display positions consistent with membership (except V10). The VI data were obtained from the ARO and processed using ARAP⁴ (Lane, 2007) and DAOPHOT⁵ (Stetson, 1987). The ARO has an SBIG ST8XME CCD detector mounted upon a 35-cm telescope located near Stillwater Lake, Nova Scotia, Canada, and is a remotely operated robotic observatory (Lane, 2007). A description of the ARO observations for NGC 7062, including an analysis using VaST (Sokolovsky & Lebedev, 2005), will be provided in a subsequent study.

The VI Wesenheit diagram compiled for the δ Scuti variables (Fig. 3.5) implies that V10, V11, and V12 either exhibit spurious data, are not *bona fide* δ Scutis, or are not cluster members. V10 is too faint, as corroborated by its position in the colour-magnitude diagram (Fig. 3.5). The variability detected in V11 is marred by a low signal to noise ratio and other complications (Arentoft et al., 2005). V12 is likewise too faint (W_{VI})

⁴<http://www.davelane.ca/aro/arap.html>

⁵IRAF contains DAOPHOT, however a standalone newer edition can be obtained from Peter.Stetson@nrc-cnrc.gc.ca

and has a period beyond that typically expected for δ Sct variables (Percy, 2007). An advantage to applying the Wesenheit technique is that high- and low-order mode pulsators may be identified. V1, V2, and V6 are likely pulsating in high orders if the stars are members (Fig. 3.5). V3, V4, V7, V8, and V9 are tightly clustered and may define the $n \geq 1$ boundary (Fig. 3.5, see §3.3.3). The resulting distance to NGC 1817 is $d \simeq 1.7$ kpc, given the aforementioned mode distribution. The δ Sct distance to NGC 1817 agrees with estimates established for the cluster by other means (Arentoft et al., 2005, see references therein). However, employing mmag δ Scutis as distance indicators for open clusters is complicated by the need for independently confirmed periods and *a priori* knowledge of the pulsation modes, or the adoption of a mode distribution ($n \geq 1$) for a sizable sample (see §3.3.3). Establishing the distance to NGC 1817 or Praesepe under the latter caveat may yield a useful result, yet the ensuing distance to the α Persei cluster would be uncertain because of small statistics. α Persei certainly has more than 3 δ Scutis, however a detection bias emerges because nearby clusters exhibit large angular diameters that exceed the field of view of most CCDs. Continued research is needed.

3.4 SUMMARY AND FUTURE RESEARCH

This research aimed to outline and evaluate a *VI* Wesenheit framework for investigating cluster δ Scuti variables, an analysis that relied on securing absolute Wesenheit magnitudes from precise open cluster distances. *JHK*, ZAMS and colour-colour relations were derived from unreddened stars near the Sun with precise Hipparcos parallaxes, and were applied to infer parameters for several benchmark star clusters that host δ Scutis (Fig. 3.1, Ta-

ble 3.1). That analysis yielded constraints on the absolute Wesenheit magnitudes ($W_{VI,0}$), evolutionary status, and pulsation modes (order, n) for the cluster δ Scutis (Figs. 3.2, 3.4, Tables 3.3, 3.4). VI photometry for the variables was tabulated to facilitate further research (Table 3.4), and include new data acquired via the AAVSO's robotic telescopes (Table 3.2).

The JHK_s -established cluster distances are bolstered by the relative insensitivity of $J - K_s$ photometry to variations in $[\text{Fe}/\text{H}]$ and age over the baseline examined (§3.2.1, Table 3.1, Fig. 3.3). The deep JHK_s photometry extends into the low mass regime ($\sim 0.4M_\odot$) and indicates that the clusters have a common ZAMS in the infrared, and that $J - K_s$ remains constant with increasing magnitude ($M_J \geq 6$) for low mass M-type dwarfs, whereas $J - H$ exhibits an inversion (§3.2.1, Figs. 3.1, 3.2). The trends ensure precise ($\leq 5\%$) JHK_s ZAMS fits by providing distinct anchor points in colour-magnitude and colour-colour diagrams (Figs. 3.1, 3.2). JHK_s distances for 7 of 9 clusters within 250 pc of the Sun agree with the van Leeuwen (2009) revised Hipparcos estimates (Table 3.1). However, the JHK_s distance to the Pleiades supports the HST estimate rather than that derived from Hipparcos data (Table 3.1). van Leeuwen (2009,b) argues in favour of the revised Hipparcos distances to open clusters, and the reader is referred to that comprehensive study. Yet the distance scale can (presently) rely on a suite of clusters that are independent of the Pleiades. Models should be calibrated and evaluated using those nearby clusters where consensus exists regarding their distances (Table 3.1).

The general agreement between the JHK_s distances derived here and the van Leeuwen (2009) Hipparcos estimates is noteworthy (Table 3.1). However, there exists a 10–20% offset in distance for the Pleiades and Blanco 1. Indeed, several clusters have distance estimates

spanning nearly a factor of two, such as NGC 2453 (Majaess et al., 2007, their Table 4), ESO 096-SC04, Collinder 419, Shorlin 1, and Berkeley 44 (Turner, 2010b,c). The universal *VI* Wesenheit template could be applied to cluster δ Scutis to isolate accurate distance solutions, provided certain criteria are satisfied (§3.3.4, e.g., large statistics). A Wesenheit analysis (*VI*) is a useful means for establishing pertinent constraints on a target population of δ Sct variables, particularly in conjunction with other methods (Figs. 3.2, 3.4, 3.5, Tables 3.3, 3.4).

REFERENCES

- Alonso, A., Arribas, S., & Martinez-Roger, C. 1996, *A&A*, 313, 873
- Arentoft, T., Bouzid, M. Y., Sterken, C., Freyhammer, L. M., & Frandsen, S. 2005, *PASP*, 117, 601
- Artigau, É., Bouchard, S., Doyon, R., & Lafrenière, D. 2009, *ApJ*, 701, 1534
- Artigau, É., Lamontagne, R., Doyon, R., & Malo, L. 2010, *Proc. SPIE*, 7737,
- Balaguer-Núñez, L., Jordi, C., Galadí-Enríquez, D., & Zhao, J. L. 2004, *A&A*, 426, 819
- Benedict G. F. et al., 2002 (a), *AJ*, 123, 473
- Benedict, G. F., et al. 2002 (b), *AJ*, 124, 1695
- Benedict G. F. et al., 2007, *AJ*, 133, 1810
- Bonatto, C., Bica, E., & Santos, J. F. C. 2008, *MNRAS*, 386, 324
- Bono, G., & Marconi, M. 1999, *New Views of the Magellanic Clouds*, 190, 527
- Bono, G. 2003, *Stellar Candles for the Extragalactic Distance Scale*, 635, 85
- Bono, G., Caputo, F., Fiorentino, G., Marconi, M., & Musella, I. 2008, *ApJ*, 684, 102
- Breger, M. 2000, *Delta Scuti and Related Stars*, 210, 3
- Catelan, M. 2009, *Ap&SS*, 320, 261
- Cutri, R. M., et al. 2003, *The IRSA 2MASS All-Sky Point Source Catalog*, NASA/IPAC Infrared Science Archive.
- Dias, W. S., Alessi, B. S., Moitinho, A., & Lépine, J. R. D. 2002, *A&A*, 389, 871
- Di Criscienzo, M., Marconi, M., & Caputo, F. 2004, *ApJ*, 612, 1092
- Di Criscienzo, M., Caputo, F., Marconi, M., & Cassisi, S. 2007, *A&A*, 471, 893
- Droege T. F., Richmond M. W., Sallman M. P., Creager R. P., 2006, *PASP*, 118, 1666
- Eisenhauer, F., et al. 2005, *ApJ*, 628, 246
- Feast, M. W. 2008, *arXiv:0806.3019*
- Fox Machado, L., Pérez Hernández, F., Suárez, J. C., Michel, E., & Lebreton, Y. 2006, *A&A*, 446, 611
- Freedman, W. L., & Madore, B. F. 2010, *arXiv:1004.1856*
- Garg, A., et al. 2010, *AJ*, 140, 328
- Guinan, E. F., & Engle, S. G. 2006, *Ap&SS*, 304, 5
- Henden, A. A., & Kaitchuck, R. H. 1990, *Richmond, Va. : Willmann-Bell*, c1990.
- Henden, A. A. 2002, *JAAVSO*, 31, 11
- Henden, A. A., & Sallman, M. P. 2007, *The Future of Photometric, Spectrophotometric and Polarimetric Standardization*, 364, 139
- Henden, A., & Munari, U. 2008, *Information Bulletin on Variable Stars*, 5822, 1
- Herrnstein, J. R., et al. 1999, *Nature*, 400, 539
- Joner, M. D., Taylor, B. J., Laney, C. D., & van Wyk, F. 2006, *AJ*, 132, 111
- Kaluzny, J., Thompson, I. B., Rucinski, S. M., Pych, W., Stachowski, G., Krzeminski, W., & Burley, G. S. 2007, *AJ*, 134, 541
- Kovács, G., & Jurcsik, J. 1997, *A&A*, 322, 218

- Kovács, G., & Walker, A. R. 2001, *A&A*, 371, 579
- Kubiak M., Udalski A., 2003, *Acta Astr.*, 53, 117
- Landolt, A. U. 1983, *AJ*, 88, 439
- Landolt, A. U. 1992, *AJ*, 104, 340
- Lane D. J., 2007, 96th Spring Meeting of the AAVSO.
- Lang, D., Hogg, D. W., Mierle, K., Blanton, M., & Roweis, S. 2010, *AJ*, 139, 1782
- Li, Z. P., & Michel, E. 1999, *A&A*, 344, L41
- Li, Z. P. 2005, *AJ*, 130, 1890
- Macri, L. M., Stanek, K. Z., Bersier, D., Greenhill, L. J., & Reid, M. J. 2006, *ApJ*, 652, 1133
- Macri, L. M., & Riess, A. G. 2009, *American Institute of Physics Conference Series*, 1170, 23
- Madore B. F., 1982, *ApJ*, 253, 575
- Madore, B. F., & Freedman, W. L. 1991, *PASP*, 103, 933
- Madore, B. F., & Steer, I. 2007, *NASA/IPAC Extragalactic Database Master List of Galaxy Distances* (<http://nedwww.ipac.caltech.edu/level5/NED1D/intro.html>)
- Madore, B. F., & Freedman, W. L. 2009, *ApJ*, 696, 1498
- Majaess, D. J., Turner, D. G., & Lane, D. J. 2007, *PASP*, 119, 1349
- Majaess D. J., Turner D. G., Lane D. J., 2008, *MNRAS*, 390, 1539
- Majaess, D. J., Turner, D. G., & Lane, D. J. 2009 (a), *MNRAS*, 398, 263
- Majaess, D., Turner, D., & Lane, D. 2009 (b), *Acta Astronomica*, 59, 403
- Majaess, D. J. 2009, *arXiv:0912.2928*
- Majaess, D. 2010 (a), *Acta Astronomica*, 60, 55
- Majaess, D. J. 2010 (b), *Acta Astronomica*, 60, 121
- Majaess, D. J., Turner, D. G., Lane, D. J., Henden, A., & Krajci, T. 2010, *arXiv:1007.2300*
- Marconi, M., & Di Criscienzo, M. 2007, *A&A*, 467, 223
- Matsunaga, N., et al. 2006, *MNRAS*, 370, 1979
- McNamara, D. H., Madsen, J. B., Barnes, J., & Ericksen, B. F. 2000, *PASP*, 112, 202
- McNamara, D. H., Clementini, G., & Marconi, M. 2007, *AJ*, 133, 2752
- Mendoza, E. E. 1967, *Boletín de los Observatorios Tonantzintla y Tacubaya*, 4, 149
- Mermilliod, J.-C. 1991, *Homogeneous Means in the UBV System*, <http://vizier.u-strasbg.fr/viz-bin/VizieR?-source=II/168>
- Mermilliod, J.-C., Turon, C., Robichon, N., Arenou, F., & Lebreton, Y. 1997, *Hipparcos - Venice '97*, 402, 643
- Mermilliod, J.-C., & Paunzen, E. 2003, *A&A*, 410, 511
- Minniti, D., et al. 2010, *New Astronomy*, 15, 433
- Mochejska, B. J., Macri, L. M., Sasselov, D. D., & Stanek, K. Z. 2001, *arXiv:astro-ph/0103440*
- Nikolaev, S., Weinberg, M. D., Skrutskie, M. F., Cutri, R. M., Wheelock, S. L., Gizis, J. E., & Howard, E. M. 2000, *AJ*, 120, 3340
- Opolski A., 1983, *IBVS*, 2425, 1
- Opolski, A. 1988, *Acta Astronomica*, 38, 375
- Percy, J. R. 2007, *Understanding variable stars* / Cambridge University Press
- Paunzen, E., & Netopil, M. 2006, *MNRAS*, 371, 1641

- Paunzen, E., Heiter, U., Netopil, M., & Soubiran, C. 2010, *A&A*, 517, A32
- Pena, J. H., et al. 1998, *A&AS*, 129, 9
- Percival, S. M., Salaris, M., & Groenewegen, M. A. T. 2005, *A&A*, 429, 887
- Perryman, M. A. C., & ESA 1997, *ESA Special Publication*, 1200
- Petersen, J. O., & Høg, E. 1998, *A&A*, 331, 989
- Pietrukowicz, P., & Kaluzny, J. 2004, *Acta Astronomica*, 54, 19
- Pietrzyński, G., Gieren, W., Udalski, A., Bresolin, F., Kudritzki, R.-P., Soszyński, I., Szymański, M., & Kubiak, M. 2004, *AJ*, 128, 2815
- Poleski, R., et al. 2010, *Acta Astronomica*, 60, 1
- Reid, M. J., Menten, K. M., Zheng, X. W., Brunthaler, A., & Xu, Y. 2009, *ApJ*, 705, 1548
- Robichon, N., Arenou, F., Mermilliod, J.-C., & Turon, C. 1999 (a), *A&A*, 345, 471
- Robichon, N., Arenou, F., Lebreton, Y., Turon, C., & Mermilliod, J. C. 1999 (b), *Harmonizing Cosmic Distance Scales in a Post-HIPPARCOS Era*, 167, 72
- Rodríguez, E., López-González, M. J., & López de Coca, P. 2000, *A&AS*, 144, 469
- Romaniello, M., et al. 2008, *A&A*, 488, 731
- Samus, N. N., Durlevich, O. V., & et al. 2009, *VizieR Online Data Catalog*, 1, 2025
- Sarajedini, A., Dotter, A., & Kirkpatrick, A. 2009, *ApJ*, 698, 1872
- Skrutskie, M. F., et al. 2006, *AJ*, 131, 1163
- Skiff, B. 2010, *Catalogue of Stellar Spectral Classifications*, <http://vizier.u-strasbg.fr/viz-bin/VizieR?-source=B/mk>
- Smith, H. A. 2004, *RR Lyrae Stars*, by Horace A. Smith, pp. 166. ISBN 0521548179. Cambridge, UK: Cambridge University Press, September 2004
- Smith, M. C., Woźniak, P., Mao, S., & Sumi, T. 2007, *MNRAS*, 380, 805
- Soderblom, D. R., Nelan, E., Benedict, G. F., McArthur, B., Ramirez, I., Spiesman, W., & Jones, B. F. 2005, *AJ*, 129, 1616
- Soderblom, D. R., Laskar, T., Valenti, J. A., Stauffer, J. R., & Rebull, L. M. 2009, *AJ*, 138, 1292
- Sokolovsky, K., & Lebedev, A. 2005, *12th Young Scientists' Conference on Astronomy and Space Physics*, 79
- Soszyński, I., et al. 2002, *Acta Astronomica*, 52, 369
- Soszyński, I., et al. 2003, *Acta Astronomica*, 53, 93
- Soszyński, I., et al. 2008, *Acta Astronomica*, 58, 293
- Soszyński, I., et al. 2008 (b), *Acta Astronomica*, 58, 163
- Soszyński, I., et al. 2009, *Acta Astronomica*, 59, 1
- Soubiran, C., Le Campion, J.-F., Cayrel de Strobel, G., & Caillo, A. 2010, *A&A*, 515, A111
- Stanek, K. Z., & Udalski, A. 1999, [arXiv:astro-ph/9909346](http://arxiv.org/abs/astro-ph/9909346)
- Stauffer, J. R., Hartmann, L. W., Burnham, J. N., & Jones, B. F. 1985, *ApJ*, 289, 247
- Stauffer, J. R., Jones, B. F., Backman, D., Hartmann, L. W., Barrado y Navascués, D., Pinsonneault, M. H., Terndrup, D. M., & Muench, A. A. 2003, *AJ*, 126, 833
- Steer, I. & Madore, B. F. 2010, *NED-D: A Master List of Redshift-Independent Extragalactic Distances* (<http://nedwww.ipac.caltech.edu/Library/Distances/>)
- Stetson, P. B. 1987, *PASP*, 99, 191
- Straižys, V., & Laugalys, V. 2009, *Baltic Astronomy*, 18, 141

-
- Taylor, B. J., & Joner, M. D. 1985, *AJ*, 90, 479
- Taylor, B. J. 2008, *AJ*, 136, 1388
- Templeton, M. R. 2009, *Astronomical Society of the Pacific Conference Series*, 412, 187
- Turner, D. G. 1979, *PASP*, 91, 642
- Turner, D. G., Majaess, D. J., Lane, D. J., Szabados, L., Kovtyukh, V. V., Usenko, I. A., & Berdnikov, L. N. 2009, *American Institute of Physics Conference Series*, 1170, 108
- Turner, D. G. 2010 (a), *Ap&SS*, 326, 219
- Turner, D. G. 2011 (b), arXiv:1102.0347
- Turner, D. G. 2010 (c), *submitted*.
- Turner, D. G. 2011, , 47, 127
- Udalski A. et al., 1999, *Acta Astr.*, 49, 223
- Udalski, A., Wyrzykowski, L., Pietrzynski, G., Szewczyk, O., Szymanski, M., Kubiak, M., Soszyński, I., & Zebrun, K. 2001, *Acta Astronomica*, 51, 221
- Udalski, A. 2009, *Astronomical Society of the Pacific Conference Series*, 403, 110
- van Altena, W. F., et al. 1997, *ApJ*, 486, L123
- van Leeuwen, F. 1999, *A&A*, 341, L71
- van Leeuwen, F. 2007, *A&A*, 474, 653
- van Leeuwen, F. 2009 (a), *A&A*, 497, 209
- van Leeuwen, F. 2009 (b), *A&A*, 500, 505
- Vilardell, F., Jordi, C., & Ribas, I. 2007, *A&A*, 473, 847
- Watson, C., Henden, A. A., & Price, A. 2010, *VizieR Online Data Catalog*, 1, 2027
- Zacharias, N., Monet, D. G., Levine, S. E., Urban, S. E., Gaume, R., & Wycoff, G. L. 2004, *Bulletin of the American Astronomical Society*, 36, 1418
- Zhang, X.-B., Zhang, R.-X., & Li, Z.-P. 2005, *CJAA*, 5, 579

CHAPTER 4

δ CEP CLUSTER

New Evidence Supporting Cluster Membership for the Keystone

Calibrator δ Cephei

Abstract: New and existing $UBVJHK_s$, spectroscopic, NOMAD, HST, and revised HIP observations are employed to determine properties for δ Cep and its host star cluster. The multi-faceted approach ensured that uncertainties were minimized ($\sigma/d \sim 2\%$). The following fundamental parameters were inferred for δ Cep: $E(B - V) = 0.073 \pm 0.018(\sigma)$, $\log \tau = 7.9 \pm 0.1$, and $d = 272 \pm 3(\sigma_{\bar{x}}) \pm 5(\sigma)$ pc. The cluster exhibits a turnoff near spectral type B6 ($M_*/M_{\odot} \simeq 5$), and the brightest host cluster members are the supergiants ζ Cep (K1.5Ib) and δ Cep. To within the uncertainties, the two stars share common astrometric parameters (π , μ_{α} , μ_{δ} , and $RV \simeq -17$ km/s) and are tied to bluer members of similar evolutionary age according to the cluster's UBV and JHK_s colour-colour and colour-magnitude diagrams. The cluster's existence is bolstered by the absence of a sequence of early-type stars in colour-magnitude diagrams for comparison fields. NOMAD data provide a means to identify potential cluster members ($n \sim 30$) and double the existing sample. That number could increase with forthcoming precise proper motions (DASCH) for faint main-sequence stars associated with classical Cepheids (e.g., δ Cep), which may invariably foster efforts to strengthen the Galactic Cepheid calibration and reduce uncertainties tied to H_0 .

4.1 INTRODUCTION

Cepheid variables are utilized to establish extragalactic distances and constrain cosmological models (Macri & Riess, 2009; Shappee & Stanek, 2011; Riess et al., 2011). However, the reliability of the derived parameters is invariably tied to the Cepheid calibration. Freedman et al. (2001) noted that ambiguities related to the zero-point of the calibration account for a sizable fraction of the total uncertainty associated with H_0 . That uncertainty hinders efforts to constrain the equation of state of dark energy which is acutely dependent on an accurate Hubble constant ($\sigma_w \sim 2\sigma_{H_0}$, Macri & Riess, 2009). The next generation follow-up to the HST key project to measure H_0 (the Carnegie Hubble project, Freedman & Madore, 2010) aims to resolve that problem by relying on LMC and Galactic calibrators (Benedict et al., 2002a, 2007; Turner, 2010; Storm et al., 2011). Consequently, bolstering the Galactic calibration should support efforts by the Carnegie Hubble, Araucaria, and SH_0ES projects to determine H_0 to within 2 – 4% (Gieren et al., 2005; Riess et al., 2011).

In this study, $UBVJHK_s$, spectroscopic, NOMAD, HST, and revised HIP observations for stars physically associated with δ Cep are employed to constrain its fundamental parameters: age ($\log \tau$), colour excess (E_{B-V}), distance, progenitor mass, and absolute Wesenheit magnitude ($W_{VIc,0}$).

4.2 ANALYSIS

4.2.1 REVISED HIP OBSERVATIONS FOR CEP OB6

In a comprehensive study de Zeeuw et al. (1999) discovered that δ Cep is a member of a group denoted as Cep OB6 (see also Hoogerwerf et al., 1997). The 20 stars identified by de Zeeuw et al. (1999) as Cep OB6 members are presented in Table 4.1. Stars with spectral

Table 4.1. Cep OB6 Member List (Z99)

HIP ID	HIP π (mas) ⁵	V07 π (mas) ⁵	μ_α, μ_δ (mas/yr) ⁶	m.p. (Z99) ¹	m.p. ²	$E(B - V)$ ³
109426	3.8 ± 0.7	3.6 ± 0.5	$16.6 \pm 0.6, 4.1 \pm 0.5$	94	m	
109492	4.5 ± 0.5	3.9 ± 0.1	$13.3 \pm 0.4, 4.4 \pm 0.3$	97	m	
110266	3.9 ± 0.6	4.4 ± 0.3	$19.0 \pm 0.5, 5.1 \pm 0.5$	96	m	0.070
110275	4.0 ± 1.0	4.0 ± 0.9	$14.7 \pm 1.0, 5.7 \pm 0.9$	89	m	
110356	3.4 ± 0.7	2.9 ± 0.5	$11.7 \pm 0.6, 3.2 \pm 0.6$	100	m	0.085
110497	3.8 ± 0.6	3.2 ± 0.4	$17.4 \pm 0.5, 4.8 \pm 0.5$	98	m	0.060
110648	3.9 ± 1.0	3.3 ± 0.9	$16.2 \pm 1.0, 6.2 \pm 0.8$	84	m	
110807	4.0 ± 0.6	3.5 ± 0.4	$16.1 \pm 0.5, 5.4 \pm 0.4$	92	m	0.060
110925	4.3 ± 0.9	5.1 ± 0.8	$21.3 \pm 1.1, 4.8 \pm 0.8$	86	m	0.060 ⁴
110988	3.4 ± 0.6	3.7 ± 0.5	$16.4 \pm 0.7, 4.7 \pm 0.7$	100	m	0.085 ⁴
111060	5.0 ± 0.8	5.3 ± 0.7	$17.2 \pm 0.7, 4.5 \pm 0.7$	100	m	
112141	3.2 ± 0.8	3.4 ± 0.6	$14.6 \pm 0.7, 2.1 \pm 0.6$	89	m	
113255	4.3 ± 0.7	4.5 ± 0.5	$19.8 \pm 0.6, 3.0 \pm 0.6$	99	m	0.095
113316	3.2 ± 0.7	3.6 ± 0.4	$14.1 \pm 0.7, 3.2 \pm 0.6$	99	m	0.100
δ Cep	3.3 ± 0.6	3.8 ± 0.2	$16.4 \pm 0.6, 3.5 \pm 0.6$	89	m	
110459	4.1 ± 0.9	4.5 ± 0.7	$16.2 \pm 0.9, 5.2 \pm 0.7$	100	nm	
111069	3.2 ± 0.9	3.1 ± 0.8	$15.1 \pm 0.8, 6.9 \pm 0.7$	79	nm	
112473	3.6 ± 0.8	5.0 ± 0.7	$13.9 \pm 0.8, 2.8 \pm 0.8$	97	nm	
112998	2.5 ± 0.6	2.6 ± 0.3	$12.7 \pm 0.6, 2.2 \pm 0.5$	98	nm	
113993	3.8 ± 0.7	3.7 ± 0.4	$14.3 \pm 0.6, 3.9 \pm 0.5$	79	nm	

¹Membership probability assigned by de Zeeuw et al. (1999, Z99).

²Membership inferred from $UBVJHK_s$ and spectroscopic observations (Figs. 4.1, 4.2).

³Reddenings derived from UBV colour-colour analysis (Fig. 4.1).

⁴Stars in close proximity to δ Cep.

⁵Parallaxes from Perryman & ESA (1997, HIP) and van Leeuwen (2007, V07).

⁶Proper motion data from NOMAD (Zacharias et al., 2004).

types inconsistent with cluster membership based on their UBV and JHK_s colour-colour and colour-magnitude positions were flagged as probable non-members. For example, HIP 110459 was previously assigned a membership probability of 100% (Table 4.1), yet the star exhibits JHK_s photometry and a late-type temperature class (K5, Skiff, 2010) indicative of a field red clump giant (Fig. 4.2). UBV and JHK_s photometry were obtained from Mermilliod (1991) and 2MASS (Cutri et al., 2003). Spectral types were assigned to stars according to the Catalogue of Stellar Spectral Classifications (Skiff, 2010).

Revised HIP parallaxes (van Leeuwen, 2007) were tabulated for 15 stars in Table 4.1

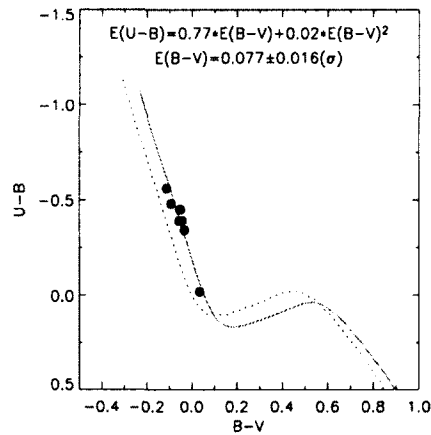


Figure 4.1 Colour-colour diagram for stars in Table 4.1 with UBV photometry that are associated with δ Cep. The sample is offset from the intrinsic relation (dotted line) by $E(B - V) = 0.077 \pm 0.016(\sigma)$ (solid line). The result confirms the reddening established for δ Cep by Benedict et al. (2002a). The intrinsic relation and reddening law for the region were adopted from Turner (1976, 1989). The uncertainties are smaller than the symbol size.

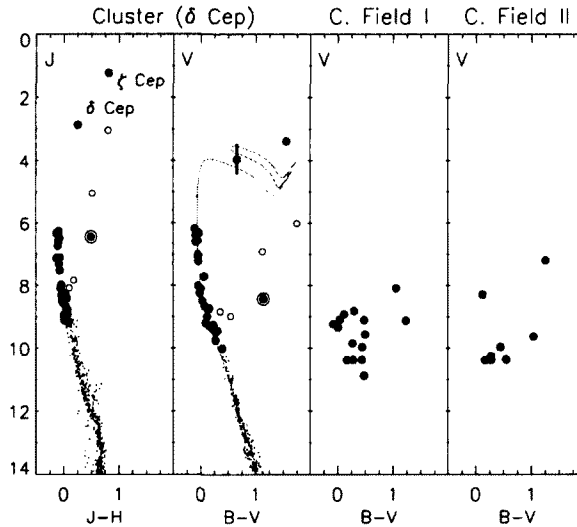


Figure 4.2 Left to right, JH and BV colour-magnitude diagrams for the Table 4.1 and NOMAD samples (panels 1, 2), and comparison fields (panels 3, 4). Small dots denote calibration stars from Majaess et al. (2011), which were employed to tie the cluster distance to a geometrically anchored scale (van Leeuwen, 2009; Majaess et al., 2011). Large dots characterize stars with $\mu_\alpha = 11 - 19$ mas/yr and $\mu_\delta = 2 - 7$ mas/yr. Open circles are likely field stars (Table 4.1). HIP 110459 (circled dot) was previously identified as a cluster member, yet $BVJHK_s$ photometry imply the object is a field star. In panel 2 a Padova $\log \tau = 7.9$ isochrone was applied. The brightest likely cluster members are the supergiants ζ Cep (K1.5Ib) and δ Cep (amplitude variation indicated). An early-type cluster sequence is absent from the comparison fields (HIP data for the cluster μ_α/μ_δ).

that were identified as probable cluster members. The revised HIP parallaxes exhibit a $\sim 30\%$ reduction in uncertainties relative to existing data (Perryman & ESA, 1997), and the parallaxes for δ Cep and HD 213307 ($r \sim 0.7'$) increased from $\pi = 3.32 \pm 0.58$ and 3.43 ± 0.64 mas to $\pi = 3.77 \pm 0.16$ and 3.69 ± 0.46 mas. A mean distance for the revised cluster sample outlined in Table 4.1 is $d = 271 \pm 11(\sigma_{\bar{x}}) \pm 42(\sigma)$ pc (see also de Zeeuw et al., 1999, and their appendix B).

4.2.2 REDDENING

UBV and JHK_s colour-colour analyses permit an assessment of the sample's extinction properties. UBV data are particularly efficient at identifying early-type stars because of the U -band's sensitivity to the Balmer decrement (e.g., Turner, 1989; Carraro et al., 2006).

Cluster members with UBV photometry (Mermilliod, 1991) are offset from the intrinsic UBV colour-colour relation by $E(B - V) = 0.077 \pm 0.016(\sigma)$ (Table 4.1, Fig. 4.1). That supports the field reddening determined for δ Cep by Benedict et al. (2002a), and is consistent with that established from spectroscopic and JHK_s observations. However, uncertainties associated with the latter hamper a precise determination. The minimal spread of $E(B - V) \simeq 0.06 - 0.10$ (Table 4.1) may be indicative of marginal differential reddening, rotation, binarity, or photometric uncertainties.

4.2.3 AGE

UBV and JHK_s colour-colour analyses imply a cluster turnoff near spectral type B5-B7 ($M_*/M_{\odot} \simeq 5$) according to intrinsic relations (Padova models, and Straižys & Lazauskaitė, 2009; Turner, 1976, 1989, 2011). A $\log \tau = 7.9 \pm 0.1$ isochrone was subsequently adopted based on the main-sequence turnoff (Fig. 4.1, Table 4.1) and because the implied evolu-

tionary track (Fig. 4.2) matches bluer and redder evolved cluster members (δ and ζ Cep). The result agrees with the Cepheid's predicted age (Turner, 1996; Bono et al., 2005). The temporal match is pertinent evidence in support of cluster membership for δ Cep.

4.2.4 CLUSTER DISTANCE

A precise distance may be established because two of four principal parameters associated with isochrone fitting are constrained by the UBV and JHK_s colour-colour and spectroscopic analyses, namely the reddening and age (spectral type at the turnoff). δ Cep exhibits solar abundances, and hence the remaining parameter is the shift required in magnitude space to overlay the intrinsic relation upon the data. The resulting distance is $d = 277 \pm 15$ pc (Fig. 4.2). The zero-point is tied to seven benchmark open clusters ($d < 250$ pc) that exhibit matching JHK_s and revised Hipparcos distances (the Hyades, α Per, Praesepe, Coma Ber, IC 2391, IC 2609, and NGC 2451, van Leeuwen, 2009; Majaess et al., 2011). A redetermination of the HST parallax for the Hyades supports that scale (McArthur et al., 2011). Isochrones, models, and the distance scale should be anchored and evaluated using clusters where consensus exists, rather than by the discrepant case (i.e. the Pleiades). A ratio of total to selective extinction R_J was adopted from Majaess et al. (2011c) (see also Bonatto et al., 2004), whereas a value for R_V was adopted from Turner (1976). An advantage of employing JHK_s observations is that the cluster reddening is negligible in that part of the spectrum ($E_{J-H} \simeq 0.3 \times E_{B-V}$, Majaess et al., 2008; Bonatto et al., 2004, and references therein), which consequently mitigates the impact of uncertainties in R_λ ($J_0 = J - E_{J-H} \times R_J$).

The distance derived from the cluster colour-magnitude diagrams (Fig. 4.2) is tied to ad-

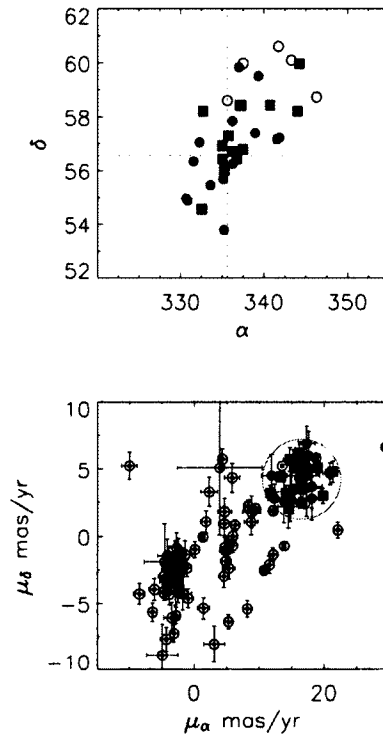


Figure 4.3 Top, J2000 RA/DEC positions for probable (squares) and non-members (open circles) presented in Table 4.1, and new potential members (filled circles) outlined in Table 4.2. Bottom, dotted open circles represent all HIP stars near the (approximate) cluster centre. The red circle represents the δ Cep cluster.

ditional potential cluster members identified using NOMAD (Zacharias et al., 2004). That database was queried for stars with $\mu_\alpha = 11 - 19 \text{ mas yr}^{-1}$ and $\mu_\delta = 2 - 7 \text{ mas yr}^{-1}$ (Table 4.1). Stars fainter than $J \simeq 9.2$ were culled from the resulting sample to reduce field contamination. Proper motions may be less reliable for such stars, and spectroscopic and UBV observations are typically unavailable. Stars redder than $J - H \simeq 0.4$ were likewise removed to mitigate contamination from field red clump giants. In addition, stars with anomalous positions in the multiband colour-colour and colour-magnitude diagrams were removed. The remaining stars double the number of existing potential cluster members, and are presented in Table 4.2. The stars in Tables 4.1 and 4.2 are potential members pending

Table 4.2. Additional Potential Cluster Members

ID	V	$B - V$	$U - B$	J	H	K_s	μ_α, μ_δ (mas/yr) ³	μ_α, μ_δ (mas/yr) ⁴
HD 210071 ¹	6.39	-0.10	-0.45	6.49	6.57	6.58	$16.3 \pm 0.4, 2.5 \pm 0.4$	$16.3 \pm 0.4, 2.4 \pm 0.4$
HD 209636 ²	7.01	-0.05	-0.23	7.10	7.17	7.16	$15.0 \pm 0.5, 2.7 \pm 0.5$	$15.0 \pm 0.5, 2.6 \pm 0.5$
HD 214259	8.72	0.15	0.10	8.27	8.24	8.24	$18.1 \pm 1.6, 3.7 \pm 1.6$	$18.4 \pm 1.3, 4.3 \pm 1.3$
HD 214512	8.74	0.15	-	8.30	8.29	8.29	$17.6 \pm 1.8, 6.0 \pm 1.8$	$-21.5 \pm 1.6, 53.1 \pm 1.6$
HD 212093	8.25	-0.02	-0.29	8.31	8.36	8.35	$15.0 \pm 1.6, 3.3 \pm 1.6$	$14.1 \pm 1.2, 2.5 \pm 1.2$
HD 210480	8.71	0.15	0.08	8.41	8.35	8.31	$14.5 \pm 1.6, 2.2 \pm 1.6$	$14.9 \pm 1.3, 2.3 \pm 1.3$
HD 211226	8.65	0.07	0.03	8.45	8.49	8.47	$17.3 \pm 1.3, 6.9 \pm 1.3$	$15.4 \pm 1.2, 6.7 \pm 1.2$
HD 215879	8.98	0.12	-	8.65	8.62	8.59	$13.8 \pm 1.6, 2.6 \pm 1.6$	$13.4 \pm 1.3, 4.4 \pm 1.2$
HD 212711	9.25	0.23	-	8.78	8.72	8.66	$17.3 \pm 2.2, 3.6 \pm 2.1$	$16.7 \pm 1.9, 5.2 \pm 1.9$
HD 240052	9.44	0.30	-	8.79	8.74	8.71	$18.1 \pm 1.6, 2.8 \pm 1.6$	$17.3 \pm 1.3, 4.1 \pm 1.2$
HD 212137	9.19	0.09	-	8.95	8.95	8.94	$12.4 \pm 1.1, 2.8 \pm 1.1$	$12.9 \pm 1.2, 1.8 \pm 1.2$
BD+54°2675	9.48	0.28	-	9.04	9.01	8.94	$11.9 \pm 1.6, 4.5 \pm 1.6$	$12.2 \pm 1.8, 7.5 \pm 1.7$
HD 239949	10.01	0.39	-	9.11	9.10	9.06	$16.8 \pm 2.5, 4.5 \pm 2.3$	$5.4 \pm 1.6, -0.8 \pm 1.5$
BD+59°2523	9.75	0.27	-	9.16	9.07	9.11	$14.8 \pm 2.3, 3.3 \pm 2.2$	$15.3 \pm 1.6, 4.2 \pm 1.6$

¹ $\pi = 5.06 \pm 0.33$ mas (van Leeuwen, 2007).

¹ $\pi = 5.54 \pm 0.39$ mas (van Leeuwen, 2007).

²NOMAD proper motions (Zacharias et al., 2004).

³The PPMXL catalog (Roeser et al., 2010).

further evidence. The NOMAD proper motions are consistent with estimates from the PPMXL catalog (Table 4.2). UBV and JHK_s photometry was taken from Mermilliod (1991), 2MASS (Cutri et al., 2003), and other sources. For example, new observations acquired from the Bright Star Monitor (BSM), which is part of the AAVSO's robotic telescope network, provided BV photometry for HD 239949: $V = 10.013 \pm 0.031$ and $B - V = 0.392 \pm 0.048$. The cluster reddening was redetermined ($E_{B-V} = 0.073 \pm 0.018(\sigma)$) using four of the early-type stars in Table 4.2 with UBV photometry.

Cluster members appear to congregate near J2000 coordinates $22^{\text{h}}22.5^{\text{m}}, +56^{\circ}34'$ (Fig. 4.3). δ Cep lies at the periphery of the density enhancement and within the confines of the cluster, because the corona extends further (Kholopov, 1969; Turner, 1985). The Cepheid is $r \simeq 2^{\circ}$ from the those coordinates, which is equivalent to a linear projected separation of $\simeq 9$ pc. The revised HIP and HST parallaxes for δ Cep and HD 213307 ($r \simeq 0.7'$ from δ

Cep), together with their apparent positions, suggest that the distance to the cluster centre and Cepheid is the same to within the uncertainties.

4.2.5 MEAN DISTANCE TO δ CEP

The mean HIP parallax for the cluster (§4.2.1) agrees with the HIP parallax for δ Cep ($\pi = 3.77 \pm 0.16$ mas), the HST parallax for δ Cep ($\pi = 3.66 \pm 0.15$ mas, Benedict et al., 2002a), and the distance inferred for the host cluster from $UBVJHK_s$ and spectroscopic observations (Figs. 4.1, 4.2). If equal weight is assigned to each method, the mean of the four distances for δ Cep is $d = 272 \pm 3(\sigma_{\bar{x}}) \pm 5(\sigma)$ pc. That agrees with the Storm et al. (2011) determination from the infrared surface brightness technique (IRSB, Fouque & Gieren, 1997). The associated standard error and deviation provide a realistic estimate for the systematic uncertainty, which is often difficult to characterize.

The resulting VI_c Wesenheit magnitude for δ Cep is $W_{VI_c,0} = -5.12$ ($R_{VI_c} = 2.55$), consistent with results established for classical Cepheids displaying similar pulsation periods: CV Mon, V Cen, Y Sgr, and CS Vel (Benedict et al., 2007; Turner, 2010; Majaess et al., 2011c).

4.3 CONCLUSION AND FUTURE RESEARCH

The evidence presented bolsters the assertion by de Zeeuw et al. (1999) that δ Cep is a constituent of an intermediate-age cluster. The brightest cluster member is the K1.5Ib supergiant ζ Cep. δ Cep and ζ Cep share similar HIP parallaxes ($\pi = 3.77 \pm 0.16$ mas and $\pi = 3.90 \pm 0.10$ mas), proper motions, radial velocities ($RV \simeq -17$ km/s), and evolutionary ages (Fig. 4.2). In conjunction with the aforementioned evidence, the cluster's existence is supported by the absence of early-type stars in the comparison fields (Fig 4.2). NOMAD

data were employed to identify additional potential cluster members (Tables 4.1, 4.2).

The Cepheid exhibits parameters of $E(B - V) = 0.073 \pm 0.018(\sigma)$, $\log \tau = 7.9 \pm 0.1$, and $d = 272 \pm 3(\sigma_{\bar{x}}) \pm 5(\sigma)$ pc (Table 4.1, Figs. 4.1, 4.2). The results are tied in part to spectroscopic and $UBVJHK_s$ observations, and may be adopted to refine classical Cepheid period-colour, period-age, period-mass, period-luminosity, and period-Wesenheit relations (e.g., Turner, 2010).

Potential future research entails establishing precise proper motions for fainter stars near Cepheids using photographic plates stored at the Harvard-Smithsonian Center for Astrophysics (CfA), as described by Grindlay (2007, DASCH),¹ thereby extending the astrometric coverage provided by HIP. The plate collection at the CfA offers unmatched multi-epoch observations spanning roughly a 100 year temporal baseline. A concurrent venture pertains to employing new VVV JHK_s observations for young clusters in Galactic spiral arms to calibrate adjacent long-period classical Cepheids (Minniti et al., 2010; Moni Bidin et al., 2011; Majaess et al., 2011c). Those initiatives, in conjunction with the analysis presented here, will complement a suite of diverse efforts aimed at reducing uncertainties associated with H_0 in order to constrain cosmological models (e.g., Benedict et al., 2007; Feast, 2008; Gerke et al., 2011; Ngeow, 2011; Steer & Madore, 2011).

The agreement between the distances inferred for δ Cep from cluster membership and the IRSB technique suggests that the systematic uncertainties have been marginalized. An analysis of $n = 20$ cluster Cepheids with revised IRSB distances (Storm et al., 2011) yields a mean fractional difference of $-3 \pm 3\%$. That result is reassuring, and subsequent research on the discrepant Cepheid calibrators (e.g., S Vul, SU Cas, in prep.) may reduce the remaining

¹Digital Access to a Sky Century @ Harvard (DASCH), <http://hea-www.harvard.edu/DASCH/>

offset. Further research is likewise required on the candidate cluster members associated with δ Cep (Tables 4.1, 4.2).

REFERENCES

- Benedict, G. F., McArthur, B. E., Fredrick, L. W., et al. 2002, *AJ*, 124, 1695
Benedict, G. F., McArthur, B. E., Feast, M. W., et al., 2007, *AJ*, 133, 1810
Bonatto, C., Bica, E., & Girardi, L. 2004, *A&A*, 415, 571
Bono, G., Marconi, M., Cassisi, S., et al. 2005, *ApJ*, 621, 966
Carraro, G., Chaboyer, B., & Perencevich, J. 2006, *MNRAS*, 365, 867
Cutri, R. M., Skrutskie, M. F., van Dyk, S., et al. 2003, *The IRSA 2MASS All-Sky Point Source Catalog*.
de Zeeuw, P. T., Hoogerwerf, R., de Bruijne, J. H. J., Brown, A. G. A., & Blaauw, A. 1999, *AJ*, 117, 354
Feast, M. W. 2008, *First Middle East-Africa, Regional IAU Meeting*, held 5-10 April, 2008 in Cairo, Egypt.
Fouque, P., & Gieren, W. P. 1997, *A&A*, 320, 799
Freedman, W. L., Madore, B. F., Gibson, B. K., et al. 2001, *ApJ*, 553, 47
Freedman, W. L., & Madore, B. F. 2010, *ARA&A*, 48, 673
Gerke, J. R., Kochanek, C. S., Prieto, J. L., Stanek, K. Z., & Macri, L. M. 2011, arXiv:1103.0549
Gieren, W., Pietrzyński, G., Soszyński, I., et al. 2005, *ApJ*, 628, 695
Grindlay, J. E. 2007, *The Central Engine of Active Galactic Nuclei*, 373, 711
Hoogerwerf, R., de Bruijne, J. H. J., Brown, A. G. A., et al. 1997, *Hipparcos - Venice '97*, 402, 571
Kholopov, P. N. 1969, *Soviet Ast.*, 12, 625
Macri, L. M., & Riess, A. G. 2009, *AIP Conference Series*, 1170, 23
Majaess D. J., Turner D. G., Lane D. J., 2008, *MNRAS*, 390, 1539
Majaess, D. J., Turner, D. G., Lane, D. J., & Krajci, T. 2011 (a), *JAAVSO*, in press
Majaess, D., Turner, D., Moni Bidin, C., et al. 2011 (b), *ApJ*, 741, L27
McArthur, B. E., Benedict, G. F., Harrison, T. E., & van Altena, W. 2011, *AJ*, 141, 172
Mermilliod, J-C. 1991, *Homogeneous Means in the UBV System*, *VizieR catalog*.
Minniti, D., Lucas, P. W., Emerson, J. P., et al. 2010, *New Astronomy*, 15, 433
Moni Bidin, C., Mauro, F., Geisler, D., et al. 2011, *A&A*, 535, A33
Ngeow, C.-C. 2011, *Proceedings of the 9th Pacific Rim Conference on Stellar Astrophysics (PRCSA2011)*, Lijiang, China, April 2011 (arXiv:1111.2094)
Perryman, M. A. C., & ESA 1997, *ESA Special Publication*, 1200
Riess, A. G., Macri, L., Casertano, S., et al. 2011, *ApJ*, 730, 119
Roeser, S., Demleitner, M., & Schilbach, E. 2010, *AJ*, 139, 2440
Shappee, B. J., & Stanek, K. Z. 2011, *ApJ*, 733, 124
Skiff, B. 2010, *General Catalogue of Stellar Spectral Classifications*, *VizieR catalog*.
Steer, I., Madore, B., 2011, *NED-D: a Master List of Extragalactic Distances*.
Storm, J., Gieren, W., Fouqué, P., et al. 2011, *A&A*, 534, A94
Straizys, V., & Lazauskaitė, R. 2009, *Baltic Astronomy*, 18, 19

-
- Turner, D. G. 1976, *AJ*, 81, 1125
Turner, D. 1985, *IAU Colloq. 82: Cepheids: Theory and Observation*, 209
Turner, D. G. 1989, *AJ*, 98, 2300
Turner, D. G. 1996, *JRASC*, 90, 82
Turner, D. G. 2010, *Ap&SS*, 326, 219
Turner, D. G. 2011, *RMxAA*, 47, 127
van Leeuwen, F. 2007, *A&A*, 474, 653
van Leeuwen, F. 2009, *A&A*, 497, 209
Zacharias, N., Monet, D. G., Levine, S. E., et al. 2004, *Bulletin of the AAS*, 36, 1418

CHAPTER 5

TW NOR/LYNGA 6

New Evidence Supporting Membership for TW Nor in Lyngå 6 and the Centaurus Spiral Arm

Abstract: The putative association between the 10.8^d classical Cepheid TW Nor and the open cluster Lyngå 6 has generated considerable debate in the literature. New *JHK_s* photometry in conjunction with existing radial velocities for Lyngå 6 stars imply cluster membership for TW Nor, and establish the variable as a high-weight calibrator for classical Cepheid relations. Fundamental mean parameters determined for Lyngå 6 are: $d = 1.91 \pm 0.10$ kpc, $E(J - H) = 0.38 \pm 0.02$, and $\log \tau = 7.9 \pm 0.1$. The Benedict et al. (2007)/Turner (2010) Galactic VI_c Wesenheit function was revised using TW Nor's new parameters: $W_{VI,0} = (-3.37 \pm 0.08) \times \log P_0 - 2.48 \pm 0.08$. TW Nor/Lyngå 6 lie beyond the Sagittarius-Carina spiral arm and occupy the Centaurus arm, along with innumerable young Cepheids and clusters (e.g., VW Cen and VVV CL070).

5.1 INTRODUCTION

Cluster membership provides a means to constrain the distance, colour excess, and age of a Cepheid (Turner et al., 1992). The parameters are subsequently employed to calibrate Cepheid period-luminosity, period-Wesenheit, and period-age relationships (Turner, 2010). Such functions bolster efforts to map the Galaxy's local spiral structure (Majaess et al., 2009, and references therein), establish the extragalactic distance scale (Pietrzyński et al.,

2004; Macri & Riess, 2009), and determine the Hubble constant (Freedman & Madore, 2010). Establishing a connection between the 10.8^d classical Cepheid TW Nor and open cluster Lyngå 6 is consequently desirable.

Tsarevsky et al. (1966) first noted that TW Nor may be a member of Lyngå 6. However, Moffat & Vogt (1975) doubted the cluster's existence after evaluating $UBV-H\beta$ photometry for 18 stars. Madore (1975) obtained UBV photoelectric photometry for 8 stars and argued for cluster parameters of $d \simeq 2.5$ kpc and $E(B-V) = 1.37 \pm 0.02$. Madore (1975) remarked that the luminosity implied for TW Nor from cluster membership matched expectations from period-luminosity calibrations. van den Bergh & Harris (1976) provided BV photoelectric and photographic photometry for 38 stars, and revised the cluster distance downward ($d \simeq 1.6$ kpc). di Prospero (1976) concluded that evolutionary models yielded similar ages for TW Nor and Lyngå 6 (40 Myr), thereby supporting cluster membership for the Cepheid. Lyngå (1977) supplemented existing data with $uvby\beta$ photometry and temperature classifications (objective prism spectra) for several stars, and corroborated the parameters cited for Lyngå 6 by van den Bergh & Harris (1976).

Uncertainties tied to TW Nor's reddening (van den Bergh & Harris, 1976; Fernie & McGonegal, 1983) and distance complicated efforts to calibrate classical Cepheid relations throughout the 1980s. For example, McGonegal et al. (1983) included TW Nor in their calibration after adopting a mean of the Madore (1975) and van den Bergh & Harris (1976) distances to Lyngå 6.

Walker (1985) acquired deep BVI_c CCD observations that extended existing photometry to $V \simeq 20$, and determined cluster parameters of $d = 2.0 \pm 0.2$ kpc and $\tau \simeq 10^8$ years. The

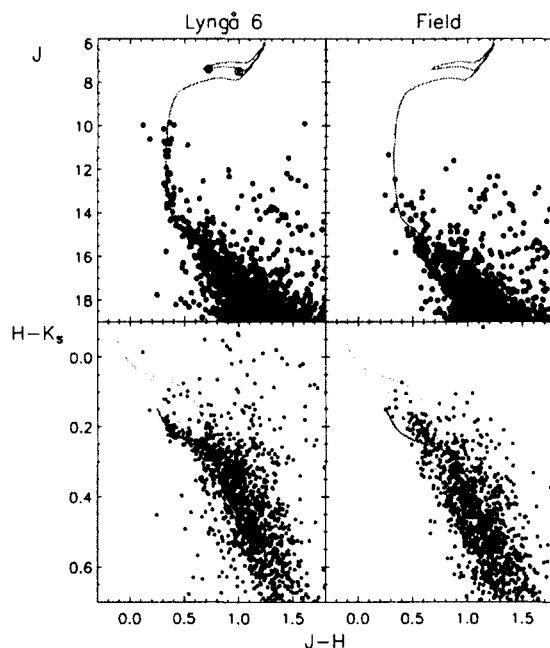


Figure 5.1 VVV colour-magnitude and colour-colour diagrams for Lynga 6 stars and a comparison field. A population of mid-to-late B-type cluster stars is absent from the latter. Stars left of the cyan line are typically earlier than $\simeq F5$ (Straizys & Lazauskaitė, 2009; Turner, 2011). The isochrone and intrinsic fit were adjusted (reddened) to match the observed data. Ly6-4 (an evolved red star, Lynga, 1977) and the classical Cepheid TW Nor (circled dots) share a common radial velocity (Mermilliod et al., 1987, 2008). Applying the intrinsic colour-colour relation of Turner (2011) and a $\log \tau = 7.9 \pm 0.1$ Padova isochrone to Lynga 6 stars yields $E(J-H) = 0.38 \pm 0.02$ and $d = 1.91 \pm 0.10$ kpc. The extinction laws adopted are described in the text.

age is older than that estimated for TW Nor and Lynga 6 by di Prospero (1976). An independent cluster reddening could not be established by Walker (1985) because the B-star sequence is parallel to the reddening vector in $B-V$ vs. $V-I_c$ colour-colour diagrams. Walker (1985) adopted the van den Bergh & Harris (1976) reddening to evaluate the distance to Lynga 6. The di Benedetto (1994) pulsational parallax for TW Nor disagreed with the cluster distance adopted, and $UBVRI$ polarization measurements by Orsatti et al. (2001) exhibited a $\geq 2\sigma$ mismatch between cluster members and TW Nor. Hoyle et al. (2003) supplied new UBV CCD photometry and established $d \simeq 1.7$ kpc and $E(B-V) = 1.36 \pm 0.08$

for Lyngå 6. By contrast, Laney & Caldwell (2007) advocated a smaller reddening for the Cepheid of $E(B-V)=1.17$, and Kaltcheva (2009) determined a closer distance to Lyngå 6 ($d = 1.36$ kpc) based on $uvby\beta$ photometry for five stars. The latter result negates cluster membership for TW Nor.

In summary, parameters for TW Nor/Lyngå 6 and their putative association have been debated for nearly a half century. In this study, new JHK_s VVV (ESO Public Survey ‘VISTA Variables in the Vía Láctea’) photometry is presented that substantiates the cluster’s existence, bolsters cluster membership for TW Nor, and provides a reliable set of fundamental parameters to permit the subsequent calibration of classical Cepheid relations.

5.2 VVV PHOTOMETRY

The VVV survey aims to establish precise multi-epoch photometry for fields in the Galactic bulge and near the Galactic plane ($\ell = 295 - 10^\circ$, Minniti et al., 2010). VVV images extend magnitudes fainter and exhibit increased spatial resolution versus 2MASS, which is particularly important for mitigating contaminated photometry in crowded regions near the Galactic centre and the cores of globular clusters (M15, Majaess et al., 2011a). The VVV survey will provide precise multi-epoch photometry for stars and variables in $\sim 3 \times 10^2$ open clusters and ≥ 39 globular clusters (e.g., NGC 6441).

Details of the pipeline constructed to process and extract VVV photometry are discussed in Mauro et al. (2012, in preparation). PSF photometry performed using DAOPHOT was subsequently tied to 2MASS JHK_s standards (see Moni Bidin et al., 2011).

5.3 ANALYSIS

A colour-colour diagram was compiled for Lyngå 6 stars within $\sim 2'$ of J2000 coordinates 16:04:54.42, $-51:57:31.6$ (Fig. 5.1). A diagram was likewise constructed for a comparison field $20'$ adjacent to Lyngå 6. Reddening laws characterizing dust along the line of sight were derived to evaluate the colour excess. The reddening vector may be determined by tracking deviations of red clump stars from their mean intrinsic colour because of extinction. The mean intrinsic colour was inferred from nearby red clump stars ($d \leq 50$ pc) with revised Hipparcos parallaxes (van Leeuwen et al., 2007). Reddening corrections were neglected because the calibrating sample lies in close proximity to the Sun. Spurious data were removed, and the resulting mean parameters for red clump stars are presented in Table (5.1). The values correspond to a K0 III star as inferred from catalogued¹ spectroscopic classifications. A reddening vector of $E(J - H)/E(H - K_s) = 1.94 \pm 0.03$ was determined, and is supported by the work of Straizys & Laugalys (2008).

Applying the reddening vector to the Lyngå 6 colour-colour diagram reveals a prominent sequence of mid-to-late B stars with $E(J-H) = 0.38 \pm 0.03$ (Fig. 5.1). The corresponding value of $E(B - V)$ is sensitive to the conversion from $E(J - H)$ adopted (see Majaess et al., 2008, and references therein), but lies within the range of 1.13 to 1.40 mag. A visible sequence of young cluster stars is absent from the comparison field. Lyngå 6 stars terminate near B5 according to the intrinsic JHK_s relations of Straizys & Lazauskaitė (2009) and Turner (2011).

Colour-magnitude diagrams for Lyngå 6 and an adjacent comparison field are shown

¹Catalogue of Stellar Spectral Classifications (B. Skiff), <http://vizier.cfa.harvard.edu/viz-bin/VizieR?-source=B/mk>

Table 5.1. Intrinsic Parameters for Red Clump Stars

M_J	M_H	M_{K_s}	$(J - H)_0$	$(H - K_s)_0$	$(J - K_s)_0$
-1.04 ± 0.04	-1.52 ± 0.04	-1.59 ± 0.04	0.48 ± 0.06	0.07 ± 0.06	0.55 ± 0.06

in Fig. 5.1. The population of cluster stars is absent from the comparison field. A $\log(\tau) = 7.9 \pm 0.1$ Padova isochrone (Bonatto et al., 2004) was adopted based on the reddening and spectral types inferred from the colour-colour diagram. That age provides an evolutionary track that aptly matches bluer cluster stars, an evolved red star at J2000 coordinates 16:04:54.42, -51:57:32.5 (hereafter Ly6-4, Lyngå, 1977), and TW Nor.

Radial velocity measurements from Mermilliod et al. (1987, 2008) for Ly6-4 agree with that established for TW Nor ($RV \simeq -56$ km/s). The radial velocity/distance gradient along of the line of sight as predicted from Galactic rotation is steep, indicating that two stars exhibiting a common radial velocity are likely associated. The radial velocity ties TW Nor to that star, and both are surrounded by bluer cluster members that adhere to the expected evolutionary track. The pair of stars lie near the cluster core and are separated by $22''$. The stars are brighter than the saturation limit of the VVV survey and thus the JHK_s photometry was taken from 2MASS. The colour-magnitude and colour-colour diagrams compiled from VVV photometry establish Lyngå 6 as a *bona fide* open cluster (Fig. 5.1).

Orsatti et al. (2001) concluded that a 2σ mismatch exists between polarization measurements for cluster members and TW Nor. JHK_s photometry for the Orsatti et al. (2001) sample confirm that the polarization measurements efficiently segregate cluster members

from field stars. Yet polarization measurements imply cluster membership for Ly6-4 (the evolved red star, Fig 5.1). A contradiction consequently emerges because CORAVEL measurements by Mermilliod et al. (1987, 2008) link that star and TW Nor to a common radial velocity. The stars lie at the cluster's core and are separated by $22''$. Incidentally, 2MASS JHK_s colours for Ly6-4 are inconsistent with a G-type classification (Lyngå, 1977), for the cluster's reddening. The anomalous JHK_s and UBV colours may be tied to the star's binary nature (Mermilliod et al., 1987, 2008).

A ratio of total to selective extinction (R) for the field was determined to evaluate the distance to Lyngå 6. The precision and faintness attained by the VVV survey permits an independent assessment of R using red clump stars via the variable extinction method (Turner, 1976). The expression for computing the distance to red clump stars simplifies because mean intrinsic parameters may be adopted:

$$J - M_J - R_J \times ((J - H) - (J - H)_0) = \mu_0$$

$$J = R_J \times (J - H) + \text{constant}$$

A determination of R follows by correlating J and $J-H$ for a sample of red clump stars at a common distance. A histogram of the colour-magnitude diagram reveals a sizable population of red clump stars ~ 5 kpc distant. Comparing J and $J-H$ photometry for that group of red clump stars yields $A_J/E(J - H) = R_J = 2.75 \pm 0.07$. The extinction ratios for the field follow from $A_J/E(J - H)$ and $E(J - H)/E(H - K_s)$ via:

$$A_J/A_H = (A_J/E_{J-H}) / (A_J/E_{J-H} - 1)$$

$$A_J/A_{K_s} = \left(\frac{A_J}{A_H} \frac{E_{J-H}}{E_{H-K_s}} \right) / \left(\frac{E_{J-H}}{E_{H-K_s}} - \frac{A_J}{A_H} + 1 \right)$$

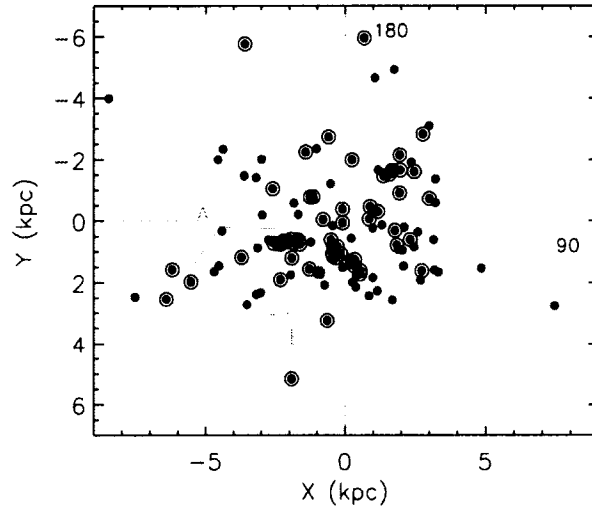


Figure 5.2 A map of local spiral structure as delineated by long period classical Cepheids (dots) and young clusters (circled dots) (see also Majaess et al., 2009). The Carina (A) and Centaurus (E) spiral arms are indicated on the diagram. TW Nor/Lyngå 6 (red dot) reside in the Centaurus spiral arm.

The resulting extinction ratios ($A_J/A_H : A_J/A_{K_s} = 1.57 : 2.22$) agree with the canonical values (e.g., Bonatto et al., 2004).

The final parameters for Lyngå 6 are $d = 1.91 \pm 0.10$ kpc, $E(J - H) = 0.38 \pm 0.02$, and $\log \tau = 7.9 \pm 0.1$. The zero-point of the Padova isochrone employed matches a distance scale anchored to seven benchmark clusters with equivalent revised Hipparcos and JHK_s ZAMS distances (Majaess et al., 2011), to within the uncertainties. The benchmark clusters are the Hyades, α Per, Praesepe, Coma Ber, IC 2391, IC 2609, and NGC 2451 (van Leeuwen, 2009; Majaess et al., 2011). The distance scale can (presently) rely on a suite of clusters that are independent of the Pleiades, and where consensus exists regarding the distances (Majaess et al., 2011). Models should be calibrated and evaluated using those seven nearby clusters where consensus exists regarding the distances, rather than the one discrepant cluster (i.e. the Pleiades).

A map of local spiral structure (Fig. 5.2) illustrates the location of TW Nor/Lynga 6 within the broader context of the Milky Way. Fig. 5.2 employs young open clusters and long period classical Cepheids to trace the Galaxy's spiral structure. The new distance established here implies that TW Nor lies beyond the Sagittarius-Carina arm and lies in the Centaurus arm (Fig. 5.2). That conclusion is supported by the distance determined for TW Nor via the infrared surface brightness technique (Storm et al., 2011). The long period classical Cepheids KQ Sco, QY Cen, VW Cen, OO Cen, and KN Cen likewise delineate the Centaurus arm (see also Majaess et al., 2009). The classical Cepheids are listed in order of decreasing Galactic longitude (ℓ). The young open clusters VVV CL070 (Borissova et al., 2011), and Hogg 15 occupy the Centaurus arm. Deep JHK_s , VVV and UKIDSS (Lucas et al., 2008) photometry will provide further constraints on the Galaxy's morphology by facilitating the discovery of Cepheids and star clusters (Minniti et al., 2011; Moni Bidin et al., 2011).

TW Nor may be used as a high-weight calibrator for the universal Wesenheit template (Majaess et al., 2011a,b) and classical Cepheid relations. A recent version of the Galactic VI_c Wesenheit calibration consists of 10 nearby classical Cepheids with precise HST parallaxes and 24 cluster Cepheids (Benedict et al., 2007; Turner, 2010), referred to hereafter as the hybrid relation. The new parameters for TW Nor place the Cepheid near the mean Wesenheit trend (Fig. 5.3). The Wesenheit magnitude for TW Nor ($W_{VI_c,0} = -5.80$) agrees with that established for calibrators exhibiting similar periods (ζ Gem and V340 Nor). The hybrid Galactic VI_c Wesenheit function was updated to include the revised parameters for

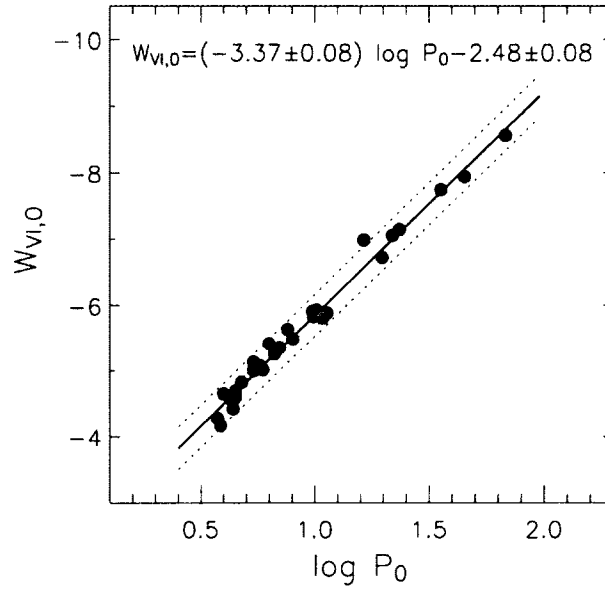


Figure 5.3 The hybrid Galactic VI_c Wesenheit function for 32 classical Cepheid calibrators (Benedict et al., 2007; Turner, 2010). The Wesenheit magnitude for TW Nor (red dot) is tied to the revised distance for Lynga 6.

TW Nor:

$$W_{VI_c,0} = (-3.37 \pm 0.08) \log P_0 - 2.48 \pm 0.08 \quad (5.1)$$

The canonical extinction law was employed ($R_{VI_c} = 2.55$). The short period classical Cepheid SU Cas was excluded from the derivation and Fig. 5.3 because its parameters are being revised by Turner (see also Storm et al., 2011).

5.4 CONCLUSION

Colour-magnitude and colour-colour diagrams constructed from precise JHK_s VVV photometry substantiate the existence of the open cluster Lynga 6 (Fig. 5.1). The diagrams have a sequence of mid-to-late B-type stars exhibiting a mean colour excess of $E(J-H) = 0.38 \pm 0.02$ (Fig. 5.1). That sequence is absent from an adjacent comparison field. The brightest cluster

members are the classical Cepheid TW Nor and Ly6-4 (an evolved red star, Fig. 5.1). The objects share equivalent radial velocities and are surrounded by bluer cluster stars that follow a $\log(\tau) = 7.9 \pm 0.1$ isochrone track. The distance to Lyngå 6 ($d = 1.91 \pm 0.10$ kpc) results after correcting for extinction using reddening laws inferred from red clump stars ($E(J - H)/E(H - K_s) = 1.94 \pm 0.03$). The result agrees with the distance to TW Nor obtained by Storm et al. (2011) via the infrared surface brightness technique, which likewise implies membership for the Cepheid in Lyngå 6 and the Centaurus spiral arm. The revised parameters for TW Nor were employed to update the Benedict et al. (2007)/Turner (2010) Galactic VI_c period-Wesenheit function (Fig. 5.3), and to establish the Cepheid's position within the Centaurus arm (Fig. 5.2). TW Nor may be used as a high-weight calibrator for classical Cepheid relations. Continued work on the Galactic calibration is needed.

REFERENCES

- Benedict G. F. et al., 2007, *AJ*, 133, 1810
Bonatto, C., Bica, E., & Girardi, L. 2004, *A&A*, 415, 571
Borissova, J., et al. 2011, *A&A*, 532, A131
di Benedetto, G. P. 1994, *A&A*, 285, 819
di Prospero, L. 1976, *Mem. Soc. Astron. Italiana*, 47, 255
Fernie, J. D., & McGonegal, R. 1983, *ApJ*, 275, 732
Freedman, W. L., & Madore, B. F. 2010, *ARA&A*, 48, 673
Hoyle, F., Shanks, T., & Tanvir, N. R. 2003, *MNRAS*, 345, 269
Kaltcheva, N. 2009, *PASP*, 121, 1326
Laney, C. D., & Caldwell, J. A. R. 2007, *MNRAS*, 377, 147
Lucas, P. W., et al. 2008, *MNRAS*, 391, 136
Lyngå, G. 1977, *A&A*, 54, 311
Madore, B. F. 1975, *A&A*, 38, 471
Macri, L. M., & Riess, A. G. 2009, *American Institute of Physics Conference Series*, 1170, 23
Majaess D. J., Turner D. G., Lane D. J., 2008, *MNRAS*, 390, 1539
Majaess, D. J., Turner, D. G., & Lane, D. J. 2009, *MNRAS*, 398, 263
Majaess, D. J., Turner, D. G., Lane, D. J., Henden, A., & Krajci, T. 2011, *JAAVSO*, 39, 122
Majaess, D. J., Turner, D. G., Lane, D. J., & Krajci, T. 2011, *JAAVSO*, 39, 217
McGonegal, R., McAlary, C. W., McLaren, R. A., & Madore, B. F. 1983, *ApJ*, 269, 641
Mermilliod, J. C., Mayor, M., & Burki, G. 1987, *A&AS*, 70, 389
Mermilliod, J. C., Mayor, M., & Udry, S. 2008, *A&A*, 485, 303
Minniti, D., et al. 2010, *New Astronomy*, 15, 433
Minniti, D., et al. 2011, *A&A*, 527, A81
Moffat, A. F. J., & Vogt, N. 1975, *A&AS*, 20, 155
Moni Bidin, C., Mauro, F., Geisler, D., et al. 2011, in press, *A&A*(arXiv:1109.1854)
Orsatti, A. M., Vega, E. I., & Marraco, H. G. 2001, *A&A*, 380, 130
Pietrzyński, G., & Gieren, W. 2004, *IAU Colloq. 193: Variable Stars in the Local Group*, 310, 87
Storm, J., Gieren, W., Fouqué, P., et al. 2011, *A&A*, 534, A94
Straizys, V., & Laugalys, V. 2008, *Baltic Astronomy*, 17, 253
Straizys, V., & Lazauskaitė, R. 2009, *Baltic Astronomy*, 18, 19
Tsarevsky, G. S., Ureche, V., & Efremov, Y. N. 1966, *Astronomicheskij Tsirkulyar*, 367, 1
Turner, D. G. 1976, *AJ*, 81, 1125
Turner, D. G., Forbes, D., & Pedreros, M. 1992, *AJ*, 104, 1132
Turner, D. G. 2010, *Ap&SS*, 326, 219
Turner, D. G. 2011, *RMxAA*, 47, 127
van Leeuwen, F. 2007, *A&A*, 474, 653

- van Leeuwen, F. 2009, *A&A*, 497, 209
van den Bergh, S., & Harris, G. L. H. 1976, *ApJ*, 208, 765
Walker, A. R. 1985, *MNRAS*, 213, 889

CHAPTER 6

ζ GEM CLUSTER

Discovery of the Host Cluster for the Fundamental Cepheid

Calibrator ζ Gem

Abstract: New and existing CORAVEL, $UBVJHK_s$, HST, HIP/Tycho, ARO, KPNO, and DAO observations imply that the fundamental Cepheid calibrator ζ Gem is a cluster member. The following parameters were inferred for ζ Gem from cluster membership and are tied to new spectral classifications (DAO) established for 26 nearby stars (e.g., HD 53588/B7.5 IV, HD 54692/B9.5 IV): $E_{B-V} = 0.02 \pm 0.02$, $\log \tau = 7.85 \pm 0.15$, and $d = 355 \pm 15$ pc. The mean distance to ζ Gem from cluster membership and six recent estimates (e.g., IRSB) is $d = 363 \pm 9(\sigma_{\bar{x}}) \pm 26(\sigma)$ pc. The results presented here support the colour-excess and HST parallax derived for the Cepheid by Benedict et al. (2007). Forthcoming precise proper motions (DASCH) and Chandra/XMM-Newton observations of the broader field may be employed to identify cluster members, bolster the cluster's existence, and provide stronger constraints on the Cepheid's fundamental parameters.

6.1 INTRODUCTION

An independent distance determination for ζ Gem is desirable because HST and HIP parallaxes for the classical Cepheid exhibit an unsatisfactory spread: $d = 358 - 422$ pc (Perryman & ESA, 1997; van Leeuwen et al., 2007; Benedict et al., 2007). Establishing reliable parameters for ζ Gem is particularly important given that the Carnegie Hubble and SH_0ES

projects (Macri & Riess, 2009; Freedman & Madore, 2010) are relying on HST calibrators (Benedict et al., 2007) to break degeneracies hindering the selection of a cosmological model (Riess et al., 2011). The Carnegie Hubble project will likewise employ Galactic calibrators tied to open clusters (Turner, 2010) with IRSB corroborated distances (Gieren et al., 2005; Storm et al., 2011). The classical Cepheid ζ Gem is the second longest period calibrator possessing a precise HST parallax (Benedict et al., 2002a, 2007), and a solid calibration for such stars is needed because longer-period Cepheids may be less affected by (insidious) photometric contamination (Macri et al., 2006, their Fig. 17). Moreover, longer-period Cepheids are detectable in distant galaxies because of their higher luminosity relative to shorter-period Cepheids (e.g., Gieren et al., 2009, their Fig. 1). Sampling remote galaxies in the Hubble flow mitigates uncertainties tied to peculiar velocity corrections and hence H_0 (Freedman et al., 2001, their Fig. 1).

In this study, CORAVEL, $UBVJHK_s$, HST, HIP/Tycho, KPNO and DAO spectroscopic observations are employed to identify stars potentially associated with ζ Gem, thereby permitting its fundamental properties to be deduced from cluster membership ($\log \tau$, E_{B-V} , $W_{VIc,0}$).

6.2 ANALYSIS

HIP/Tycho data were examined for stars surrounding ζ Gem that exhibit similar proper motions: $-10 < \mu_\alpha < -2$ mas/yr and $-7 < \mu_\delta < 2$ mas/yr (Perryman & ESA, 1997; van Leeuwen et al., 2007). Stars that display proper motions that deviate significantly from ζ Gem were eliminated via those limits. However, countless field stars likewise exhibit proper motions marginally offset from zero. The available proper motions could not be employed

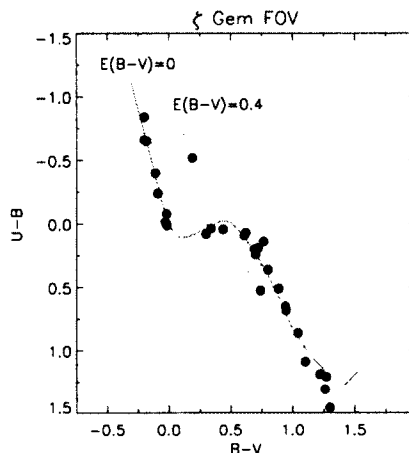


Figure 6.1 Colour-colour diagram for all stars $r \leq 4^\circ$ from ζ Gem with UBV photometry (Mermilliod, 1991). The field is comparatively unreddened. The intrinsic UBV relation and reddening law for the region were adopted from Turner (1976, 1989). Most objects in the diagram are not associated with ζ Gem. The uncertainties are smaller than the symbol size.

to substantiate the cluster’s existence given their uncertainties (Majaess et al., 2012, see their Fig. 3 for δ Cep). Stars redder than $B - V \simeq 0.14$ were culled to further mitigate field contamination (e.g., red clump giants). $UBVJHK_s$ photometry was tabulated for the remaining sample using the compilations of Mermilliod (1991), Perryman & ESA (1997), and Cutri et al. (2003).

6.2.1 REDDENING AND AGE

An analysis of all stars near ζ Gem with UBV photometry (Mermilliod, 1991) confirms that the field is comparatively unreddened (Fig. 6.1). The mean colour excess inferred from new DAO spectra (Fig. 6.2) for probable cluster members in Table 6.1 is $E(B - V) = 0.019 \pm 0.017$. The findings support the reddening determined for ζ Gem by Benedict et al. (2007).

The cluster age can be constrained by examining the spectral types of members near the turnoff. A distinct sequence of B-stars is visible in the BV and JH colour-magnitude

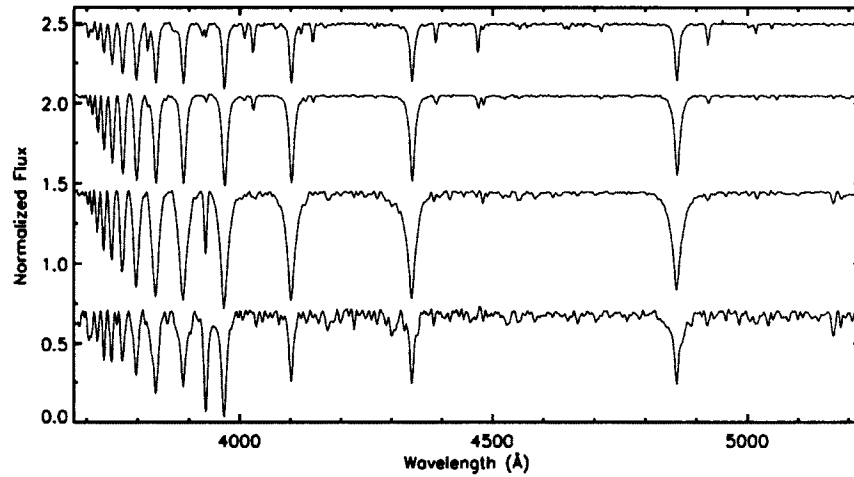


Figure 6.2 A subset of the new DAO spectra obtained for objects in the field of the classical Cepheid ζ Gem. From top to bottom the spectra correspond to HD 50767, HD 53588, HD 52474, and ζ Gem B.

diagrams (Fig. 6.3, $r \leq 2.5^\circ$ from ζ Gem). The stars HD 51102, HD 51353, HD 53588, and HD 55919 aggregate near the turnoff and have B6-B7 spectral classes (Table 6.1). For example, HD 53588 has UBV colours and a DAO spectrum consistent with spectral type B7.5 IV (Table 6.1). The star's radial velocity ($RV = 10 \pm 3$ km/s) is consistent with that established for ζ Gem ($RV \sim 7$ km/s). However, cluster membership cannot be established solely on the basis of consistent radial velocities because the predicted RV -distance gradient along $\ell \sim 197^\circ$ is shallow. Membership for the two earliest type stars examined is less certain (HD 50767, HD 51354, Table 6.1). A spectroscopic parallax for HD 50767 implies that the star is well behind the cluster. The spectroscopic and HIP parallaxes for HD 50767 disagree. The intrinsic colours for HD 51354 ($(B - V)_0 = -0.18$, $(U - B)_0 = -0.65$) and the DAO spectrum indicate that the star is a B3 Vne dwarf ($H\beta$ emission). A mean of the HIP parallaxes established for HD 51354 (Table 6.1) is consistent with that for ζ Gem ($\pi = 2.78 \pm 0.18$ mas, Benedict et al., 2007). The Perryman & ESA (1997) parallax for HD

51354 is $\pi = 2.57 \pm 0.81$ mas, whereas the revised HIP parallax is $\pi = 3.75 \pm 0.47$ mas (van Leeuwen et al., 2007). Spectroscopic parallaxes for emission-line stars (i.e., HD 51354) are unreliable.

A $\log \tau = 7.85 \pm 0.15$ Padova isochrone¹ provides the best match to the data (Fig. 6.3). The age agrees with that predicted for stars near the turnoff and the age inferred for ζ Gem from its pulsation period (Turner, 1996; Bono et al., 2005).

6.2.2 LOWER-MASS CLUSTER MEMBERS

Turner & Fernie (1978) noted that ζ Gem B (J2000 07:04:12.73, +20:34:21.3) may be associated with ζ Gem. The stars are separated by $r \simeq 1.4'$. A mean radial velocity was determined for ζ Gem B from six CORAVEL measurements obtained at l'Observatoire de Haut-Provence (OHP).² The radial velocities acquired from the OHP span the interval -16.2 to 36.9 km/s, with a mean of 9.9 km/s. ζ Gem B is thus a spectroscopic binary because the uncertainty tied to an individual measurement is ± 1.4 km/s. The mean radial velocity matches that established for the Cepheid, to within the uncertainties. However, as noted in §6.2.1, the shallow radial velocity-distance gradient along the line of sight requires that cluster membership be secured by independent means. *UBV* photometry by Fernie (1969) indicates that ζ Gem B is an F-type star (Turner & Fernie, 1978). That is corroborated by the 2MASS colours for the object ($(J-H) = 0.206$, $(H-K) = 0.056$), which are indicative of an unreddened F5-F8 V star (Straizys & Lazauskaitė, 2009). A spectrogram of the star was acquired on HJD = 2444122.995 with the 2.1-m telescope at Kitt Peak. That spectrogram and a DAO spectrum confirm that ζ Gem B is an F4 V dwarf (Table 9.1, Fig. 6.2). The

¹<http://pleiadi.pd.astro.it/>

²M. Mayor kindly obtained CORAVEL observations of ζ Gem B for D. Turner.

result is supported by Benedict et al. (2007), who classified the star as F3.5 V. The spectral type and luminosity class for ζ Gem B are consistent with what is expected for a cluster member at the star's location in the BV and JH colour-magnitude diagrams (Fig. 6.3).

DAO spectra were obtained for two additional stars in close proximity to ζ Gem ($r < 6'$). The spectral type and luminosity class for 2MASS 07041267+2030196 are consistent with what is expected for a cluster member at the star's location in the BV and JH colour-magnitude diagrams (Fig. 6.3, Table 9.1). The same is true for 2MASS 07035262+2035162. Benedict et al. (2007) inferred a similar classification for 2MASS 07035262+2035162 (F6 V). Four additional stars in close proximity to ζ Gem have multiband photometry consistent with late-type (potential) cluster members. New BV observations for those stars were acquired from the Abbey Ridge Observatory (ARO, Lane, 2008; Majaess et al., 2008). The data were processed via ARAP (Lane, 2008) and DAOPHOT (Stetson, 1987), and subsequently standardized to photometry obtained from the New Mexico State University 1-m telescope (T. Harrison priv. communication, see also Benedict et al. 2007). The following equations were derived to place the instrumental ARO photometry on the Johnson system:

$$B - V = (0.99 \pm 0.06) \times (b - v) - (0.57 \pm 0.08)$$

$$V - v = -0.86 \pm 0.02$$

Observations from the AAVSO's Bright Star Monitor (BSM) provided additional data for ζ Gem B and 2MASS 07041267+2030196. The BSM is located at the Astrokolkhoz telescope facility near Cloudcroft, New Mexico.

HST WFC3 images (HST Proposal 12215, Evans, 2009) reveal a star $15''$ west of the Cepheid at J2000 07:04:05.5, +20:34:12.0. The object was identified after subtracting (nor-

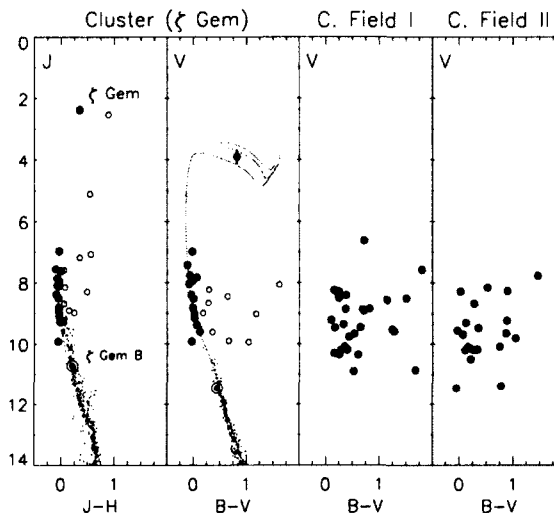


Figure 6.3 Left to right, JH and BV colour-magnitude diagrams for HIP/Tycho stars with $r \leq 2.5^\circ$ of ζ Gem exhibiting $-10 < \mu_\alpha < -2$ mas/yr and $-7 < \mu_\delta < 2$ mas/yr. An early type cluster sequence is absent from the comparison fields (panels 3, 4, HIP/Tycho), which encompass $r \leq 4^\circ$. Small dots denote calibration stars from Majaess et al. (2011), which were employed to tie the cluster distance to a geometrically anchored scale (van Leeuwen, 2009; Majaess et al., 2011). Open circles are likely field stars. In panel 2 a Padova $\log \tau = 7.85$ isochrone is shown. ζ Gem (amplitude variation indicated) and its companion ζ Gem B (circled dot) is the brightest cluster member.

malized) the ζ Gem image from a master, which was constructed (median combine) using Cepheids observed for proposal 12215. The object displays a signal-to-noise ratio greater than 20 in both WFC3 images. However, N. Evans (private communication) noted that the star’s photometry is not consistent with cluster membership.

Later-type stars associated with ζ Gem may exhibit X-ray emission (Evans, 2011). Additional observations are required to assess the candidates (e.g., Chandra/XMM-Newton). The objects are not in the ROSAT catalogs.

6.2.3 CLUSTER DISTANCE

A precise cluster distance may be determined because the reddening, age, and chemical composition of the sample are constrained ($[\text{Fe}/\text{H}]_{\zeta\text{Gem}} \simeq 0$, Luck et al., 2011). The magnitude shift required to overlay the intrinsic relation upon the data yields $d = 355 \pm 15$

pc (Fig. 6.3). The zero-point is tied to seven benchmark open clusters ($d < 250$ pc) that exhibit matching JHK_s and revised HIP distances (e.g., the Hyades, α Per, Coma Ber, van Leeuwen, 2009; Majaess et al., 2011). A redetermination of the HST parallax for the Hyades supports that scale (McArthur et al., 2011). The scale employed here is anchored to clusters where consensus exists, rather than to the discrepant case (i.e., the Pleiades). A ratio of total to selective extinction R_J was adopted from Majaess et al. (2011c) (see also Bonatto et al., 2004); whereas a value for R_V was adopted from Turner (1976). Deviations from the canonical reddening law are mitigated because the field is comparatively unreddened (Fig. 6.1, note that $V_0 = V - E_{B-V} \times R_V$).

A mean distance inferred from potential members with revised HIP parallaxes is $d = 366 \pm 57(\sigma_{\bar{x}}) \pm 196(\sigma)$ pc. Certain stars were excluded from the derivation because they have uncertainties greater than the cited parallax, deviate significantly from the mean, or have negative parallaxes (e.g., HD 49824, $\pi = -0.74 \pm 0.89$ mas). Stars with spectral types inconsistent with cluster membership were likewise removed (e.g., HD 50767, §6.2.1).

Three HIP parallaxes exist for ζ Gem: $\pi = 2.79 \pm 0.81$ mas, 2.37 ± 0.30 mas, and 2.71 ± 0.17 mas (Perryman & ESA, 1997; van Leeuwen, 2007; van Leeuwen et al., 2007). The results inferred from cluster membership and HST observations for ζ Gem ($\pi = 2.78 \pm 0.18$ mas, Benedict et al., 2007) support the van Leeuwen et al. (2007) HIP determination. Distances to ζ Gem are also available from the infrared surface brightness technique ($d = 386 \pm 9$ pc, Storm et al., 2011) and the PTI (Palomar Testbed Interferometer, $d = 336 \pm 44$ pc, Lane et al., 2000, and references therein). A straight mean of the 6 (+2 cluster-based) estimates for ζ Gem yields $d = 363 \pm 9(\sigma_{\bar{x}}) \pm 26(\sigma)$ pc. A weighted mean of $d = 368$ pc

Table 6.1. Stars Near ζ Gem

ID	V	$B - V$	$U - B$	J	H	K_s	SpT	π (P97)	π (V07)
ζ Gem	3.90	0.82	-	2.38	2.03	2.14	-	2.79 ± 0.81	2.37 ± 0.30
HD 49381	6.80	0.01	-	6.66	6.70	6.65	A0 III	3.87 ± 0.96	3.12 ± 0.47
HD 50634	6.98	-0.02	-	6.96	7.00	6.96	B9.5 II	2.41 ± 0.98	3.91 ± 0.60
HD 51354	7.12	-0.18	-0.65	7.20	7.18	7.05	B3 Vnne	2.57 ± 0.81	3.75 ± 0.47
HD 53588	7.20	-0.11	-0.40	7.33	7.44	7.44	B7.5 IV	4.67 ± 0.87	3.96 ± 0.56
HD 51102	7.42	-0.12	-	7.56	7.66	7.70	B6 V	0.36 ± 1.00	1.59 ± 0.52
HD 55919	7.43	-0.09	-	7.60	7.68	7.72	B7 IV-V	3.98 ± 0.79	3.86 ± 0.60
HD 52372	7.58	0.03	-	7.42	7.45	7.43	A1 III	1.94 ± 0.93	2.17 ± 0.86
HD 50767	7.70	-0.20	-0.84	8.09	8.20	8.25	B2 V	2.15 ± 1.01	2.52 ± 0.74
HD 51353	7.76	-0.07	-	7.86	7.93	7.92	B7 V	2.00 ± 0.94	3.22 ± 0.64
HD 52474	7.83	0.06	-	7.62	7.62	7.59	A2 V	3.07 ± 1.02	2.79 ± 0.66
HD 52422	7.93	-0.01	-	7.95	7.98	7.97	B9 IV	2.03 ± 1.10	3.65 ± 0.86
HD 52371	8.00	-0.07	-	8.12	8.16	8.23	B7 V:	1.43 ± 0.97	1.13 ± 0.83
HD 50509	8.04	-0.08	-	8.09	8.16	8.16	B8 V	-1.28 ± 1.06	0.88 ± 0.72
HD 57070	8.14	-0.04	-	8.19	8.25	8.24	B9 IV	1.07 ± 1.05	1.26 ± 0.66
HD 54404	8.40	-0.05	-	8.38	8.47	8.45	B9 IV	3.12 ± 1.05	1.49 ± 0.86
HD 54692	8.52	0.00	-	8.49	8.54	8.53	B9.5 IV	3.29 ± 1.12	2.26 ± 0.84
HD 50107	8.84	-0.01	-	8.83	8.80	8.78	-	-	-
HD 53230	8.84	0.09	-	8.59	8.54	8.51	-	1.92 ± 1.24	2.56 ± 1.02
HD 53288	8.84	-0.02	-0.08	8.81	8.85	8.84	B9.5 V	2.29 ± 1.05	1.53 ± 0.83
HD 50164	8.94	-0.07	-	8.91	8.96	8.92	B9 Vnn	3.82 ± 1.33	3.34 ± 1.19
HD 49824	8.97	0.10	-	8.70	8.66	8.67	-	0.33 ± 1.25	-0.74 ± 0.89
HD 263791	8.98	-0.05	-	8.99	9.12	9.06	B9 V	0.38 ± 1.36	0.17 ± 1.24
HD 51187	9.02	0.02	-	8.93	8.97	8.92	A0 V	-	-
HD 53473	9.16	0.02	-	9.09	9.13	9.07	A0 V	0.92 ± 1.18	0.30 ± 0.99
HD 51971	9.38	0.06	-	9.28	9.30	9.22	A1 V	-	-
TYC 1352-582-1	9.60	0.12	-	9.26	9.22	9.15	-	-	-
BD+18° 1470	9.92	-0.03	-	9.92	9.97	9.98	B9.5 VpCr-Eu	-	-
ζ Gem B	11.47	0.42:	-	10.72	10.51	10.46	F4 V	-	-
07:03:23.1 +20:37:59.5	11.71	0.38:	-	11.06	10.87	10.85	-	-	-
07:04:12.7 +20:30:19.7	11.83	0.57:	-	10.79	10.49	10.44	F6 V	-	-
07:03:38.7 +20:40:59.0	12.00	0.59:	-	10.95	10.68	10.61	-	-	-
07:03:52.6 +20:35:16.3	12.34	0.54:	-	11.37	11.11	11.06	F7 V	-	-
07:04:28.6 +20:34:47.3	12.37	0.53:	-	11.46	11.24	11.17	-	-	-
07:04:40.4 +20:35:13.1	12.45	0.46:	-	11.66	11.51	11.47	-	-	-

¹Stars classified by D. Turner (DAO spectrum).

²The star ζ Gem B is a spectroscopic binary (§6.2.2). Benedict et al. (2007) classified ζ Gem B as F3.5 V.

³Perryman & ESA (1997, P97), van Leeuwen (2007, V07).

⁴van Leeuwen et al. (2007) cite $\pi = 2.71 \pm 0.17$ mas for ζ Gem.

was obtained by assigning unit weights to the HIP and PTI estimates, and double weights for the rest.

6.3 CONCLUSION AND FUTURE RESEARCH

The evidence indicates that the 10^d classical Cepheid calibrator ζ Gem belongs to a newly identified cluster (Fig. 6.3). Potential members were identified on the basis of new and existing CORAVEL, $UBVJHK_s$, HST, HIP/Tycho, KPNO and DAO ($n = 26$) spectroscopic observations. The analysis indicates that the field is comparatively unreddened (Fig. 6.1), with ζ Gem reddened by $E(B - V) = 0.019 \pm 0.017$ (§6.2.1). The age and distance were

inferred from spectroscopic and multiband $UBVJHK_s$ analyses of cluster stars, yielding $\log \tau = 7.85 \pm 0.15$ and $d = 355 \pm 15$ pc (Fig. 6.3). The results support the parameters derived for ζ Gem by Benedict et al. (2007). However, the breadth of the standard deviation tied to several recent estimates for ζ Gem is unsatisfactory (§6.2.3, $d = 363 \pm 9(\sigma_{\bar{x}}) \pm 26(\sigma)$), and continued research is required. CORAVEL, KPNO, and DAO observations indicate that ζ Gem B is an F-type spectroscopic binary. DAO spectra were likewise obtained for two other low-mass members in close proximity to ζ Gem. Additional observations are required to highlight *bona fide* members on the candidate list (Table 6.1). Those stars are potential members pending further evidence. Membership identification may be facilitated by obtaining precise proper motions for fainter stars near ζ Gem from photographic plates stored at the CfA (Grindlay, 2007, DASCH).³ The plates offer multi-epoch coverage spanning a ~ 100 year baseline, and uncertainties are further mitigated because of sizable statistics ($\sim (5 - 10) \times 10^2$ plates per object). Searching for X-ray emission from low-mass stars near ζ Gem is likewise a useful pursuit for corroborating membership (Evans, 2011; Evans et al., 2011). However, the star Polaris B is of a similar spectral type to ζ Gem B (Turner, 1977) and does not exhibit X-ray emission (Evans et al., 2010).

At least two classical Cepheids with HST parallaxes are cluster members (δ Cep and ζ Gem, de Zeeuw et al., 1999; Majaess et al., 2012). Cluster membership provides a means to secure independent fundamental parameters ($\log \tau$, E_{B-V} , $W_{V I_c, 0}$, $\log L_*/L_\odot$, M_V). The results will complement a suite of diverse efforts with a common objective to reduce uncertainties associated with H_0 in order to constrain cosmological models (Feast, 2008; Shappee & Stanek, 2011; Gerke et al., 2011; Ngeow, 2011, 2012; Steer & Madore, 2011).

³Digital Access to a Sky Century @ Harvard (DASCH), <http://hea-www.harvard.edu/DASCH/>

REFERENCES

- Benedict, G. F., McArthur, B. E., Fredrick, L. W., et al. 2002, *AJ*, 124, 1695
- Benedict G. F. et al., 2007, *AJ*, 133, 1810
- Bonatto, C., Bica, E., & Girardi, L. 2004, *A&A*, 415, 571
- Bono, G., Marconi, M., Cassisi, S., et al. 2005, *ApJ*, 621, 966
- Cutri, R. M., et al. 2003, The IRSA 2MASS All-Sky Point Source Catalog, NASA/IPAC Infrared Science Archive.
- de Zeeuw, P. T., Hoogerwerf, R., de Bruijne, J. H. J., Brown, A. G. A., & Blaauw, A. 1999, *AJ*, 117, 354
- Dias, W. S., Alessi, B. S., Moitinho, A., & Lépine, J. R. D. 2002, *A&A*, 389, 871
- Evans, N. 2009, HST Proposal, 12215
- Evans, N. R., Guinan, E., Engle, S., et al. 2010, *AJ*, 139, 1968
- Evans, N. R. 2011, IAU Symposium, 272, 537
- Evans, N. R., DeGioia-Eastwood, K., Gagné, M., et al. 2011, *ApJS*, 194, 13
- Feast, M. W. 2008, First Middle East-Africa, Regional IAU Meeting, held 5-10 April, 2008 in Cairo, Egypt (arXiv:0806.3019).
- Fernie, J. D. 1969, *JRASC*, 63, 133
- Freedman, W. L., Madore, B. F., Gibson, B. K., et al. 2001, *ApJ*, 553, 47
- Freedman, W. L., & Madore, B. F. 2010, *ARA&A*, 48, 673
- Gerke, J. R., Kochanek, C. S., Prieto, J. L., Stanek, K. Z., & Macri, L. M. 2011, *ApJ*, 743, 176
- Gieren, W., Pietrzyński, G., Soszyński, I., et al. 2005, *ApJ*, 628, 695
- Gieren, W., Pietrzyński, G., Soszyński, I., et al. 2009, *ApJ*, 700, 1141
- Grindlay, J. E. 2007, The Central Engine of Active Galactic Nuclei, 373, 711
- Lane, B. F., Kuchner, M. J., Boden, A. F., Creech-Eakman, M., & Kulkarni, S. R. 2000, *Nature*, 407, 485
- Lane, D. J. 2008, *JAAVSO*, 36, 143
- Luck, R. E., Andrievsky, S. M., Kovtyukh, V. V., Gieren, W., & Graczyk, D. 2011, *AJ*, 142, 51
- Macri, L. M., Stanek, K. Z., Bersier, D., Greenhill, L. J., & Reid, M. J. 2006, *ApJ*, 652, 1133
- Macri, L. M., & Riess, A. G. 2009, American Institute of Physics Conference Series, 1170, 23
- Majaess, D. J., Turner, D. G., Lane, D. J., & Moncrieff, K. E. 2008, *JAAVSO*, 36, 90
- Majaess, D. J., Turner, D. G., Lane, D. J., & Krajci, T. 2011 (a), *JAAVSO*, 39, 219
- Majaess, D., Turner, D., Moni Bidin, C., et al. 2011 (b), *ApJ*, 741, L27
- Majaess, D. J., Turner, D. G., & Gieren, W. 2012, *ApJ*, in press (arXiv:1201.0993)
- McArthur, B. E., Benedict, G. F., Harrison, T. E., & van Altena, W. 2011, *AJ*, 141, 172
- Mermilliod, J-C. 1991, Homogeneous Means in the UBV System, Vizier catalog.

-
- Ngeow, C.-C. 2011, Proceeding submitted for the 9th Pacific Rim Conference on Stellar Astrophysics (PRCSA2011), Lijiang, China, April 2011 (arXiv:1111.2094)
- Ngeow, C.-C. 2012, ApJS, in press (arXiv:1202.0339)
- Paunzen, E. 2008, Contributions of the Astronomical Observatory Skalnaté Pleso, 38, 435
- Perryman, M. A. C., & ESA 1997, ESA Special Publication, 1200
- Riess, A. G., Macri, L., Casertano, S., et al. 2011, ApJ, 730, 119
- Shappee, B. J., & Stanek, K. Z. 2011, ApJ, 733, 124
- Skiff, B. 2010, General Catalogue of Stellar Spectral Classifications, Vizier catalog.
- Steer, I., Madore, B. 2011, NED-D: A Master List of Redshift-Independent Extragalactic Distance, <http://ned.ipac.caltech.edu/Library/Distances/>
- Stetson, P. B. 1987, PASP, 99, 191
- Storm, J., Gieren, W., Fouqué, P., et al. 2011, A&A, 534, A94
- Straižys, V., & Lazauskaitė, R. 2009, Baltic Astronomy, 18, 19
- Turner, D. G. 1976, AJ, 81, 1125
- Turner, D. G. 1977, PASP, 89, 550
- Turner, D. G., & Fernie, J. D. 1978, Information Bulletin on Variable Stars, 1509, 1
- Turner, D. G. 1989, AJ, 98, 2300
- Turner, D. G. 1996, JRASC, 90, 82
- Turner, D. G. 2010, Ap&SS, 326, 219
- van Leeuwen, F., Feast, M. W., Whitelock, P. A., & Laney, C. D. 2007, MNRAS, 379, 723
- van Leeuwen, F. 2007, A&A, 474, 653
- van Leeuwen, F. 2009, A&A, 497, 209

CHAPTER 7

R CRU/NGC4349

Strengthening the Open Cluster Distance Scale via VVV Photometry

Abstract: Approximately 14% of known Galactic open clusters have absolute errors $\leq 20\%$ as evaluated from $n \geq 3$ independent distance estimates, and the statistics for age estimates are markedly worse. That impedes such diverse efforts as calibrating standard candles and constraining masses for substellar companions. New data from the VVV survey may be employed to establish precise cluster distances with comparatively reduced uncertainties ($\leq 10\%$). That is illustrated by deriving parameters for Pismis 19 and NGC 4349, two pertinent open clusters which hitherto have sizable uncertainties (60%). Fundamental parameters determined for Pismis 19 from new VVV JHK_s photometry are $d = 2.40 \pm 0.15$ kpc, $\langle E_{J-H} \rangle = 0.34 \pm 0.04$, and $\log \tau = 9.05 \pm 0.10$, whereas for NGC 4349 the analysis yields $d = 1.63 \pm 0.13$ kpc, $E_{J-H} = 0.09 \pm 0.02$, and $\log \tau = 8.55 \pm 0.10$. The results exhibit a significant ($\geq 5\times$) reduction in uncertainties and indicate that: *i*) existing parameters for the substellar object NGC 4349 127b require revision, in part because the new cluster parameters imply that the host star is 20% less-massive ($\mathcal{M}_*/\mathcal{M}_\odot \simeq 3.1$); *ii*) R Cru is not a member of NGC 4349 and should be excluded from period-Wesenheit calibrations that anchor the distance scale; *iii*) and results for Pismis 19 underscore the advantages gleaned from employing deep VVV JHK_s data to examine obscured ($A_V \simeq 4$) and differentially reddened intermediate-age clusters.

7.1 INTRODUCTION

Approximately 30% of the 395 open clusters with $n \geq 3$ independent distance estimates exhibit absolute errors $\geq 20\%$ (Paunzen & Netopil, 2006, their Fig. 2). There are $\geq 2 \times 10^3$ catalogued Galactic open clusters (Dias et al., 2002), implying that merely $\sim 14\%$ of the known sample have errors $\leq 20\%$ as evaluated by three distance estimates. The uncertainties permeate into analyses that rely on the cluster zero-point, such as the calibration of any constituent standard candles or substellar companions (Lovis & Mayor, 2007; Majaess et al., 2011c). Consider that published parameters for NGC 4349 span $d = 900 - 2200$ pc and $\tau = 0.1 - 0.6$ Gyr (§7.3.2). Yet physical parameters for the substellar companion to TYC 8975-2601-1 (Lovis & Mayor, 2007; Kashyap et al., 2008) rely on those inferred for the host from cluster membership (NGC 4349). Furthermore, the nearer distance and younger age for NGC 4349 potentially imply cluster membership for the classical Cepheid *R Cru*, which lies within the cluster corona. Establishing cluster membership would enable the subsequent calibration of Cepheid period-luminosity and period-Wesenheit relations (Turner, 2010). Such functions support efforts to establish extragalactic distances and solidify the zero-point for the SNe Ia scale (e.g., Pietrzyński & Gieren, 2004). The examples underscore the broad ramifications of an uncertain cluster distance scale. Admittedly, age estimates for open clusters are less reliable because a third exhibit absolute errors $> 50\%$ (Paunzen & Netopil, 2006, $n \geq 3$), and presumably the statistics worsen for obscured clusters near the Galactic plane.

In this study, new VVV (VISTA Variables in the Vía Láctea) JHK_s photometry is employed to illustrate the marked improvement that can be achieved *vis à vis* open cluster

distances. Two important clusters possessing particularly discrepant published parameters are examined, namely Pismis 19 and NGC 4349. Distances for the clusters display a $\sim 60\%$ spread with individual uncertainties of $\sim 30\%$. Efforts to secure precise parameters for Pismis 19 via optical photometry have been complicated by differential reddening and $A_V \simeq 4$ magnitudes of obscuring dust. Parameters for Pismis 19 and NGC 4349 derived here exhibit a marked ($> 5\times$) reduction in uncertainties (§7.3), and highlight the advantages of using VVV data to determine reliable cluster distances and compliment existing efforts.

7.2 VVV PHOTOMETRY

The VVV survey aims to establish precise multi-epoch JHK_s photometry for fields in the Galactic bulge and near the Galactic plane ($\ell = 295^\circ - 10^\circ$, Minniti et al., 2010; Catelan et al., 2011; Saito et al., 2011). VVV images exhibit increased angular resolution relative to 2MASS, and extend ~ 4 magnitudes fainter for Galactic disk stars. The deep JHK_s photometry facilitates isochrone fitting by revealing the target cluster’s evolutionary morphology, which is particularly important when investigating highly reddened clusters. The VVV survey will provide standardized (2MASS) JHK_s photometry for stars in $\geq 3 \times 10^2$ open clusters and ≥ 39 globular clusters (e.g., M28). Details of the pipeline constructed to process and extract the VVV photometry employed here are discussed in Mauro et al. (2012, in preparation). PSF photometry was performed using DAOPHOT and subsequently tied to 2MASS JHK_s standards (Fig. 7.1, see also Moni Bidin et al., 2011). However, as with any nascent large scale survey, adjustments to the zero-point may occur as improvements and systematic errors are identified.

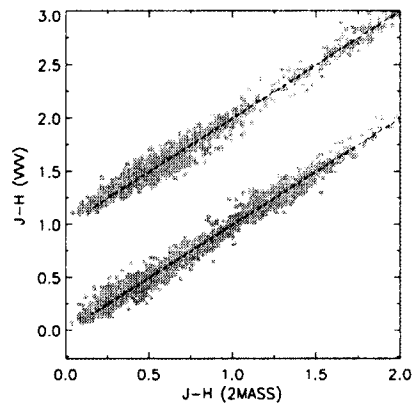


Figure 7.1 A comparison between 2MASS and VVV $J-H$ photometry for the regions encompassing Pismis 19 and NGC 4349. A 1:1 correlation (red line) exists to within the uncertainties. The data for Pismis 19 were deliberately offset from zero for presentation purposes. Pertinent details regarding the pipeline employed here to process the VVV data are described in Moni Bidin et al. (2011) and Mauro et al. (2012, in preparation.).

7.2.1 THE ADVANTAGES OF JHK_s PHOTOMETRY

Precise JHK_s observations of stellar clusters are desirable because total and differential reddening are less deleterious than in the optical ($A_J \simeq 0.2 \times A_V$). Sizable extinction may shift a significant fraction of the main-sequence near/beyond the limiting magnitude where uncertainties are largest. Consider that merely $\sim 3^m$ of the cluster sequence for Pismis 19 was sampled in existing optical surveys because of significant reddening, which subsequently complicated efforts to make an accurate zero-age main-sequence (ZAMS) fit. The JHK_s reddening vector provides direct solutions for the intrinsic colours of stars across much of the main-sequence. The JHK_s reddening vector can be determined from red clump stars along the line of sight (Straižys & Laugalys, 2008; Majaess et al., 2011c), and the ratio of total-to-selective extinction can be inferred in certain instances using red clump stars via the variable extinction method (e.g., Majaess et al., 2011c). Straižys & Laugalys (2008)

demonstrated that $E(J - H)/E(H - K_s)$ is (rather) constant for dust occupying the inner Galaxy. A consensus exists that any variations in the infrared would be marginal relative to those expected for the optical.

JHK_s photometry is particularly suited for detecting and characterizing the heavily obscured pre-main-sequence population of young clusters (Bonatto & Bica, 2010). For later-type stars, JHK_s photometry is relatively insensitive to variations in chemical composition (e.g., the Hyades anomaly, Turner, 1979; Majaess et al., 2011, see also Straižys & Lazauskaitė 2009). That claim is supported in part by the establishment of seven benchmark open clusters ($d < 250$ pc) that exhibit matching JHK_s ZAMS and revised Hipparcos distances (the Hyades, α Per, Praesepe, Coma Ber, IC 2391, IC 2609, and NGC 2451, van Leeuwen, 2009; Majaess et al., 2011). The zero-point of the Padova isochrone employed (§7.3) matches that scale, to within the uncertainties. Isochrones, models, and the distance scale should be anchored and evaluated using clusters where consensus exists, rather than for the discrepant case (i.e., the Pleiades). The 2MASS survey provides invaluable all-sky JHK_s photometric standards. A similar survey tied to Johnson-Cousins $UBVRI$ photometry is desirable. U -band photometry is particularly challenging to standardize and zero-point errors are common (§7.3.2, see also Cousins & Caldwell, 2001). However, UBV colour-colour analyses permit crucial dereddening for younger stars.

In summary, the VVV survey is aptly tailored to foster cluster research (Minniti et al., 2011; Borissova et al., 2011; Moni Bidin et al., 2011; Majaess et al., 2011c). Admittedly, acquiring precise and standardized $UBVJHK_s$ photometry is ideal, and enables the characterization of potential systemic errors. UBV data by Turner and Forbes (unpublished) and

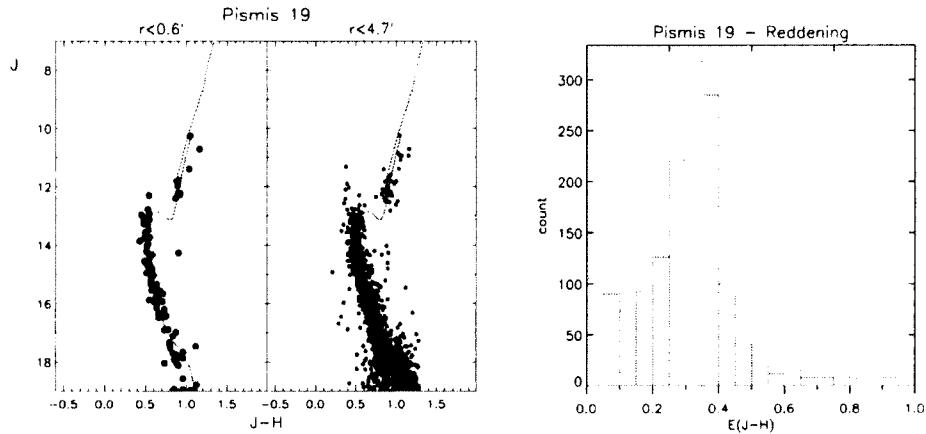


Figure 7.2 VVV colour-magnitude diagrams for Pismis 19 at varying radii. JHK_s Padova isochrones (Bonatto et al., 2004) were employed. Individual reddenings were determined via the approach outlined in §7.3.1. Photometric errors and binary contamination artificially broaden the breadth of the differential reddening.

Carraro (2011) are employed to corroborate parameters determined via VVV photometry.

7.3 ANALYSIS

7.3.1 PISMIS 19

Pismis 19 is a heavily reddened open cluster (Piatti et al., 1998; Carraro & Munari, 2004). The cluster’s non-symmetric appearance in optical images is indicative of differential reddening. Piatti et al. (1998) and Carraro & Munari (2004) acquired BVI photometry for Pismis 19 stars. However, separate conclusions were reached regarding the cluster’s fundamental parameters. Piatti et al. (1998) found $E(B - V) = 1.45 \pm 0.10$, $d = 2.40 \pm 0.88$ kpc, and $\tau = 1.0 \pm 0.2$ Gyr, whereas Carraro & Munari (2004) obtained $E(B - V) = 1.48 \pm 0.15$, $d = 1.5 \pm 0.4$ kpc, and $\tau \simeq 0.8$ Gyr. The reddenings and distances agree to within the mutual uncertainties, however the individual uncertainties are large because of the challenging task of analyzing highly obscured clusters solely via optical photometry. Carraro (2011) built upon analyses by Piatti et al. (1998) and Carraro & Munari (2004) by obtaining deeper

photometry, and derived $d = 2.5 \pm 0.5$ kpc.

Individual reddenings for stars in Pismis 19 were determined as follows. Any point on the dereddening line (dl) for the i^{th} star is given by: $(J - H)_i = E_{J-H}/E_{H-K_s} \times (H - K_s)_i + b$; $b = (J - H)_i - E_{J-H}/E_{H-K_s} \times (H - K_s)_i$; $(J - H)_{dl} = E_{J-H}/E_{H-K_s} \times (H - K_s)_{dl} + b$. The intersect between the dereddening line and the intrinsic relation was determined by minimizing the difference as a function of $(H - K_s)_0$: $|(J - H)_{dl} - (J - H)_{0,z}| = E_{J-H}/E_{H-K_s} \times (H - K_s)_{0,z} + (J - H)_i - E_{J-H}/E_{H-K_s} \times (H - K_s)_i - (J - H)_{0,z}$. The reddening vector (E_{J-H}/E_{H-K_s}) characterizing dust along the line of sight was derived by tracking deviations of red clump stars from their mean intrinsic colour because of extinction. The mean intrinsic colour was adopted from Majaess et al. (2011c), who inferred the result from nearby red clump stars ($d \leq 50$ pc) with revised Hipparcos parallaxes (van Leeuwen et al., 2007). The reddening vector determined from red clump stars is $E(J-H)/E(H-K_s) = 2.02$. That result agrees with a determination for the region from 2MASS photometry (Straizys & Laugalys, 2008). A reddening diagram was subsequently compiled (Fig. 7.2), with the mean reddening being $\langle E(J-H) \rangle = 0.34 \pm 0.04$. Cluster main-sequence stars display a turnoff near spectral type F2 according to the intrinsic JHK_s relation of Straizys & Lazauskaitė (2009).

A colour-magnitude diagram was compiled for Pismis 19 stars surrounding J2000 coordinates of 14:30:40.54, -60:53:32.2 (Fig. 7.2).¹ A $\log \tau = 9.05 \pm 0.10$ Padova isochrone (Bonatto et al., 2004) was adopted based on the reddening and spectral types inferred (Fig. 7.2), and because that age provides an evolutionary track that matches cluster members ranging from \sim M0 dwarfs to evolved stars. A precise fit was obtained through several factors.

¹The coordinates cited for the cluster centre in Simbad require updating.

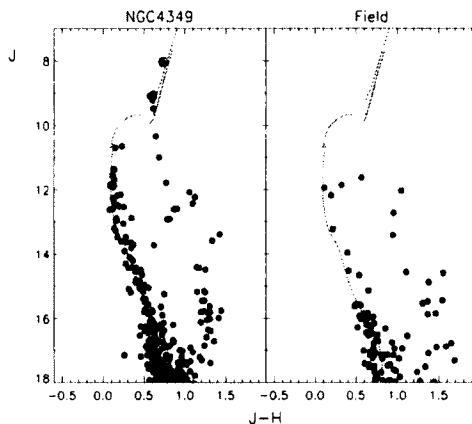


Figure 7.3 Colour-magnitude diagrams constructed for NGC 4349 and an adjacent comparison field using VVV/2MASS JHK_s photometry. The circled dot near the tip of the giant branch is TYC 8975-2606-1, which hosts a substellar companion (Lovis & Mayor, 2007). To reduce contamination the CMDs contain stars within $r < 1.2'$. Seven evolved red stars beyond that radius were added to the CMD for NGC 4349.

First, two of three free parameters associated with isochrone fitting were constrained by the colour-colour analysis, namely the reddening and age (spectral type at the turnoff). The remaining parameter (excluding metallicity) is the shift required in magnitude space to overlay the isochrone upon the data. The best fit and uncertainties were established via the traditional visual approach (e.g., Carraro & Munari, 2004; Bonatto & Bica, 2010), and the latter represents the limit where a mismatch is clearly perceived. Paunzen & Netopil (2006, and references therein) note that errors tied to isochrone fitting via computer algorithms are comparable to those associated with the traditional approach. Secondly, field star contamination was reduced because the surface density of cluster members is an order of magnitude larger, and furthermore, cluster members occupy a heavily reddened locus separated from less-reddened field stars (Fig. 7.2). Lastly, deep VVV photometry provided excellent anchor points for isochrone fitting.

The final parameters for Pismis 19 are $d = 2.40 \pm 0.15$ kpc, $\langle E(J - H) \rangle = 0.34 \pm 0.04$,

and $\log \tau = 9.05 \pm 0.10$. The distance is tied to a ratio of total to selective extinction (R) derived by Majaess et al. (2011) (see also Bonatto et al., 2004, and references therein). The distance derived here agrees with the latest estimate from optical photometry (Carraro, 2011).

7.3.2 NGC 4349

Kholopov (1956) and Kraft (1957) noted that the 5.8^d classical Cepheid *R Cru* may be a member of NGC 4349. That assessment was based in part on the Cepheid's proximity and brightness relative to cluster members. Cepheids are typically among the brightest members of their host clusters. Lohmann (1961) employed *UBV* photographic photometry to derive cluster parameters of $d = 1700$ pc and $\tau = 600$ Myr. Fernie (1963) obtained photoelectric *BV* photometry from the Cape Observatory and established a cluster distance of $d = 900$ pc for $E(B - V) = 0.31$. The distance to NGC 4349 cited by Fernie (1963) is approximately half that derived by Lohmann (1961). Fernie (1963) concluded that *R Cru* is unassociated with NGC 4349 because the Cepheid lies towards the cluster's periphery. Cluster Cepheids known during that era had been discovered near the cluster centre (e.g., *S Nor* in NGC 6087). Incidentally, the distance to NGC 4349 established by Fernie (1963) is consistent with that inferred for *R Cru* from present day period-Wesenheit relations (Benedict et al., 2007; Majaess et al., 2011c). Lindoff (1968) revised the Lohmann (1961) age estimate for NGC 4349 downward to $\log \tau = 8.04$. Loktin & Matkin (1994) computed the following properties for NGC 4349 based on a reanalysis of existing photometry: $d = 2176$ pc, $E(B - V) = 0.384$, and $\log \tau = 8.315$. In sum, established distances to NGC 4349 span the range $d = 900 - 2200$ pc.

A reddening vector of $E(J - H)/E(H - K_s) = 2.04$ was determined from red clump stars along the line of sight (see also Straižys & Laugalys, 2008). The reddening vector was subsequently adopted to establish a reddening of $E(J-H) = 0.09 \pm 0.02$. Stars catalogued by Lohmann (1961) as likely cluster members were employed to derive that result. New photoelectric *UBV* photometry² obtained for stars in NGC 4349 were likewise used to constrain the cluster reddening and age. A comparison of the photoelectric *UBV* photometry and the photographic photometry of Lohmann (1961) reveals that the latter is offset from the standard system by $B - V = (1.02 \pm 0.02) \times (B - V)_{L61} - 0.02 \pm 0.02$, $U - B = (0.96 \pm 0.02) \times (U - B)_{L61} + 0.09 \pm 0.01$, and $V = (-0.015 \pm 0.03) \times (B - V)_{L61} + 0.06 \pm 0.02 + V_{L61}$. The offset may partly explain the difference between the distances inferred from the *UBV* photometry of Lohmann (1961) and the present analysis. Applying an intrinsic *UBV* colour-colour relation to the corrected data yields a reddening of $E(B - V) = 0.32 \pm 0.03$. The canonical extinction law was employed, and may be refined once spectroscopic observations are available. Stars in NGC 4349 terminate near B8–A0 according to the intrinsic *JHK_s* and *UBV* relations (e.g., Straižys & Lazauskaitė, 2009; Turner, 2011). Published reddenings for *R Cru* (Ferne, 1990) are nearly half that derived for the cluster, implying that the Cepheid lies in the foreground. That is consistent with the Cepheid’s parameters as inferred from the latest period-Wesenheit relations (e.g., Benedict et al., 2007), which indicate that *R Cru* is less than 1 kpc distant.

A colour-magnitude diagram for NGC 4349 is shown in Fig. 7.3. A $\log \tau = 8.55 \pm 0.10$ Padova isochrone (Bonatto et al., 2004) was adopted based on the reddening and

²Obtained with the 0.6 m Helen Sawyer Hogg Telescope that was stationed at Cerro Las Campanas, Chile.

spectral types inferred from the colour-colour diagram, and because that age provides an evolutionary track that aptly matches both bluer and redder evolved members. NGC 4349 contains evolved stars brighter than the saturation limit of the VVV survey. Therefore, JHK_s photometry for those stars was taken from 2MASS. The colour-magnitude diagram for NGC 4349 was restricted to stars within $\leq 1.2'$ to reduce field star contamination. The final parameters for NGC 4349 are $d = 1.63 \pm 0.13$ kpc, $E(J - H) = 0.09 \pm 0.02$, and $\log \tau = 8.55 \pm 0.10$. A ratio of total to selective extinction (R) was adopted from Majaess et al. (2011c) (see also Bonatto et al., 2004, and references therein). The distance and reddening agree with that established by Claria & Lapasset (1989, $d = 1.74 \pm 0.65$ kpc and $E_{B-V} = 0.34 \pm 0.03$).

In their comprehensive survey Lovis & Mayor (2007) discovered that TYC 8975-2606-1 hosts a substellar companion (designated NGC 4349 127b). Lovis & Mayor (2007) adopted cluster parameters of $d = 2200$ pc and $\tau = 200$ Myr, which implied a $3.9M_{\odot}$ host. However, the distance and age established here for NGC 4349 are 30% nearer and 150 Myr older, respectively. The parent star exhibits the following parameters according to the Padova isochrone applied: $M_*/M_{\odot} \sim 3.1$ and $\log L/L_{\odot} \sim 2.7$. Yet the principal source of uncertainty hindering a reliable determination of the orbital parameters remains the sparsely sampled radial velocity curve (Lovis & Mayor, 2007), as indicated by simulations conducted using the *Systemic Console* (Meschiari et al., 2009). Nevertheless, a minimum mass for the substellar companion of $M/M_J \sim 17$ was obtained. Kashyap et al. (2008) derived an X-ray luminosity for the system in order to evaluate whether giant planets in close proximity to the host are catalysts for magnetic activity. That determination was based on a distance to

NGC 4349 of $d = 2176$ pc, thereby reaffirming the importance of a precise distance scale.

7.4 CONCLUSION

VVV JHK_s observations may be employed to help establish precise cluster distances that have comparatively reduced uncertainties ($\leq 10\%$). That is illustrated by deriving fundamental parameters for Pismis 19 and NGC 4349, two important clusters which hitherto exhibit sizable distance uncertainties (60%, §7.3.1 and 7.3.2). A precise distance determination for Pismis 19 from optical photometry was hampered in part by significant reddening (Fig. 7.2, $A_V \simeq 4$). Parameters derived for Pismis 19 are $d = 2.40 \pm 0.15$ kpc, $\langle E(J - H) \rangle = 0.34 \pm 0.04$, and $\log \tau = 9.05 \pm 0.10$ (Fig. 7.2), whereas the parameters for NGC 4349 are $d = 1.63 \pm 0.10$ kpc, $E(J - H) = 0.09 \pm 0.02$, and $\log \tau = 8.55 \pm 0.10$ (Fig. 7.3). The nature of the VVV survey ensured that the revised results, which have pertinent ramifications, complement existing estimates and display a marked improvement ($\geq 5\times$) in precision. New VVV JHK_s observations for stars in NGC 4349 and Pismis 19 imply that: existing physical parameters derived for NGC 4349 127b need to be redetermined, in part because the mass for the host star was revised downward to $\mathcal{M}_*/\mathcal{M}_\odot \sim 3.1$ (§7.3.2), the classical Cepheid *R Cru* is not a member of NGC 4349 (§7.3.2), and VVV JHK_s photometry is particularly suited for constraining parameters of obscured and differentially reddened intermediate-age clusters (e.g., Pismis 19, $A_V \sim 4$, Fig. 7.2).

The VVV and UKIDSS surveys (Lucas et al., 2008; Minniti et al., 2010) may be employed to achieve significant gains toward strengthening the open cluster distance scale. Yet considerable work remains, and unknown systematic errors may be discovered, given the nascent nature of the surveys. Consequently, obtaining independent multiband observations

is desirable to corroborate derived cluster parameters (e.g., Carraro, 2011).

REFERENCES

- Benedict, G. F., McArthur, B. E., Feast, M. W., et al. 2007, *AJ*, 133, 1810
- Bonatto, C., Bica, E., & Girardi, L. 2004, *A&A*, 415, 571
- Bonatto, C., & Bica, E. 2010, *A&A*, 516, A81
- Borissova, J., et al. 2011, *A&A*, 532, A131
- Carraro, G., & Munari, U. 2004, *MNRAS*, 347, 625
- Carraro, G. 2011, *A&A*, 536, A101
- Catelan, M., Minniti, D., Lucas, P. W., et al. 2011, *RR Lyrae Stars, Metal-Poor Stars, and the Galaxy*, 145
- Claria, J. J., & Lapasset, E. 1989, *MNRAS*, 241, 301
- Cousins, A. W. J., & Caldwell, J. A. R. 2001, *MNRAS*, 323, 380
- Dias, W. S., Alessi, B. S., Moitinho, A., & Lépine, J. R. D. 2002, *A&A*, 389, 871
- Fernie, J. D. 1963, *The Observatory*, 83, 33
- Fernie, J. D. 1990, *ApJS*, 72, 153
- Lindoff, U. 1968, *Arkiv for Astronomi*, 5, 1
- Lohmann, W. 1961, *Astronomische Nachrichten*, 286, 105
- Loktin, A. V., & Matkin, N. V. 1994, *A&AT*, 4, 153
- Lovis, C., & Mayor, M. 2007, *A&A*, 472, 657
- Lucas, P. W., et al. 2008, *MNRAS*, 391, 136
- Kashyap, V. L., Drake, J. J., & Saar, S. H. 2008, *ApJ*, 687, 1339
- Kholopov, P. N. 1956, *Peremennye Zvezdy*, 11, 325
- Kraft, R. P. 1957, *ApJ*, 126, 225
- Majaess, D., Turner, D., Lane, D., & Krajci, T. 2011 (a), *JAAVSO*, 39, 219
- Majaess, D., Turner, D., Moni Bidin, C., et al. 2011 (b), *ApJ*, 741, L27
- Meschiari, S., Wolf, A. S., Rivera, E., et al. 2009, *PASP*, 121, 1016
- Minniti, D., et al. 2010, *New Astronomy*, 15, 433
- Minniti, D., et al. 2011, *A&A*, 527, A81
- Moni Bidin, C., Mauro, F., Geisler, D., et al. 2011, *A&A*, 535, A33
- Paunzen, E., & Netopil, M. 2006, *MNRAS*, 371, 1641
- Piatti, A. E., Clariá, J. J., Bica, E., Geisler, D., & Minniti, D. 1998, *AJ*, 116, 801
- Pietrzyński, G., & Gieren, W. 2004, *IAU Colloq. 193: Variable Stars in the Local Group*, 310, 87
- Saito, R. K., Hempel, M., Minniti, D., et al. 2011, *A&A*, in press (arXiv:1111.5511)
- Straižys, V., & Laugalys, V. 2008, *Baltic Astronomy*, 17, 253
- Straižys, V., & Lazauskaitė, R. 2009, *Baltic Astronomy*, 18, 19
- Turner, D. G. 1979, *PASP*, 91, 642
- Turner, D. G. 2010, *Ap&SS*, 326, 219
- Turner, D. G. 2011, *RMxAA*, 47, 127
- van Leeuwen, F. 2007, *A&A*, 474, 653
- van Leeuwen, F. 2009, *A&A*, 497, 209

CHAPTER 8

TYPE I/II CEPHEIDS IN NGC 5128

The Cepheids of Centaurus A (NGC 5128) and Implications for H_0

Abstract: A *VI* Wesenheit and period-colour analysis based on new OGLE observations confirms the Ferrarese et al. discovery of 5 Type II Cepheids in NGC 5128 (Centaurus A). The distance to that comparatively unreddened population is $d = 3.8 \pm 0.4(\sigma_{\bar{x}})$ Mpc. The classical Cepheids in NGC 5128 are the most obscured in the extragalactic sample ($n = 30$) surveyed, whereas groups of Cepheids tied to several SNe host galaxies have negative reddenings. Adopting an anomalous extinction law for Cepheids in NGC 5128 as a result of observations of SN 1986G ($R_V \simeq 2.4$) is not favoured, although SNe Ia may follow smaller R_V . The distances to classical Cepheids in NGC 5128 exhibit a dependence on colour and CCD chip that may arise in part from photometric contamination. Applying a colour cut to minimize contamination yields $d \simeq 3.5$ Mpc ($V - I \leq 1.3$), while the entire sample's mean is $d \simeq 3.1$ Mpc. The distance was established via the latest *VI* Galactic Wesenheit functions that include the 10 HST calibrators, which imply a shorter distance scale than that of Sandage et al. (2004) by $\geq 10\%$ at $P \simeq 25^d$. HST monitored classical Cepheids in NGC 5128, and the SNe host galaxies NGC 3021 and NGC 1309 follow a shallower *VI* Wesenheit slope than ground-based calibrations of the Milky Way, LMC, NGC 6822, SMC, and IC 1613. The discrepancy is unrelated to metallicity because the latter group share a common slope over a sizable abundance baseline ($\alpha = -3.34 \pm 0.08(2\sigma)$, $\Delta[\text{Fe}/\text{H}] \simeq 1$).

A negligible distance offset between OGLE classical Cepheids and RR Lyrae variables in the LMC, SMC, and IC 1613 bolsters assertions that VI -based Wesenheit functions are relatively insensitive to chemical abundance. In sum, a metallicity effect (in VI) is not the chief source of uncertainty associated with the Cepheid distance to NGC 5128 or the establishment of the Hubble constant, but rather it may be the admittedly challenging task of obtaining precise, commonly standardized, multi-epoch, multi-band, comparatively uncontaminated extragalactic Cepheid photometry.

8.1 INTRODUCTION

Ferrarese et al. (2007) discovered at least 51 classical Cepheids and 5 Type II Cepheid candidates in NGC 5128 (Centaurus A). Their comprehensive survey provides an opportunity to determine the distance to NGC 5128 from Population I and II standard candles. That is particularly important given that the classical Cepheid distance to NGC 5128 conflicts with independent indicators. The discrepancy has been attributed to an anomalous extinction law and ambiguities surrounding the sensitivity of VI -based Cepheid relations to chemical abundance. Yet alternative rationale are favored in the present study.

Type II Cepheids continue to garner attention as a means of establishing the distances to globular clusters, the Galactic centre, and galaxies (Kubiak & Udalski, 2003; Majaess et al., 2009,c; Majaess, 2010a,b). Indeed, at least 21 Type II Cepheids were observed beyond the local group in M106 (Macri et al., 2006; Majaess et al., 2009c). The distance inferred to that galaxy from Type II Cepheids agrees with estimates established by masers and classical Cepheids ($D_{TII} \simeq 7.3$ Mpc, Herrnstein et al., 1999; Macri et al., 2006; Majaess et al., 2009c). Discovering Type II Cepheids and RR Lyrae variables in galaxies hosting classical

Cepheids offers an opportunity to constrain the effects of chemical composition on their luminosities and intrinsic colours (Freedman & Madore, 1996; Udalski et al., 2001; Majaess et al., 2009,c; Majaess, 2010a,b, see also the historic precedent outlined in Tammann et al. 2008). However, the statistics must be suitable for the task, while the degeneracies posed by other uncertainties require resolution (e.g., photometric contamination via blending and crowding).

In this study additional evidence is presented to secure membership for 5 Type II Cepheid candidates observed by Ferrarese et al. (2007) in NGC 5128 (§8.2). In §8.3 distances are computed for the galaxy’s population of classical and Type II Cepheids, namely by employing the latest *VI* Galactic calibration that includes the new HST parallaxes for 10 nearby classical Cepheids, and a calibration inferred from recent *VI* observations for 197 Type II Cepheids in the LMC (OGLE). The associated uncertainties in the derived parameters are discussed, and pertain directly to the Cepheid distance scale and the establishment of H_0 . It is advocated that an anomalous extinction law (§8.3) and variations in chemical composition among Cepheids (§8.4.1) are unrelated to a significant disparity between the Cepheid distance to NGC 5128 and independent indicators. The discrepancy may stem from the difficulties inherent to obtaining extragalactic Cepheid photometry (§8.4.2).

8.2 TYPE II CEPHEIDS IN NGC 5128

Ferrarese et al. (2007) identified several potential Type II Cepheids in NGC 5128, with an emphasis placed on the following variables that exhibit Cepheid-like light curves: C43, C50, C52, C54, and C56. However, the absence of a *VI* calibrating dataset hampered efforts to secure the classification (footnote 9, Ferrarese et al., 2007). The relevant data would be

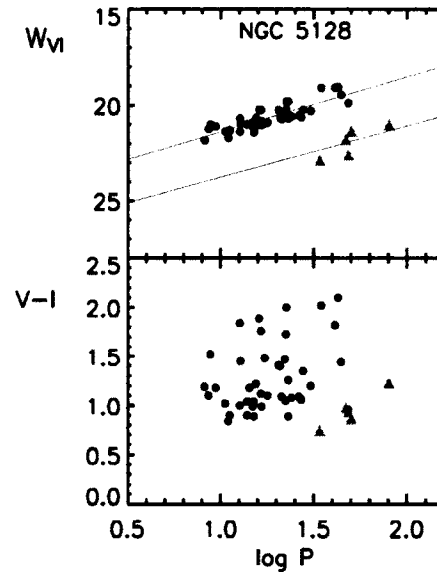


Figure 8.1 *VI* Wesenheit and period-colour diagrams confirm the Ferrarese et al. (2007) discovery of five Type II Cepheids in NGC 5128. Type II and classical Cepheids are indicated by red triangles and black dots respectively, and are distinctly separated by ~ 2 magnitudes in Wesenheit space. The Wesenheit magnitudes were evaluated using $W_{VI} = V - R_{VI} \times (V - I)$, where $R_{VI} = 2.55$ is the canonical extinction law. The slopes of the Wesenheit functions are variants of the LMC calibration (Majaess et al., 2009c, OGLE photometry). Long-period classical Cepheids in NGC 5128 exhibit a sizable colour excess. The error bars are suppressed for clarity.

published a year later by the OGLE consortium, who observed 197 Type II LMC Cepheids in *V* and *I* (Soszyński et al., 2008). The candidates presented by Ferrarese et al. (2007) may now be reassessed via *VI* Wesenheit and period-colour diagrams (Fig. 8.1). There are drawbacks to applying only those diagnostics to secure a Type II Cepheid designation (Majaess et al., 2009c). The former diagnostic is degenerate because variables of separate classes may overlap the Type II Cepheid Wesenheit relation, stars such as semi-regulars (Soszyński et al., 2007; Soszyński et al., 2008; Soszyński et al., 2009b; Pellerin et al., 2009; Majaess et al., 2009c). The latter diagnostic is problematic because of differential reddening displacing a variable from the intrinsic or mean Type II Cepheid trend. A strict adherence

to the mean period-colour criterion led Majaess et al. (2009c) to reduce their preliminary sample of ≥ 100 extragalactic Type II Cepheids (excluding the LMC) by nearly $\sim 50\%$. Additional diagnostics are needed, including period-amplitude diagrams and Fourier analyses of the light curves. Yet RV Tau stars, which constitute the brightest subclass of Type II Cepheids (Szabados, 2010) and are therefore often detected in extragalactic surveys, exhibit somewhat chaotic and non-unique light curves that hamper efforts to solidify a designation. The matter is exacerbated because observations for Type II Cepheid candidates in remote galaxies are typically sparse and uncertain, particularly because the stars are often sampled fortuitously near the limiting magnitude of surveys seeking to discover more luminous classical Cepheids.

All the candidates presented by Ferrarese et al. (2007) fall on the *VI* Wesenheit relation characterizing Type II Cepheids (Fig. 8.1). The Wesenheit function is defined and discussed by van den Bergh (1968), Madore (1982), Opolski (1983, 1988), Madore & Freedman (1991, 2009), and Turner (2010). The relation is reddening-free and relatively insensitive to the width of the instability strip. The period-magnitude relations of Type II and classical Cepheids are distinctly separated by ~ 2 magnitudes in Wesenheit space. BL Her, W Vir, and RV Tau stars do not follow the same linear *VI* Wesenheit function (Soszyński et al., 2008, although see Matsunaga et al. 2006, 2009; Feast 2010). However, the linear relations displayed in Figure 8.1 merely identify and segregate the Cepheid populations (Majaess et al., 2009c). A separate relation that accounts for the reputed non-linearity of the *VI* Type II Cepheid Wesenheit function is employed to establish distances (Majaess et al., 2009).

The *VI* period-colour diagram demonstrates that the Type II Cepheid candidates ex-

hibit apparent colours that are similar to or somewhat bluer than their classical Cepheid counterparts (Fig. 8.1). That agrees with the trend noted for classical and Type II Cepheids in the LMC and M31 (Majaess et al., 2009c, photometry from Udalski et al. 1999; Bonanos et al. 2003). Semi-regulars, by contrast, are typically redder than Cepheids. The sparse sampling results in large uncertainties for the deduced mean magnitudes, periods, and hence classifications for the Type II Cepheid candidates. The variables exhibit pulsation periods likely matching an RV Tau subclassification. RV Tau stars may display alternating minima and maxima (see the interesting discussion in Wils & Otero, 2008), however that effect cannot be detected in the present data because of the limited sampling and uncertainties (one cycle $\simeq 44^d$).

8.3 THE CEPHEID DISTANCE TO NGC 5128

The distance to the Type II Cepheids in NGC 5128 may be determined via the *VI* reddening-free relation established by Majaess et al. (2009) from OGLE LMC calibrators (Udalski et al., 1999; Soszyński et al., 2008). Likewise, the distance to the classical Cepheids may be computed using a *VI* Galactic Cepheid calibration (Majaess et al., 2008). That calibration is based primarily on the efforts of fellow researchers who established classical Cepheids as members of Galactic open clusters (e.g., Sandage, 1958; Madore & van den Bergh, 1975; Turner et al., 1992) and obtained precise trigonometric parallaxes (HST, Benedict et al., 2007). The resulting mean distance to the classical and Type II Cepheids in NGC 5128 is

$$D_{TI} = 3.06 \pm 0.07(\sigma_{\bar{x}}) \pm 0.54(\sigma) \text{ Mpc} \text{ and } D_{TII} = 3.8 \pm 0.4(\sigma_{\bar{x}}) \pm 0.8(\sigma) \text{ Mpc.}^1$$

¹ $\sigma_{\bar{x}}$ and σ are the internal standard error and standard deviation. The Ferrarese et al. 2007 error budget is provided in their Table 7. Note that the Cepheid distances deviate as a function of colour and CCD chip by upwards of ~ 0.4 Mpc (§8.4.2, Fig. 8.5).

Cepheid distance is essentially that determined by Ferrarese et al. for a canonical extinction law ($D_{TI} \simeq 3.1$ Mpc, see their Table 6). The agreement is expected given that the Galactic classical Cepheid calibration yields a distance modulus to the LMC of $\mu_0 \simeq 18.45$ (Majaess et al. 2008, Majaess 2010a, photometry from Udalski et al., 1999; Sebo et al., 2002; Soszyński et al., 2008b), which is comparable to the zero-point of the distance relation they employed. Ferrarese et al. (2007) consider and invariably adopt an anomalous extinction law for NGC 5128's Cepheids based on observations of supernova 1986G ($R_V = 2.4$, Hough et al., 1987), thereby increasing their estimate to $D_{TI} \simeq 3.4$ Mpc, which is the distance cited throughout the literature. Yet recent observations indicate that SNe Ia may follow a smaller R_V value than the canonical extinction law (Elias-Rosa et al., 2006; Wang et al., 2006; Goobar, 2008; Nobili & Goobar, 2008). Riess et al. (2009b) cite a consensus value of $R_V \simeq 2.5$ for SNe Ia, which is consistent with that found by Hough et al. (1987) for the supernova in NGC 5128 (SN 1986G). Adopting an anomalously low extinction law for Cepheids in NGC 5128 based solely on observations of SN 1986G is not favoured.

The mean classical Cepheid distance to NGC 5128 disagrees with other indicators by roughly -20% (Harris et al., 2009, see also the NASA/IPAC Extragalactic Database (NED) master list of galaxy distances² by Madore & Steer 2007). The distances cited above should be interpreted cautiously.

²<http://nedwww.ipac.caltech.edu/level5/NED1D/intro.html>

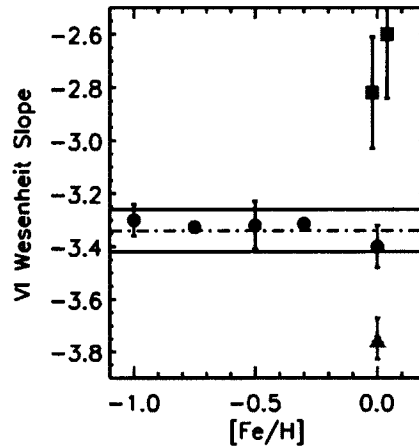


Figure 8.2 The slope of the *VI* classical Cepheid Wesenheit relation is relatively insensitive to metallicity. HST observations of classical Cepheids in NGC 5128, NGC 1309, and NGC 3021 (blue squares) follow a different metallicity dependence relative to the latest ground-based observations of variables in the Milky Way, LMC, NGC 6822, SMC, and IC 1613 (black dots, $\alpha = -3.34 \pm 0.08(2\sigma)$). The slope of the Sandage et al. (2004) Galactic calibration, based upon the best available data at the time of derivation and represented by the red triangle, disagrees with that inferred from the new HST parallaxes and (revised) cluster Cepheids ($\alpha \simeq -3.4$).

8.4 UNCERTAINTIES ASSOCIATED WITH THE CEPHEID DISTANCE TO NGC 5128

8.4.1 THE (NULL) ROLE OF METALLICITY

It has been argued that metal-rich classical Cepheids may follow a shallower (and steeper) Wesenheit slope than metal-poor ones, thereby introducing a potential source of uncertainty into the present analysis, because the chemical composition of Cepheids in NGC 5128 is unknown. However, a plot of the Wesenheit slopes inferred from ground-based observations of classical Cepheids in the Milky Way, LMC, NGC 6822, SMC, and IC 1613, demonstrates that the galaxies are characterized by a common *VI* slope over a sizable abundance baseline (Fig. 8.2, $\alpha = -3.34 \pm 0.08(2\sigma)$ and $\Delta[\text{Fe}/\text{H}] \simeq 1$). The slope of the *VI* Wesenheit function is therefore insensitive to metallicity to within the uncertainties.

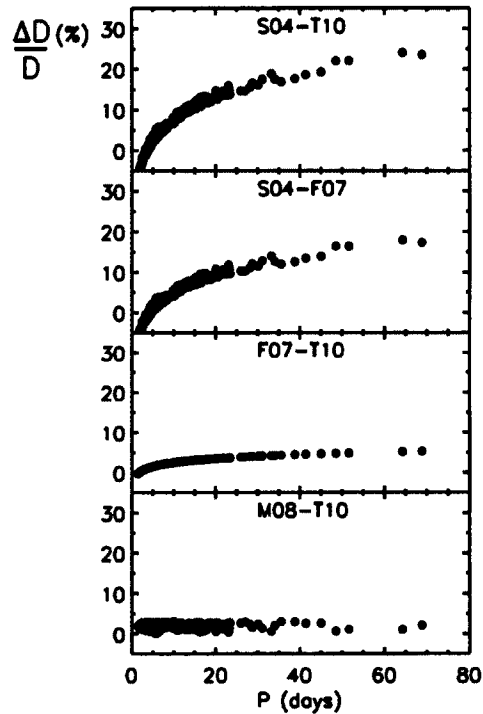


Figure 8.3 A comparison of the distances established to Galactic classical Cepheids via the *VI* Wesenheit calibrations of Sandage et al. (2004) (S04), Fouqué et al. (2007, F07), Majaess et al. (2008, M08), and Turner (2010, T10). The latter three calibrations include HST trigonometric parallaxes for 10 nearby classical Cepheids (Benedict et al., 2007). The Sandage et al. (2004) distance scale diverges from that of Fouqué et al. (2007) and Turner (2010) by $\geq +10\%$ at $P \simeq 25^d$.

The Galactic calibration employed to secure the distance to NGC 5128 and construct figure 8.2 is based in part on the HST parallaxes for 10 nearby classical Cepheids (Benedict et al., 2007), which anchored the Milky Way calibration. Tammann et al. (2008) questioned the reliability of the HST parallaxes because the resulting period- $M_{V,I}$ relations inferred from that sample do not match their functions (Tammann et al., 2003; Sandage et al., 2004), which were constructed from the best available data at the time. Their relations were derived prior to the publication of the HST parallaxes, and the parameters for longer-period classical Cepheids tied to Galactic associations have since been revised (Turner,

2010), although continued work is needed to secure new calibrators and revise existing ones.³ The implied assertion that the HST parallaxes are awry is not supported by the results of Turner (2010) or figure 8.2. A central conclusion of Turner (2010) was that the classical Cepheid period-luminosity relation tied to the HST sample is in agreement with that inferred from cluster Cepheids. Moreover, the slope of the *VI* Wesenheit function inferred from HST parallaxes matches that of ground-based observations of classical Cepheids in the LMC, NGC 6822, SMC, and IC 1613 (Fig. 8.2). The *VI* Galactic Wesenheit functions of Fouqué et al. (2007), Majaess et al. (2008), and Turner (2010) establish a distance scale that is $\geq 10\%$ nearer than that of Sandage et al. (2004) at $P \simeq 25^d$ (Fig. 8.3). The *VI* Galactic Wesenheit calibration established by Fouqué et al. (2007), partly on the basis of infrared surface brightness and interferometric Baade-Wesselink parallaxes, matches the Turner (2010) hybrid HST/cluster Cepheid-based relation within $\leq 5\%$ (Fig. 8.3). Lastly, regarding the construction of Fig. 8.2, it is noted that the slope characterizing longer period Cepheids in IC 1613 is steeper than that describing the short period regime. Moreover, the SMC exhibits a significant break in the *VI* Wesenheit function (see also Soszyński et al., 2010, and references therein). The LMC displays a separate trend, and efforts continue to characterize the discrepancy and its source. The reader is likewise referred to the research of Ngeow et al. (2009).

Kennicutt et al. (1998), Macri et al. (2006), and Scowcroft et al. (2009) suggest that the classical Cepheid *VI* Wesenheit relation exhibits a zero-point dependence on metallicity (see also the review of Romaniello et al., 2005, 2008), again introducing a potential source of uncertainty into the present analysis because the chemical composition of the Cepheids in

³Facilitated by surveys initiated at the VISTA and OMM (Minniti et al., 2010; Artigau et al., 2010).

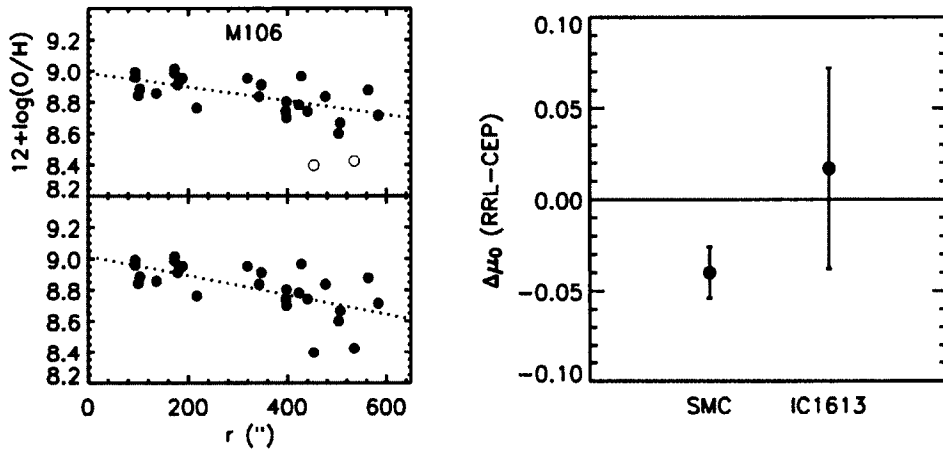


Figure 8.4 Left, the abundance gradient for M106 (Riess et al., 2009) implies that initial estimates of the *VI* classical Cepheid metallicity effect ($\gamma_i \simeq -0.3 \text{ mag dex}^{-1}$) nearly double. The exclusion of two data points implies an even larger value (left, top panel). A sizable metallicity effect contradicts evidence presented by a direct comparison of classical Cepheids, Type II Cepheids, and RR Lyrae variables at common zero-points. Right, the distance offset between RR Lyrae variables and classical Cepheids in the SMC and IC 1613 is nearly negligible. The base set of equations employed to compute the distances are OGLE *VI* Wesenheit functions of LMC classical Cepheids and RR Lyrae variables. The comparison is independent of zero-point and uncertainties tied to extinction corrections. The results, in tandem with those of Fig. 8.2, imply that the primary source of uncertainty tied to the Cepheid distance to NGC 5128 is unrelated to variations in chemical composition among Cepheids.

NGC 5128 is unknown. Those researchers endeavoured to deduce the influence of chemical composition by examining the distance offset between classical Cepheids located in the central (metal-rich) and outer (metal-poor) regions of a particular galaxy (M101, M106, M33). However, a degeneracy emerges (photometric contamination), because stellar density and surface brightness often increase toward the central region. Macri et al. (2001) noted that a substantial fraction of the difference in distance moduli between classical Cepheids occupying the inner and outer regions of M101 could arise from blending. Macri et al. (2006) and Scowcroft et al. (2009) employed criteria to reduce the impact of photometric contamination to enable an unbiased determination of the classical Cepheid metallicity effect

from observations of classical Cepheids in M106 and M33, and the reader is encouraged to consider their evidence. Yet the result inferred from variables in M106 was provided an alternative rationale by Bono et al. (2008) and Majaess et al. (2009c), who noted that the observed offset was too large to be attributed to variations in chemical composition. Indeed, the abundance gradient for M106 (Riess et al., 2009) implies that initial estimates of the classical Cepheid metallicity effect ($\gamma_i \simeq -0.3 \text{ mag dex}^{-1}$) nearly double (Fig. 8.4, or see Table 12 in Riess et al., 2009). A comparably large metallicity gradient is obtained when examining the offset between distances to classical Cepheids occupying the inner (Stetson et al., 1998) and outer (Kelson et al., 1996) regions of M101, which sample metal-rich and metal-poor variables accordingly ($\gamma \simeq -0.5 \text{ mag dex}^{-1}$, see also Majaess et al. 2009c). The results for M101 and M106 are larger than that cited for M33 ($\gamma \simeq -0.3 \text{ mag dex}^{-1}$). The results differ in yet another manner, namely the slope of the *VI* Wesenheit function inferred from classical Cepheids sampling the inner region of M106 differs from the outer region, while classical Cepheids in M33 (inner & outer) exhibit a comparable slope. The discrepancies are manifold and the proposed metallicity effect is nonetheless too large.

The sizable distance offset between the inner and outer regions of the galaxies arises from photometric contamination and other source(s). Consider the following example, in tandem with the results of Fig. 8.2, which compares the distances to classical Cepheids and RR Lyrae variables at a common zero-point (e.g., LMC, SMC, and IC 1613). The *VI* Wesenheit functions inferred from OGLE LMC classical Cepheids and RR Lyrae variables are adopted as the calibrating set (Udalski et al., 1999; Soszyński et al., 2003). RR Lyrae variables likewise follow scatter-reduced *VI* Wesenheit functions (Kovács & Jurcsik, 1997;

Soszyński et al., 2003, 2009a; Di Criscienzo et al., 2007; Majaess, 2010a,b). The distance offset between classical Cepheids and RR Lyrae variables in the SMC as established via the OGLE LMC Wesenheit relations is $\Delta\mu_0 \simeq -0.04$ (Fig. 8.4). The distance offset between classical Cepheids and RR Lyrae variables in IC 1613, as established via the OGLE LMC Wesenheit relations, is $\Delta\mu_0 \simeq +0.02$ (Fig. 8.4). The distances inferred from the standard candles agree to within the uncertainties, despite the neglect of metallicity corrections for variable types sampling different temperature, radius, and density regimes. Hence the evidence does not support a sizable metallicity effect. The comparison between the variable types is independent of zero-point and uncertainties tied to extinction corrections. Admittedly, additional *VI* observations of extragalactic RR Lyrae variables are desirable, and the Wesenheit function characterizing that population, as inferred from pulsation models, the Magellanic Clouds, and globular clusters, are marginally discrepant (Kovács & Walker, 2001; Di Criscienzo et al., 2004, 2007; Soszyński et al., 2009a). Further work is needed.

In sum, metallicity does not significantly alter the *VI* Wesenheit slope or zero-point (Figs. 8.2 and 8.4, see also Udalski et al., 2001; Pietrzyński et al., 2004; Majaess et al., 2008, 2009,c; Bono et al., 2008; Majaess, 2010a,b). Therefore, concerns are allayed regarding chemical composition being a sizable source of uncertainty for the Cepheid distance to NGC 5128, or the establishment of the Hubble constant. By contrast, caution should be used when employing *BV* relations for Cepheids and RR Lyrae variables of differing abundance (Majaess et al., 2009c, and references therein). Caution is likewise urged when deriving a galaxy's distance and reddening via a multiwavelength approach that relies on Cepheid *B*-band data.

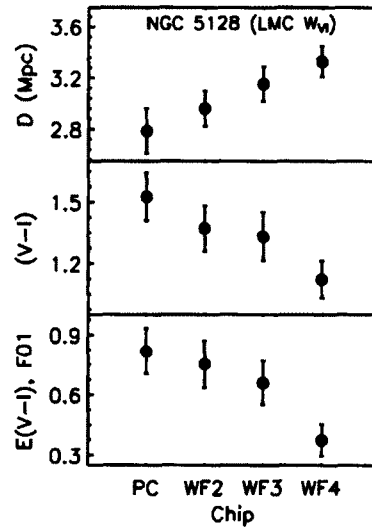


Figure 8.5 The distances of classical Cepheids in NGC 5128 exhibit a colour and CCD chip dependence, owing partly to photometric contamination. A colour-limited sample that reduces the effects of contamination yields $D \simeq 3.5$ Mpc ($V-I \leq 1.3$, see Fig. 8.1). A VI Wesenheit relation based on new OGLEIII observations was applied to infer the distance (LMC, $\mu_0 = 18.5$).

8.4.2 EXTRAGALACTIC CEPHEID PHOTOMETRY

Alternate sources that may explain the discrepancy between the Cepheid distance to NGC 5128 and independent indicators are now considered. Of particular concern is the correlation between the computed distances to classical Cepheids in NGC 5128, their colours, and the sampling CCD (Fig. 8.5). The origin of the bias may be manifold.

The excess reddening detected for a sizable fraction of the classical Cepheids in NGC 5128 may be an indication of photometric contamination (Fig. 8.1), which subsequently causes the affected stars to appear brighter and nearer (Stanek & Udalski, 1999; Mochejska et al., 2000, 2001). The most obscured Cepheids in the sample yield the nearest distances. Applying a colour cut as indicated by figure 8.1 yields $D \simeq 3.5$ Mpc ($V - I \leq 1.3$). The classical Cepheids of NGC 5128 exhibit the largest mean colour excess of the extragalactic

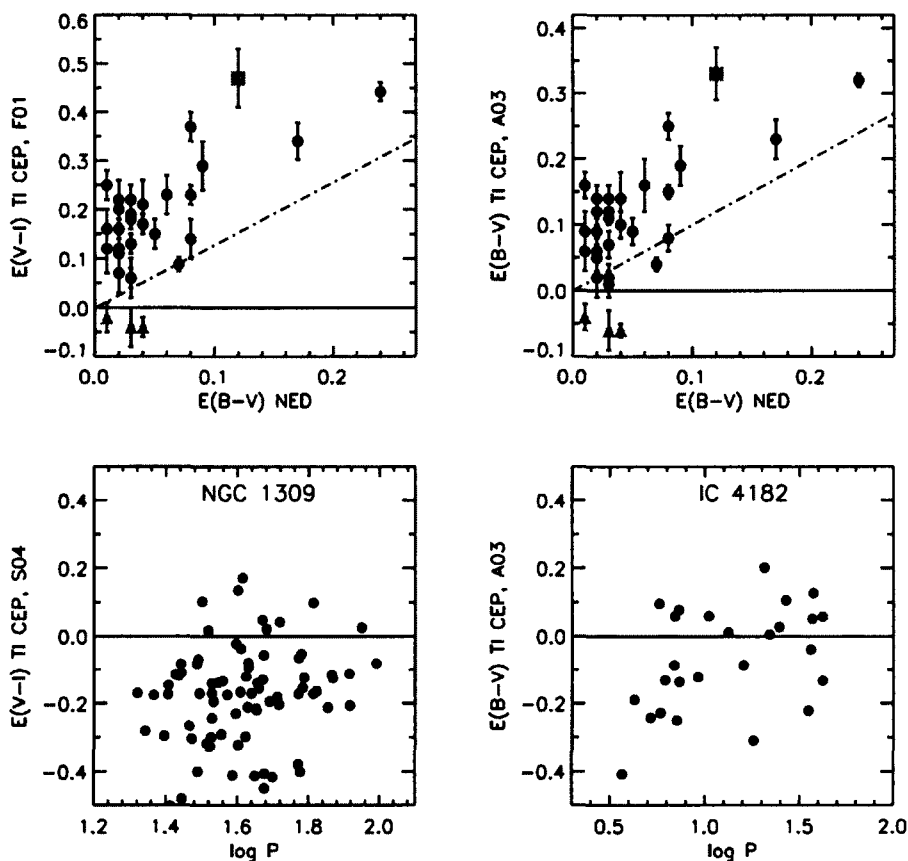


Figure 8.6 Top panels, a comparison of the reddenings established for a sample of galaxies (including NGC 5128) from classical Cepheids and the NED extinction calculator. $E(V-I)$ is tabulated according to equations adopted by Freedman et al. (2001, F01) and Sandage et al. (2004, S04), whereas $E(B-V)$ is computed following Abrahamyan (2003, A03). Extragalactic classical Cepheid reddenings lie above the relation describing unity (dashed line). The bulk of the data are offset $A_V \simeq 0.^m3$ beyond the foreground estimate. Classical Cepheids in NGC 5128 (red square) display a sizable mean colour excess (see also Figs. 8.1, 8.5). By comparison, the Cepheid-SNe calibrating galaxies NGC 1309, NGC 3021, and IC 4182 (blue triangles) exhibit negative mean reddenings (see also Saha et al., 2006).

sample examined (Fig., 8.6). By contrast, negative mean reddenings were obtained for NGC 3021, NGC 1309, and IC 4182, galaxies that host classical Cepheids and SNe (Fig. 8.6, see also Saha et al., 2006). The reddenings for the extragalactic sample (including NGC 5128) were established via the period-colour relations employed by Freedman et al. (2001) and

Abrahamyan (2003). Applying the period- $M_{V,I}$ relations of Sandage et al. (2004) would shift additional SNe-Cepheid calibrating galaxies into the negative absorption regime (see also Saha et al., 2006). That calibration yields a mean colour excess of $E_{V-I} \simeq -0.17$ for classical Cepheids in NGC 1309. Period-colour relations do not account for the temperature dependence in the strip at a given period. Consequently, reddenings computed for classical Cepheids on the hot edge of the strip will be overestimated, while reddenings computed for classical Cepheids on the cool edge of the strip will be underestimated. The photometric errors inherent to extragalactic observations, in addition to internal differential reddening, exacerbate the perceived spread. Period-colour relations will yield negative reddenings for Cepheids on the cool edge of the strip that are observed through negligible extinction, yet the mean for an entire sample of classical Cepheids should be null within the uncertainties, because of the isotropic distribution of variables within the strip (Turner, 2001). Suspicion should be cast on photometry (and the period-colour relations employed) that yields a mean extinction significantly less than the foreground estimate (Fig. 8.6). Also note that classical Cepheids observed in remote galaxies are preferentially the brightest (most massive), and may be tied to star forming regions immersed in obscuring material (longer period classical Cepheids trace spiral arms: e.g., Tammann 1970; Berdnikov & Efremov 1989; Majaess et al. 2009,b; Majaess 2010b).

The presence of floating photometric zero-points is a concern because of the difficulties inherent to achieving a common standardization, particularly across a range in colour and CCDs.

The Wesenheit relations (LMC or MW) applied to infer the distance to NGC 5128

exhibit a steeper slope. The Wesenheit slope describing classical Cepheids in NGC 5128 is $\alpha \simeq -2.9 \pm 0.3$ (Fig. 8.1, sensitive to the sample and CCD chip chosen: Fig. 8.5). Riess et al. (2009) remarked that a sample of classical Cepheids in metal-rich galaxies hosting supernovae are likewise characterized by a shallow Wesenheit slope. Photometric contamination, which may preferentially affect fainter short period Cepheids relative to brighter long period ones (e.g., Fig. 17 in Macri et al., 2006), may bias the tilt of the inferred Wesenheit relation and could in part explain shallower slopes. Applying an LMC or Galactic calibration to galaxies that exhibit vastly differing Wesenheit slopes will introduce a global bias. Consider two galaxies sharing a common distance (e.g., the Leo I group) and spurious shallow Wesenheit slope, yet hosting variables of differing period distributions. The galaxy containing classical Cepheids characterized by a shorter period distribution will have a nearer computed distance. Moreover, an inhomogeneous period distribution across the CCD chips will result in the propagation of artificial distance offsets across the detectors.

The effects described above may in sum conspire to produce figure 8.5, and the discrepancy between the Cepheid distance to NGC 5128 and that established by independent means. Admittedly, further work is needed to bolster the evidence.

Lastly, the period-reddening function derived previously by the author (Majaess et al., 2009c) was not employed here because it has become apparent that the purely numerical method pursued to derive the relation was swayed by poor calibrating statistics toward the long period regime (Majaess et al., 2008). The Galactic classical Cepheid calibration employed by the author (Majaess et al., 2008) exhibits an absence of long period variables save ℓ Car, as perhaps a too conservative philosophy was imposed requiring cluster Cepheids

used in the calibration be secured by radial velocities or proper motions. A bias is introduced because ℓ Car lies well toward the red edge of the instability strip (see Turner, 2010). The author will revisit the VI period-reddening formalism and subject elsewhere, an analysis that will be facilitated by the recent establishment of spectroscopic reddenings for a sizable sample of Galactic classical Cepheids (Kovtyukh et al., 2008).

8.5 SUMMARY & FUTURE RESEARCH

The properties of classical and Type II Cepheids in NGC 5128 are reinvestigated by employing calibrations with the latest OGLE and HST data. The significant discrepancy between the classical Cepheid distance to NGC 5128 and other indicators is likely unrelated to an anomalous extinction law or variations in chemical composition among Cepheids.

Five Type II Cepheid candidates discovered by Ferrarese et al. (2007) in NGC 5128 exhibit VI Wesenheit magnitudes and colours that are consistent with the proposed designation (Fig. 8.1). The pulsation periods could imply an RV Tau subclassification. RV Tau stars typically exhibit alternating minima and maxima (see Wils & Otero, 2008), however the presence of that effect cannot be established because the observational baseline is only one cycle ($\simeq 44^d$). Type II Cepheids are observed through marginal extinction, in contrast to their classical Cepheid counterparts (Figs. 8.1, 8.6).

The mean distance to NGC 5128's population of Type II and classical Cepheids is $D_{TII} = 3.8 \pm 0.4(\sigma_{\bar{x}}) \pm 0.8(\sigma)$ Mpc and $D_{TI} = 3.06 \pm 0.07(\sigma_{\bar{x}}) \pm 0.54(\sigma)$ Mpc. The latter estimate is essentially that obtained by Ferrarese et al. (2007) when that team employed the canonical extinction law ($R_V \simeq 3.3$, Table 6 in Ferrarese et al., 2007). Adopting an anomalous extinction law for classical Cepheids in NGC 5128 because of observations of SN

1982G ($R_V \simeq 2.4$) is not favoured. SNe Ia may follow smaller R_V values than the canonical value (Elias-Rosa et al., 2006; Wang et al., 2006; Goobar, 2008; Nobili & Goobar, 2008). Small statistics presently dominate the uncertainty in the Type II Cepheid distance to NGC 5128, affecting the estimate's importance. The mean classical Cepheid distance to NGC 5128 ($D_{TI} \simeq 3.1$ Mpc) disagrees with other indicators by $\geq -20\%$ (Harris et al., 2009).

The distance to the classical Cepheids in NGC 5128 was determined by applying the latest *VI* Galactic Wesenheit calibrations that utilize the new HST trigonometric parallaxes (Benedict et al., 2007) for 10 nearby classical Cepheids (e.g., Fouqué et al., 2007; Majaess et al., 2008; Turner, 2010). The distance scale implied by the *VI* Galactic calibrations of Fouqué et al. (2007) and Turner (2010) is $\geq 10\%$ less than that advocated by Sandage et al. (2004) at $P \simeq 25^d$ (Fig. 8.3). The Tammann et al. (2003) and Sandage et al. (2004) relations were constructed prior to the publication of the HST parallaxes for 10 nearby classical Cepheids (Benedict et al., 2007), which anchored the Milky Way calibration. The Sandage et al. (2004) relation forms the basis for an estimate of $H_0 \simeq 62 \text{ km s}^{-1} \text{ Mpc}^{-1}$ (Sandage et al., 2006). That estimate is smaller than the value espoused by Freedman et al. (2001) or Riess et al., and the discrepancy hampers efforts to constrain cosmological models (Riess et al., 2009b, Table 1). The differences displayed by the *VI* Galactic calibrations cited above may explain the bulk of the disagreement between the estimates of H_0 , however that conclusion is somewhat presumptuous. Redetermining H_0 to complement the aforementioned estimates is desirable, but requires a scrupulous inspection of all the archived data while considering advances in the field and the assertions summarized here, an effort that may be pursued elsewhere. For example, added weight will be given to calibrating galaxies that exhibit:

(i) a population of classical Cepheids that are characterized by a *VI* Wesenheit slope near $\alpha \simeq -3.34 \pm 0.08(2\sigma)$ (Fig. 8.2), where the slope is not imposed upon the data unless reaffirmed by a least-squares fit, (ii) Cepheids that have consistent moduli across the CCD chips, (iii) Cepheids that are observed through low obscuration, yet marginally greater than the foreground extinction estimate (Fig. 8.6), (iv) Cepheids that are sampled in low density and low surface brightness environments to reduce photometric contamination. Period-colour relations and the slope of the *VI* Wesenheit function may be employed to screen photometry and assess quality.

The *VI* Wesenheit functions describing classical Cepheids in NGC 5128 and the SNe hosts NGC 3021 and NGC 1309 exhibit a shallower slope than calibrations of the Milky Way, LMC, NGC 6822, SMC, and IC 1613 (Fig. 8.2). The discrepancy is not tied to variations in metallicity because ground-based observations of classical Cepheids in the Milky Way, LMC, NGC 6822, SMC, and IC 1613 yield comparable *VI* Wesenheit slopes over a sizable abundance baseline (Fig. 8.2, $\alpha = -3.34 \pm 0.08(2\sigma)$, $\Delta[\text{Fe}/\text{H}] \simeq 1$). Those galaxies exhibit the most precise photometry of all the Cepheid data inspected (Fig. 8.6). The distances computed for classical Cepheids in NGC 5128 display a dependence on colour and CCD chip that is likely attributable in part to photometric contamination (Figs. 8.1 and 8.5, see text). Applying a colour cut yields $d \simeq 3.5$ Mpc ($V - I \leq 1.3$, see Fig. 8.1). The classical Cepheids otherwise exhibit the largest mean colour excess of the extragalactic sample examined (Figs. 8.1, 8.6). By contrast, and perhaps disconcertingly, Cepheids tied to several galaxies hosting SNe have negative (or near negligible) mean reddenings (Fig. 8.6, see also Saha et al., 2006). The extragalactic classical Cepheid sample displays a mean $A_V \simeq$

0.^m3 offset beyond the foreground extinction estimate inferred from dust maps (Fig. 8.6). Fig. 8.6 confirms that reddenings inferred from foreground dust extinction maps for distant galaxies are likely underestimated.

A zero-point metallicity correction is not the chief source of uncertainty tied to the *VI*-based Cepheid distance for NGC 5128, or the establishment of the Hubble constant. The abundance gradient for M106 (Riess et al., 2009) implies that initial estimates of the classical Cepheid metallicity effect nearly double (Fig. 8.4). That value is too large, and contradicts a direct comparison of OGLE classical Cepheids and RR Lyrae variables in the Magellanic Clouds and IC 1613, which exhibit a negligible distance offset ($\Delta\mu_0 \simeq +0.01 \pm 0.06$, Fig. 8.4). Moreover, the metallicity effect cited in the literature and inferred from observations of M33, M101, and M106 is discrepant in its zero-point and slope. In sum, the evidence indicates that the slope and zero-point of the classical Cepheid *VI* Wesenheit function are largely insensitive to variations in chemical abundance (Figs. 8.2 & 8.4, see also Udalski et al., 2001; Pietrzyński et al., 2004; Majaess et al., 2008, 2009,c; Bono et al., 2008; Majaess, 2010a,b). A primary source of uncertainty tied to the Cepheid distance to NGC 5128, and that hampering efforts to constrain cosmological models, may be the admittedly challenging task of obtaining precise, commonly standardized, multi-epoch, multi-band, comparatively uncontaminated extragalactic Cepheid photometry.

REFERENCES

- Abrahamyan, G. V. 2003, *Astrophysics*, 46, 304
- Artigau, E., Doyon, R., & Lamontagne, R. 2010, *Proc. SPIE*, 7737, 63
- Benedict G. F. et al., 2007, *AJ*, 133, 1810
- Berdnikov, L. N., & Efremov, U. N. 1989, *Soviet Astronomy*, 33, 274
- Bonanos, A. Z., Stanek, K. Z., Sasselov, D. D., Mochejska, B. J., Macri, L. M., & Kaluzny, J. 2003, *AJ*, 126, 175
- Bono, G., Caputo, F., Fiorentino, G., Marconi, M., & Musella, I. 2008, *ApJ*, 684, 102
- Di Criscienzo, M., Marconi, M., & Caputo, F. 2004, *ApJ*, 612, 1092
- Di Criscienzo, M., Caputo, F., Marconi, M., & Cassisi, S. 2007, *A&A*, 471, 893
- Elias-Rosa, N., et al. 2006, *MNRAS*, 369, 1880
- Feast, M. W. 2010, *Variable Stars, the Galactic halo and Galaxy Formation*, 45
- Ferrarese, L., Mould, J. R., Stetson, P. B., Tonry, J. L., Blakeslee, J. P., & Ajhar, E. A. 2007, *ApJ*, 654, 186
- Freedman, W. L., & Madore, B. F. 1996, *Clusters, Lensing, and the Future of the Universe*, 88, 9
- Freedman W. L. et al., 2001, *ApJ*, 553, 47
- Fouqué P. et al., 2007, *A&A*, 476, 73
- Goobar, A. 2008, *ApJ*, 686, L103
- Harris, G. L. H., Rejkuba, M., & Harris, W. E. 2009, arXiv:0911.3180
- Herrnstein, J. R., et al. 1999, *Nature*, 400, 539
- Hough, J. H., Bailey, J. A., Rouse, M. F., & Whittet, D. C. B. 1987, *MNRAS*, 227, 1P
- Kelson, D. D., et al. 1996, *ApJ*, 463, 26
- Kennicutt, R. C., Jr., et al. 1998, *ApJ*, 498, 181
- Kovács, G., & Jurcsik, J. 1997, *A&A*, 322, 218
- Kovács, G., & Walker, A. R. 2001, *A&A*, 371, 579
- Kovtyukh, V. V., Soubiran, C., Luck, R. E., Turner, D. G., Belik, S. I., Andrievsky, S. M., & Chekhonadskikh, F. A. 2008, *MNRAS*, 389, 1336
- Kubiak M., Udalski A., 2003, *Acta Astr.*, 53, 117
- Macri, L. M., et al. 2001, *ApJ*, 549, 721
- Macri, L. M., Stanek, K. Z., Bersier, D., Greenhill, L. J., & Reid, M. J. 2006, *ApJ*, 652, 1133
- Madore, B. F., & van den Bergh, S. 1975, *ApJ*, 197, 55
- Madore B. F., 1982, *ApJ*, 253, 575
- Madore, B. F., & Freedman, W. L. 1991, *PASP*, 103, 933
- Madore, B. F., & Steer, I. 2007, *NASA/IPAC Extragalactic Database Master List of Galaxy Distances* (<http://nedwww.ipac.caltech.edu/level5/NED1D/intro.html>)
- Madore, B. F., & Freedman, W. L. 2009, *ApJ*, 696, 1498
- Majaess D. J., Turner D. G., Lane D. J., 2008, *MNRAS*, 390, 1539
- Majaess, D. J., Turner, D. G., & Lane, D. J. 2009, *MNRAS*, 398, 263

- Majaess, D. J., Turner, D. G., & Lane, D. J. 2009 (b), *JAAVSO*, 37, 179
- Majaess, D., Turner, D., & Lane, D. 2009 (c), *Acta Astronomica*, 59, 403
- Majaess, D. J. 2009, arXiv:0912.2928
- Majaess, D. 2010, *Acta Astronomica*, 60, 55
- Matsunaga, N., et al. 2006, *MNRAS*, 370, 1979
- Matsunaga, N., Kawadu, T., Nishiyama, S., Nagayama, T., Hatano, H., Tamura, M., Glass, I. S., & Nagata, T. 2009, *MNRAS*, 399, 1709
- Minniti, D., et al. 2010, *New Astronomy*, 15, 433
- Mochejska, B. J., Macri, L. M., Sasselov, D. D., & Stanek, K. Z. 2000, *AJ*, 120, 810
- Mochejska, B. J., Macri, L. M., Sasselov, D. D., & Stanek, K. Z. 2001, arXiv:astro-ph/0103440
- Ngeow, C.-C., Kanbur, S. M., Neilson, H. R., Nanthakumar, A., & Buonaccorsi, J. 2009, *ApJ*, 693, 691
- Nobili, S., & Goobar, A. 2008, *A&A*, 487, 19
- Opolski A., 1983, *IBVS*, 2425, 1
- Opolski, A. 1988, *Acta Astronomica*, 38, 375
- Pellerin, A., Macri, L. M., Bradshaw, A. K., & Stanek, K. Z. 2009, *American Institute of Physics Conference Series*, 1170, 40
- Pietrzyński, G., Gieren, W., Udalski, A., Bresolin, F., Kudritzki, R.-P., Soszyński, I., Szymański, M., & Kubiak, M. 2004, *AJ*, 128, 2815
- Pritzl B. J., Smith H. A., Stetson P. B., Catelan M., Sweigart A. V., Layden A. C., Rich R. M., 2003, *AJ*, 126, 1381
- Riess, A. G., et al. 2009 (b), *ApJ*, 699, 539
- Riess, A. G., et al. 2009, *ApJS*, 183, 109
- Romaniello, M., Primas, F., Mottini, M., Groenewegen, M., Bono, G., & François, P. 2005, *A&A*, 429, L37
- Romaniello, M., et al. 2008, *A&A*, 488, 731
- Saha, A., Thim, F., Tammann, G. A., Reindl, B., & Sandage, A. 2006, *ApJS*, 165, 108
- Sandage, A. 1958, *ApJ*, 128, 150
- Sandage, A., Tammann, G. A., & Reindl, B. 2004, *A&A*, 424, 43
- Sandage, A., Tammann, G. A., Saha, A., Reindl, B., Macchetto, F. D., & Panagia, N. 2006, *ApJ*, 653, 843
- Scowcroft, V., Bersier, D., Mould, J. R., & Wood, P. R. 2009, *MNRAS*, 396, 1287
- Sebo, K. M., et al. 2002, *ApJS*, 142, 71
- Soszyński, I., et al. 2003, *Acta Astronomica*, 53, 93
- Soszyński, I., et al. 2007, *Acta Astronomica*, 57, 201
- Soszyński, I., et al. 2008, *Acta Astronomica*, 58, 293
- Soszyński, I., et al. 2008 (b), *Acta Astronomica*, 58, 163
- Soszyński, I., et al. 2009, *Acta Astronomica*, 59, 1
- Soszyński, I., et al. 2009, *Acta Astronomica*, 59, 239
- Soszyński, I., et al. 2010, arXiv:1003.4518
- Stanek, K. Z., & Udalski, A. 1999, arXiv:astro-ph/9909346
- Stetson, P. B., et al. 1998, *ApJ*, 508, 491
- Szabados, L. 2010, *Variable Stars, the Galactic halo and Galaxy Formation*, 37

-
- Tammann, G. A. 1970, *The Spiral Structure of our Galaxy*, 38, 236
- Tammann, G. A., Sandage, A., & Reindl, B. 2003, *A&A*, 404, 423
- Tammann, G. A., Sandage, A., & Reindl, B. 2008, *ApJ*, 679, 52
- Turner, D. G., Forbes, D., & Pedreros, M. 1992, *AJ*, 104, 1132
- Turner, D. G. 2001, *Odessa Astronomical Publications*, 14, 166
- Turner, D. G. 2010, *Ap&SS*, 326, 219
- Udalski A. et al., 1999, *Acta Astr.*, 49, 223
- Udalski, A., Wyrzykowski, L., Pietrzynski, G., Szewczyk, O., Szymanski, M., Kubiak, M., Soszyński, I., & Zebrun, K. 2001, *Acta Astronomica*, 51, 221
- van den Bergh S., 1968, *JRASC*, 62, 145
- Wang, X., Wang, L., Pain, R., Zhou, X., & Li, Z. 2006, *ApJ*, 645, 488
- Wils, P., & Otero, S. 2008, *JAAVSO*, 36, 29

CHAPTER 9

METALLICITY EFFECTS

The Impact of Metallicity on Cepheid Distances

Abstract: Evidence is presented that supports findings that the classical Cepheid VI_C period-Wesenheit function is insensitive to metallicity. The viability of a recently advocated strong metallicity dependence was evaluated by applying the proposed correction ($\gamma = -0.8$ mag/dex) to distances established for the Magellanic Clouds via a Galactic VI_C Wesenheit calibration, which is anchored to ten nearby classical Cepheids with measured HST parallaxes. The resulting γ -corrected distances to the Magellanic Clouds (e.g., SMC, $\mu_{0,\gamma} \sim 18.3$) are in significant disagreement with that established from a mean of > 300 published estimates (NED-D), and a universal Wesenheit template with eleven δ Scuti, SX Phe, RR Lyrae, and Type II Cepheid variables with HST/Hipparcos parallaxes. Conversely, adopting a null correction (i.e., $\gamma = 0$ mag/dex) consolidates the estimates. In tandem with existing evidence, the results imply that variations in chemical composition among Cepheids are a negligible source of uncertainty for W_{VI_C} -based extragalactic distances and determinations of H_0 . A new approach is described that aims to provide additional Galactic Cepheid calibrators to facilitate subsequent assessments of the VI_C Wesenheit function's relative (in)sensitivity to abundance changes. VVV/UKIDSS/2MASS JHK_s photometry for clusters in spiral arms will be employed to establish a precise Galactic longitude-distance relation that can be applied in certain cases to determine the absolute Wesenheit magnitudes for

younger Cepheids.

9.1 INTRODUCTION

Classical Cepheids are integral to the establishment of the Galactic and extragalactic distance scales (Pietrzyński & Gieren, 2004; Turner, 2010) and the selection of a cosmological model (Macri & Riess, 2009; Freedman & Madore, 2010). Consequently, it is imperative to assess the effect of metallicity on VI_C Wesenheit classical Cepheid relations. In particular, are abundance differences between Cepheids comprising the calibration and target population important? Certain researchers advocate that a sizable correction is necessary when establishing the distance to benchmark metal-poor classical Cepheids in the Magellanic Clouds via a VI_C Wesenheit calibration tied to solar-abundance Galactic Cepheids. The dependence of the VI_C Wesenheit function on chemical composition is typically assessed by:

1. Evaluating the Wesenheit slopes inferred from classical Cepheids in galaxies spanning a sizable abundance baseline, such as solar to metal-poor classical Cepheids in the Milky Way, LMC, NGC 6822, SMC, and IC 1613. The galaxies are listed in order of decreasing metal abundance, and span $\Delta[\text{Fe}/\text{H}] \simeq 1$ (Luck et al., 1998; Udalski et al., 2001; Mottini et al., 2006; Tautvaišienė et al., 2007).
2. Determining whether the VI_C Wesenheit magnitude offset between different classes of pulsating stars is insensitive to the galaxy sampled. That may be evaluated by examining differences in Wesenheit space between RR Lyrae variables, δ Scuti variables (SX Phe variables), Type II Cepheids, and classical Cepheids in the Galaxy, LMC, SMC,

and IC 1613. Equivalent offsets in the absence of metallicity corrections imply that VI_C Wesenheit functions are insensitive to abundance changes. Similarly, comparing the mean colour excess inferred from various standard candles at a common zero-point (e.g., IC 1613) enables a determination of the impact of metallicity on that parameter, although marginal differences may arise because classical Cepheids (Population I objects) are often located in dustier regions. Furthermore, extinction estimates inferred from period-reddening (VI_c) relations can be compared to DIRBE/IRAS dust maps to constrain the metallicity dependence.

3. Exploiting the galactocentric metallicity gradient to deduce the Wesenheit magnitude offset between classical Cepheids observed in the outer (metal-poor) and central (metal-rich) regions of a particular galaxy. A degeneracy emerges that complicates the analysis, however, because the surface brightness and stellar density increase toward the central (metal-rich) regions, and thus photometric contamination (blending/crowding) becomes significant. Indeed, it is argued here that the (spurious) brightening (W_{VI_c}) of extragalactic Cepheids as a function of decreasing galactocentric distance (Kennicutt et al., 1998) is direct empirical evidence of photometric contamination.
4. Published metallicity corrections are evaluated by applying them to distances established for the Magellanic Clouds using a Galactic classical Cepheid calibration (e.g., Majaess et al., 2009b). The aim is to assess whether the metallicity corrected distances match expectations for the Magellanic Clouds as established from $\geq 3 \times 10^2$ published estimates (e.g., SN1987A, eclipsing binaries, RR Lyrae variables.).

In this study, evaluation (4) is conducted using the sizable metallicity effect¹ ($\gamma \simeq -0.8$ mag/dex) proposed by Shappee & Stanek (2011). Shappee & Stanek (2011) inferred their estimate by comparing the Wesenheit magnitudes of classical Cepheids occupying metal-rich and metal-poor fields in M101. Evaluation (1) is employed to assess the conclusion by Shappee & Stanek (2011, their Fig. 28) that the slope of the Wesenheit function is sensitive to abundance changes. Mager et al. (2009) analyzed the same HST images for M101² and reached alternate conclusions, namely that there is no significant dependence on metallicity for the slope, and a comparatively small dependence on the zero-point of the P-L relation exists (see also Freedman et al., 2001; Storm et al., 2011b). Published results for other galaxies (e.g., NGC 5253, Gibson et al., 2000) are likewise interpreter/sample selection/pipeline dependent, thereby highlighting an often uncharacterized source of uncertainty.

The dissenting (alternate) view conveyed here concerning a sizable γ -correction does not mitigate the broader significance of the Shappee & Stanek (2011) and Gerke et al. (2011) results. Shappee & Stanek (2011) discovered $\sim 10^3$ classical Cepheids in M101, thereby exceeding existing records for the number of extragalactic Cepheids detected in a particular galaxy beyond the Local Group. Indeed, it is hoped that their approach may be applied to discover countless Cepheids in additional galaxies. Gerke et al. (2011) demonstrated the pertinence of the Large Binocular Telescope for fostering extragalactic Cepheid research.

Both studies present seminal results.

¹Gerke et al. (2011) likewise favour a sizable metallicity dependence. The reader is referred to their comprehensive survey.

²Taken *verbatim* from their published AAS abstract, see also <http://www.stsci.edu/observing/phase2-public/11297.pdf>

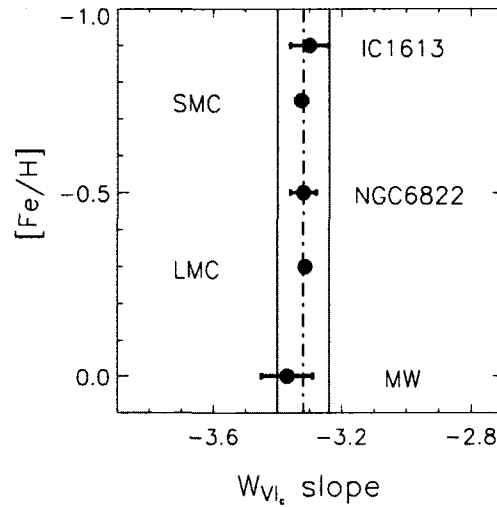


Figure 9.1 The slope of the VI_c Wesenheit function as inferred from ground-based photometry of classical Cepheids in the Milky Way (equation 9.2), LMC, NGC 6822, SMC, and IC 1613. The slope of the VI_c Wesenheit function is insensitive to metallicity over the range examined.

9.2 EVIDENCE FOR THE ABSENCE OF A METALLICITY EFFECT IN VI_C

First, evidence hitherto that indicates the relative insensitivity of VI_c intrinsic colour and Wesenheit functions to abundance changes is summarized, mainly because such pertinent evidence is often overlooked.

The results for evaluation (1) indicate that classical Cepheids in the Milky Way, LMC, NGC 6822, SMC, and IC 1613 follow a common VI_C Wesenheit slope (Majaess, 2010c, see also Pietrzyński et al. 2004; Pietrzyński & Gieren 2004; Majaess et al. 2008, 2009b; Soszyński et al. 2010), to within the uncertainties (Fig. 9.1). The galaxies span a sizable abundance baseline, thereby permitting a reliable determination of any trend. Conversely, classical Cepheids in the Milky Way and SMC exhibit differing BV Wesenheit slopes (Majaess et al., 2008, 2009b, see also Caldwell & Coulson 1985). The latter dependence appears linked to different amounts of line blanketing in BV (Caldwell & Coulson, 1985, and references

therein).

The VI_C Wesenheit results imply that the source for the following discrepancies is unrelated to a metallicity effect: (i) the slope of the VI_C Wesenheit function varies as a function of galactocentric distance for classical Cepheids in M101 and M106 (e.g., Shappee & Stanek, 2011, their Fig. 28), (ii) the slope of the VI_C Wesenheit function inferred from the Sandage et al. (2004) Galactic calibrating sample³ is too steep, yielding distances for longer-period Cepheids that are artificially too large (Majaess, 2010c, see also Benedict et al. 2007; van Leeuwen et al. 2007; Storm et al. 2011a), (iii) and conversely, classical Cepheids in several SNe host galaxies exhibit too shallow a VI_C Wesenheit slope and negative mean reddenings (IC 4128, NGC 1309, NGC 3021, Majaess, 2010c, and references therein).

Regarding evaluation (2), the Wesenheit magnitude offset between RR Lyrae variables and classical Cepheids in the LMC, SMC, and IC 1613 agree to within the uncertainties (Majaess, 2010c, see also Udalski et al. 2001; Pietrzyński & Gieren 2004; Pietrzyński et al. 2004). Distances and extinction estimates inferred for RR Lyrae, Type II Cepheid, and classical Cepheid variables in countless galaxies and globular clusters via metallicity-uncorrected period-based relations are comparable, and agree with results from DIRBE/IRAS dust maps (e.g., M33 and M54, Majaess et al., 2009b; Majaess, 2010a).

Concerning evaluation (3), results by several authors imply that the (spurious) brightening (W_{VI_c}) of extragalactic Cepheids as a function of decreasing galactocentric distance stems from the associated increase in photometric contamination rather than as a result of increasing metal abundances (Mochejska et al., 2000; Macri et al., 2001; Mochejska et al.,

³The Sandage et al. (2004) Galactic Cepheid calibration relied upon the best available data prior to the release of the HST parallaxes (Benedict et al., 2007). Moreover, Turner (2010) and Storm et al. (2011a) subsequently revised the Galactic calibration, and continued revisions will invariably ensue.

2004; Bono et al., 2008; Majaess et al., 2009b; Majaess, 2010c; Bresolin, 2011). The surface brightness and stellar density increase near the central region, and hence the effects of crowding and blending cannot be ignored. Further evidence presented below bolsters that assertion. Shappee & Stanek (2011) admit that the impact of blending was not assessed in their analysis.

9.3 EVALUATING THE VIABILITY OF $\gamma \simeq -0.8$ mag/dex

The viability of a sizable metallicity correction ($\gamma \simeq -0.8$ mag/dex) is now evaluated by applying it to distances inferred from classical Cepheids in the Magellanic Clouds via the Galactic calibration. Benedict et al. (2007) cite a Galactic VI_C Wesenheit function characterizing 10 nearby classical Cepheids with HST parallaxes as:

$$W_{VI_c,0} = (-3.34 \pm 0.17) \log P_0 - 2.52 \quad (9.1)$$

where $W_{VI_c,0}$ is the absolute Wesenheit magnitude and $\log P_0$ is the pulsation period tied to the fundamental mode. Benedict et al. (2002a, 2007) established HST parallaxes for the classical Cepheids RT Aur, T Vul, FF Aql, δ Cep, Y Sgr, X Sgr, W Sgr, β Dor, ζ Gem, and ℓ Car. Turner (2010) noted that the period-luminosity relation inferred from classical Cepheids in open clusters (e.g., DL Cas/NGC 129, Turner et al., 1992) matches that established from the Benedict et al. (2007) sample. Moreover, the revised Hipparcos parallaxes by van Leeuwen et al. (2007) are consistent with the HST parallaxes. Majaess et al. (2011) established precise JHK_s ZAMS distances to 7 of 9 benchmark open clusters that agree with the revised Hipparcos estimates (van Leeuwen, 2009). In summary, the reliability of the HST parallaxes is supported by independent means.

Majaess et al. (2011c) supplemented the HST calibration with 21 Galactic cluster Cepheids (Turner, 2010) and obtained:

$$W_{VI_c,0} = (-3.37 \pm 0.08) \log P_0 - (2.48 \pm 0.08) \quad (9.2)$$

The hybrid Galactic Wesenheit function includes the revised parameters for the classical Cepheid TW Nor in the open cluster Lyngå 6, which stemmed from an analysis of new VVV JHK_s photometry for the cluster (Minniti et al., 2010; Moni Bidin et al., 2011; Majaess et al., 2011c). That result agrees with the revised distance established from the infrared surface brightness technique (Storm et al., 2011a). The short period classical Cepheid SU Cas was excluded from the derivation because its parameters were being revised by Turner (see also discussion in Storm et al., 2011a).

VI_C Wesenheit functions determined by Soszyński et al. (2008, 2010) that characterize $\geq 10^3$ fundamental mode classical Cepheids in the Magellanic Clouds are:

$$W_{VI_c}(\text{LMC}) = (-3.314 \pm 0.009) \log P_0 + (15.838 \pm 0.006)$$

$$W_{VI_c}(\text{SMC}) = (-3.326 \pm 0.019) \log P_0 + (16.383 \pm 0.014)$$

(9.3)

A similar slope describes Galactic and Magellanic Cloud classical Cepheids that span $[\text{Fe}/\text{H}] \sim 0 \rightarrow -0.33 \rightarrow -0.75$ (equations 9.2, 9.3, Fig. 9.1). The coefficients and zero-points of the functions were confirmed by Majaess et al. (2009b) and Ngeow et al. (2009). The distance modulus follows from subtracting the Wesenheit function inferred for a target population from the Galactic calibration:

$$W_{VI_c,0} = W_{VI_c} - \mu_0$$

Table 9.1. Distances to the Magellanic Clouds

	[Fe/H] ¹	$\mu_0(\gamma = 0 \text{ mag/dex})^2$	$\mu_0(\gamma = -0.8 \text{ mag/dex})^2$	NED-D ³	$\mu_{0,univ}^4$
LMC	-0.33 ± 0.13	18.4	18.1	$18.46 \pm 0.01(\sigma_x) \pm 0.15(\sigma)$	$18.40 \pm 0.08(\sigma_x)$
SMC	-0.75 ± 0.08	18.9	18.3	$18.86 \pm 0.02(\sigma_x) \pm 0.18(\sigma)$	

¹Mean Cepheid abundances from Mottini et al. (2006), which agree with the earlier determinations by Luck et al. (1998).

²Metallicity (γ) corrected distances established from a V_{IC} Galactic classical Cepheid Wesenheit function (equation 9.1).

³Distances for the Magellanic Clouds tabulated from $> 3 \times 10^2$ published estimates (NED-D). A mean LMC distance derived from additional published estimates is forthcoming (Steer et al., in preparation).

⁴Inferred from a universal Wesenheit template with 11 nearby δ Scuti, SX Phe, RR Lyrae, and Type II Cepheids variables with HST/Hipparcos parallaxes.

$$\mu_0 = W_{V_{IC}} - W_{V_{IC},0} \quad (9.4)$$

Evaluating μ_0 for the LMC and SMC by subtracting equation (9.3) from equation (9.1) yields $\mu_0 \simeq 18.4$ and $\mu_0 \simeq 18.9$, respectively. Mottini et al. (2006) cite mean abundance estimates for classical Cepheids in the Magellanic Clouds as: $[\text{Fe}/\text{H}]_{\text{LMC}} = -0.33 \pm 0.13$ and $[\text{Fe}/\text{H}]_{\text{SMC}} = -0.75 \pm 0.08$ (see also Luck et al., 1998). The resulting distance modulus corrections tied to abundance differences between Galactic and Magellanic Cloud classical Cepheids are $\Delta\mu_{0,\gamma}(\text{LMC}) \simeq -0.26$ and $\Delta\mu_{0,\gamma}(\text{SMC}) \simeq -0.60$, for $\gamma \simeq -0.8 \text{ mag/dex}$ (Shappee & Stanek, 2011). The metallicity corrected distance estimates for the LMC and SMC are therefore $\mu_{0,\gamma} \simeq 18.1$ and $\mu_{0,\gamma} \simeq 18.3$, respectively. The results are of concern because they imply that the Magellanic Clouds are $\sim 20\%$ nearer than inferred from a mean of > 300 published estimates, including the independent distance determined below from a Universal Wesenheit template. Furthermore, the separation between the Clouds ($\Delta\mu_{0,\gamma} \simeq 0.2$) is approximately half the canonical estimate.

A consensus distance for the LMC may be derived using the NASA/IPAC Extragalactic Database NED-D (Madore & Steer, 2007). That compilation has redshift-independent

distances for 10^4 galaxies. NED-D contains $> 3 \times 10^2$ distance estimates for the Magellanic Clouds, excluding those established from classical Cepheids (e.g., Storm et al., 2011b). The mean values for the LMC and SMC are: $\mu_0 = 18.46 \pm 0.01(\sigma_{\bar{x}}) \pm 0.15(\sigma)$ and $\mu_0 = 18.86 \pm 0.02(\sigma_{\bar{x}}) \pm 0.18(\sigma)$. The results disagree with the metallicity corrected distances established using $\gamma \simeq -0.8$ mag/dex (Table 9.1). By contrast, the results inferred from NED-D agree with the W_{VI} -based distances uncorrected for metallicity differences between Magellanic Cloud and Galactic classical Cepheids (Table 9.1).

The distance to the LMC established via a universal Wesenheit template (Majaess et al., 2011a,b) with 11 nearby δ Scuti, SX Phe, RR Lyrae, and Type II Cepheids variables with HST/Hipparcos parallaxes is $\mu_0 = 18.40 \pm 0.08(\sigma_{\bar{x}})$. The prototypes RR Lyrae and SX Phe are included in the calibration because of the availability of HST and revised Hipparcos parallaxes (Benedict et al., 2002b; van Leeuwen, 2007). The distance was inferred by matching the calibrated Wesenheit template to OGLE observations of LMC variables (e.g., Poleski et al., 2010, for δ Scuti stars). The impetus for the universal Wesenheit template is to employ the statistical weight of the entire variable star demographic to establish precise distances, constrain pulsation modes, and provide broader context to identify peculiarities among certain variables (Majaess et al., 2011a,b). The reddening-free nature of the Wesenheit approach bypasses the propagation of uncertainties tied to tentative total/differential extinction corrections, ensuring that further calibration may ensue directly from published or forthcoming geometric-based distances (masers, HST, VLBA, GAIA). The distance established to the LMC from the Wesenheit template matches that from NED-D and a calibration based on classical Cepheids only (equations 9.1 and 9.2). (see

discussion in Shappee & Stanek, 2011, and their Table 10/Figure 28).

9.4 CONCLUSION AND FUTURE RESEARCH

A sizable metallicity correction ($\gamma \simeq -0.8$ mag/dex) was evaluated by applying it to distances established for classical Cepheids in the Magellanic Clouds via the Galactic W_{VIc} function (equation 9.1, Table 9.1). The ensuing metallicity corrected distances for the Magellanic Clouds are in significant disagreement with estimates from countless indicators (Table 9.1). In tandem with the evidence summarized in §9.2, the results indicate that variations in chemical composition among Cepheids are a comparatively insignificant source of uncertainty for W_{VI} -established distances and determinations of H_0 . Metallicity corrections seem unnecessary for W_{VIc} -based distances, and consequently the observed apparent brightening (W_{VIc}) of extragalactic Cepheids with decreasing galactocentric distance (Kennicutt et al., 1998; Shappee & Stanek, 2011) likely stems from the associated increase in surface brightness and stellar density toward the galaxy centre (Majaess et al., 2009b; Majaess, 2010c, see also Mochejska et al. 2000; Macri et al. 2001; Mochejska et al. 2004; Bono et al. 2008; Bresolin 2011). The disagreement with the results of Shappee & Stanek (2011) regarding the nature of the VI_C Wesenheit function's metallicity dependence does not affect the significant accomplishments achieved in their comprehensive analysis of M101. Shappee & Stanek (2011) discovered $\sim 10^3$ classical Cepheids using hybrid and modified variable star search routines. Furthermore, the results for M101 provide additional empirical constraints on photometric contamination (blending/crowding), which in conjunction with the challenges of establishing precise, standardized, multi-epoch, multi-band photometry: constitute a significant source of uncertainty for extragalactic Cepheid distances.

Future research will aim to assess the viability of establishing classical Cepheid calibrators from their membership in spiral arms, which are likewise delineated by young open clusters (e.g., Majaess et al., 2009,c). A ℓ -distance relation, where ℓ is the Galactic longitude, can be inferred from open clusters with precise parameters derived via VVV/UKIDSS/2MASS JHK_s photometry (Lucas et al., 2008; Minniti et al., 2010). The dispersion in the ℓ -distance relation is particularly limited for certain lines of sight, such as toward the Carina arm (Majaess et al., 2009,c; Majaess, 2010b). The ℓ -distance relation may be subsequently applied to classical Cepheids that are spiral arm members: e.g., SZ Vel and RY Vel. Those classical Cepheids exhibit pulsation periods of 14^d and 28^d respectively, and would bolster the longer period regime of the Galactic calibration, which is comparatively undersampled (see Benedict et al. 2007 or Fig. 3 in Majaess et al., 2011c). Securing additional long-period calibrators could resolve present uncertainties associated with the slope of the Galactic Wesenheit function (equation 9.2) and permit a more reliable determination of the parameter's insensitivity to chemical composition (Fig. 9.1). Moreover, long period classical Cepheids are particularly important because they are most often sampled in remote galaxies because of their higher luminosity relative to short period Cepheids. The Hubble flow dominates proper motions for remote galaxies, thereby minimizing uncertainties tied to the latter parameter and hence H_0 . Indeed, the debate surrounding the SNe Ia scale and H_0 (Freedman et al., 2001; Sandage et al., 2004) centres in part around the intrinsic parameters of long period Cepheids (e.g., see Fig. 3 in Majaess, 2010c).

The results presented here emphasize the importance of characterizing and correcting unreliable (e.g., contaminated) photometry tied to distant Cepheids when determining the

metallicity dependence on W_{VIc} and H_0 .

REFERENCES

- Benedict, G. F., et al. 2002, *AJ*, 124, 1695
Benedict, G. F., et al. 2002, *AJ*, 123, 473
Benedict G. F. et al., 2007, *AJ*, 133, 1810
Bono, G., Caputo, F., Fiorentino, G., Marconi, M., & Musella, I. 2008, *ApJ*, 684, 102
Bresolin, F. 2011, *ApJ*, 729, 56
Caldwell, J. A. R., & Coulson, I. M. 1985, *MNRAS*, 212, 879
Freedman, W. L., Madore, B. F., Gibson, B. K., et al. 2001, *ApJ*, 553, 47
Freedman, W. L., & Madore, B. F. 2010, *ARA&A*, 48, 673
Gerke, J. R., Kochanek, C. S., Prieto, J. L., Stanek, K. Z., & Macri, L. M. 2011, *ApJ*, 743, 176
Gibson, B. K., et al. 2000, *ApJ*, 529, 723
Kennicutt, R. C., Jr., et al. 1998, *ApJ*, 498, 181
Lucas, P. W., et al. 2008, *MNRAS*, 391, 136
Luck, R. E., Moffett, T. J., Barnes, T. G., III, & Gieren, W. P. 1998, *AJ*, 115, 605
Macri, L. M., et al. 2001, *ApJ*, 549, 721
Macri, L. M., & Riess, A. G. 2009, *American Institute of Physics Conference Series*, 1170, 23
Madore, B. F., & Steer, I. 2007, *NASA/IPAC Extragalactic Database Master List of Galaxy Distances* (<http://nedwww.ipac.caltech.edu/level5/NED1D/intro.html>)
Mager, V., Madore, B., & Freedman, W. 2009, *American Astronomical Society Meeting Abstracts #214*, 2146, #605.05
Majaess D. J., Turner D. G., Lane D. J., 2008, *MNRAS*, 390, 1539
Majaess, D. J., Turner, D. G., & Lane, D. J. 2009 (a), *MNRAS*, 398, 263
Majaess, D., Turner, D., & Lane, D. 2009 (b), *Acta Astronomica*, 59, 403
Majaess, D. J., Turner, D. G., & Lane, D. J. 2009 (c), *JAAVSO*, 37, 179
Majaess, D. J. 2010 (a), *JAAVSO*, 38, 100
Majaess, D. 2010 (b), *Acta Astronomica*, 60, 55
Majaess, D. J. 2010 (c), *Acta Astronomica*, 60, 121
Majaess, D. J., Turner, D. G., Lane, D. J., Henden, A. A., & Krajci, T. 2011 (a), *JAAVSO*, 39, 122
Majaess, D. J., Turner, D. G., Lane, D. J., & Krajci, T. 2011 (b), *JAAVSO*, 148
Majaess, D. J., Turner, D. G., Moni Bidin, C., et al. 2011, in press, *ApJL* (arXiv:1110.0830)
Minniti, D., et al. 2010, *New Astronomy*, 15, 433
Mochejska, B. J., Macri, L. M., Sasselov, D. D., & Stanek, K. Z. 2000, *AJ*, 120, 810
Mochejska, B. J., Macri, L. M., Sasselov, D. D., & Stanek, K. Z. 2004, *IAU Colloq. 193: Variable Stars in the Local Group*, 310, 41
Moni Bidin, C., Mauro, F., Geisler, D., et al. 2011, in press, *A&A* (arXiv:1109.1854)
Mottini, M., Romaniello, M., Primas, F., Bono, G., Groenewegen, M. A. T., & François, P. 2006, *Mem. Soc. Astron. Italiana*, 77, 156

-
- Ngeow, C.-C., Kanbur, S. M., Neilson, H. R., Nanthakumar, A., & Buonaccorsi, J. 2009, *ApJ*, 693, 691
- Pietrzyński, G., Gieren, W., Udalski, A., et al. 2004, *AJ*, 128, 2815
- Pietrzyński, G., & Gieren, W. 2004, *IAU Colloq. 193: Variable Stars in the Local Group*, 310, 87
- Poleski, R., et al. 2010, *Acta Astronomica*, 60, 1
- Sandage, A., Tammann, G. A., & Reindl, B. 2004, *A&A*, 424, 43
- Shappee, B. J., & Stanek, K. Z. 2011, *ApJ*, 733, 124
- Soszyński, I., et al. 2008, *Acta Astronomica*, 58, 163
- Soszyński, I., et al. 2010, *Acta Astronomica*, 60, 17
- Storm, J., Gieren, W., Fouque, P., et al. 2011 (a), in press, *A&A* (arXiv:1109.2017)
- Storm, J., Gieren, W., Fouque, P., et al. 2011 (b), in press, *A&A* (arXiv:1109.2016)
- Tautvaišienė, G., Geisler, D., Wallerstein, G., Borissova, J., Bizyaev, D., Pagel, B. E. J., Charbonnel, C., & Smith, V. 2007, *AJ*, 134, 2318
- Turner, D. G., Forbes, D., & Pedreros, M. 1992, *AJ*, 104, 1132
- Turner, D. G. 2010, *Ap&SS*, 326, 219
- Udalski, A., Wyrzykowski, L., Pietrzynski, G., Szewczyk, O., Szymanski, M., Kubiak, M., Soszyński, I., & Zebrun, K. 2001, *Acta Astronomica*, 51, 221
- van Leeuwen, F., Feast, M. W., Whitelock, P. A., & Laney, C. D. 2007, *MNRAS*, 379, 723
- van Leeuwen, F. 2007, *A&A*, 474, 653
- van Leeuwen, F. 2009, *A&A*, 497, 209

CHAPTER 10

SUMMARY AND FUTURE RESEARCH

As summarized in chapter 9, the results imply that variations in chemical composition among Cepheids are a comparatively negligible source of uncertainty for VI_c -based extragalactic distances.

The evidence indicates that classical Cepheids in the Milky Way, LMC, NGC 6822, SMC, and IC 1613 adhere to a common slope, to within the uncertainties (chapters 8, 9). Therefore, contrary to assertions by Sandage et al. (2004) (see also Shapsee & Stanek, 2011; Gerke et al., 2011) the slope of the period-magnitude (VI_c) relation appears relatively insensitive to variations in chemical abundance. The derived mean slope is shallower than that inferred from the Cepheid calibrators Sandage et al. (2004) employed to establish the SN Ia scale and secure their estimate of H_0 (chapter 8). The mean slope implies a shorter distance scale than Sandage et al. (2004) by $> 10\%$ for 25^d Cepheids. The revised slope principally affects the distances for long-period Cepheids, which are most often sampled in remote galaxies because of their greater luminosity relative to short-period Cepheids. It should be emphasized that the Sandage et al. (2004) Galactic Cepheid calibration relied upon the best available data at the time, and prior to the release of the HST parallaxes (Benedict et al., 2007). The revised slope of the Galactic calibration is steeper than that inferred from Cepheids discovered in a survey of SN host galaxies (Riess et al., 2009), which are of similar chemical composition (near solar). The results confirm the importance of establishing a solid Galactic calibration (e.g., chapter 5). Furthermore, the distances established to clusters and

galaxies using various standard candles (e.g., RR Lyrae and classical Cepheids) yield comparable results to within the uncertainties, and without applying metallicity corrections. Such a result consequently implies that the zero-point and slope of the classical Cepheid $V I_c$ period-Wesenheit relation are insensitive to abundance changes. The conclusions rely in part on the establishment of a solid calibration for Galactic classical Cepheids. In addition, cited metallicity corrections were evaluated by applying the proposed corrections ($\gamma = -0.8$ mag/dex) to distances established for the Magellanic Clouds using the derived Galactic period-Wesenheit calibration. The resulting γ -corrected distances for the Magellanic Clouds (e.g., SMC, $\mu \sim 18.3$) are in significant disagreement with that established from a mean of > 300 published estimates (NED-D), and a universal Wesenheit template (chapter 2) based on 11 delta Scuti, SX Phe, RR Lyrae, and Type II Cepheid variables with HST/Hipparcos parallaxes. Conversely, adopting a null correction (i.e., $\gamma = 0$ mag/dex) consolidates the estimates. The impetus for the universal Wesenheit template (chapter 2) is to leverage the statistical weight of the entire variable star demographic to establish precise distances, constrain pulsation modes, and to provide the broader context needed to identify peculiarities among calibrators. The reddening-free nature of the Wesenheit approach also bypasses the propagation of uncertainties tied to tentative total/differential extinction corrections, ensuring that further calibration may ensue directly from published or forthcoming geometric-based distances (masers, HST, VLBA, GAIA). For example, the maser distance to NGC 4258 (M106) permitted a suite of long-period Type II Cepheids discovered in that galaxy (Macri et al., 2006; Majaess et al., 2009) to be incorporated into the template.

By eliminating metallicity as a potential source of uncertainty, the following impor-

tant conclusions result: i) the (spurious) brightening of extragalactic Cepheids (e.g., M101, M106) as a function of decreasing galactocentric distance stems from the associated increase in photometric contamination rather than as a result of increasing metal abundances with decreasing galactocentric distance (Freedman & Madore, 2010, and references therein). The surface brightness and stellar density increase near the central regions of M87, M101, M106, and hence the effects of crowding and blending cannot be ignored; ii) a Cepheid metallicity effect is not the chief source of uncertainty associated with the establishment of H_0 or the equation of state of dark energy.

Freedman et al. (2001), in their summary of the final results from the HST key project to measure H_0 , noted that the zero-point of the Cepheid calibration accounts for a sizable fraction of the total uncertainty. Again, that uncertainty hampers efforts to constrain cosmological models, which are acutely dependent on establishing an accurate Hubble constant. A principal aim of the Ph.D. research was devoted to strengthening the Galactic Cepheid calibration to address that aspect of the error budget, in addition to constraining the impact of metallicity. In chapter 9 a new approach is proposed to strengthen Galactic period-magnitude relations by doubling the number of long-period Cepheid calibrators, which are presently undersampled. Remote extragalactic Cepheids observed using HST typically exhibit periods greater than 10 days because their shorter-period counterparts are fainter. A well-sampled calibration with long-period Cepheids is consequently desirable. Uncertainties tied to Cepheid-based determinations of H_0 could be reduced by an unprecedented 25-50%, assuming an optimistic outcome. This Ph.D. thesis focused on reducing a third of the uncertainty associated with H_0 by constraining the impact of chemical compo-

sition on Cepheid distances, whereas future postdoctoral research aims to reduce a sizable fraction of the remaining uncertainty by bolstering the base calibration. In particular, the postdoctoral research aims to pursue the assertion that Cepheids in the Galaxy's spiral arms can be employed as calibrators. The spiral arms are likewise delineated by young clusters. Distances to star clusters can be determined more reliably than individual Cepheids, provided deep multiband photometry and intermediate-resolution spectra are acquired. It was surmised that a ℓ -distance relation, where ℓ is the Galactic longitude, can be inferred from young clusters in spiral arms with parameters derived with new infrared-optical ESO VVV/ Pan-STARRS photometry. The dispersion for the ℓ -distance relation is particularly limited for certain lines of sight, such as toward the Carina spiral arm. The ℓ -distance relation may be subsequently applied to long-period Cepheids such as SZ Vel and RY Vel, which are spiral arm members. Those Cepheids have pulsation periods of 14^d and 28^d respectively, and would therefore improve the long-period regime of the Galactic calibration which hitherto contains only seven calibrators with $P > 11$ days (1 HST + 6 association Cepheids). Preliminary tests indicate that number may be doubled through the envisioned research. The spiral arm Cepheid calibrators are predicted to exhibit uncertainties on the order of that cited for the HST sample (Benedict et al., 2007).

A concurrent means of refining the Cepheid calibration using Chandra-XMM-Newton X-ray data will likewise be pursued. As discussed (chapters 4, 6), new and existing CORAVEL, $UBVJHK_s$, HST, Hipparcos/Tycho, and spectroscopic observations imply that ζ Gem and δ Cep are cluster members. Bright early-type members were readily identified in both clusters because of the nature of the IMF (Initial Mass Function). The progenitors of Cepheids

are B stars (Turner, 1996, his Table 1) that are rare in a given field, thus the presence of a cluster of such stars is readily discernible. However, late-type cluster members are difficult to separate from numerous field stars that are of comparable brightness. The distances to the Cepheid clusters were established by main-sequence fitting using the empirical infrared calibration defined in chapter 3. The main-sequence fit to the Cepheid clusters may improve markedly pending the identification of late-type members. The calibration could subsequently be adjusted to match the entire main sequence, rather than relying entirely on early-type cluster stars. That would result in precise distances to the clusters and their Cepheid constituents. In turn, the Cepheid calibration may be refined with the new distances, which have smaller uncertainties. Late-type stars associated with Cepheids are expected to emit X-rays because of their comparative youth (Evans, 2011). By contrast, the field is replete with older stars. X-ray sources identified in the cluster Cepheid fields using XMM-Newton/Chandra will subsequently be correlated with 2MASS JHK_s and APASS BV data. The positions of the X-ray sources in colour-magnitude and colour-colour diagrams will be evaluated. Stars that lie near an extension of the relation defined by early-type members, and exhibit spectral types (JHK_s colour-colour analysis) consistent with that expected from the colour-magnitude diagram position will be tagged as putative members. Spectroscopic follow-up may be initiated to confirm the results. In addition, a benchmark cluster with an age near 100 Myr will be imaged in order to define a $\log L_x$ -spectral type calibration. The age is consistent with that inferred for the Cepheid clusters and the age predicted from the pulsation periods of δ Cep and ζ Gem (Turner, 1996). In particular, the α Per cluster will be imaged. Members of α Per are well defined

because of their large proper motions. For the study presented in chapter 3, coordinates were tabulated for members of α Per in addition to their spectral types from positions in the JHK_s colour-magnitude and colour-colour diagrams. Furthermore, a precise distance to the cluster was established, which is a pertinent parameter needed to determine $\log L_x$ reliably. α Per may be a more suitable cluster than the Pleiades to establish the $\log L_x$ -spectral type calibration because the JHK_s and revised Hipparcos distance to the cluster agree. van Leeuwen (2009) obtained $d = 172.4 \pm 2.7$ pc for α Per, which matches that established with the JHK_s data (chapter 3). By contrast, van Leeuwen (2009) obtained $d = 120.2 \pm 1.9$ pc for the Pleiades, whereas the JHK_s data implied $d = 138 \pm 6$ pc, and Soderblom et al. (2005) employed HST to deduce $d = 134.6 \pm 3.1$ pc (chapter 3). Using the Pleiades would introduce unnecessary ambiguity. The X-ray data requested will be combined with existing $BVJHK_s$ photometry to establish the most precise distance to ζ Gem and δ Cep, thereby demonstrating a novel approach for calibrating Cepheid relations.

REFERENCES

- Andrievsky, S. M., Luck, R. E., Martin, P., & Lépine, J. R. D. 2004, *A&A*, 413, 159
- Barnes, T. G. 2009, *American Institute of Physics Conference Series*, 1170, 3
- Benedict, G. F., McArthur, B. E., Feast, M. W., et al. 2007, *AJ*, 133, 1810
- Evans, N. R. 2011, *IAU Symposium*, 272, 537
- Freedman, W. L., Madore, B. F., Gibson, B. K., et al. 2001, *ApJ*, 553, 47
- Freedman, W. L., & Madore, B. F. 2010, *ARA&A*, 48, 673
- Gerke, J. R., Kochanek, C. S., Prieto, J. L., Stanek, K. Z., & Macri, L. M. 2011, *ApJ*, 743, 176
- Gieren, W., Storm, J., Barnes, T. G., III, et al. 2005, *ApJ*, 627, 224
- Gieren, W., Pietrzyński, G., Soszyński, I., et al. 2009, *ApJ*, 700, 1141
- Gould, A. 1994, *ApJ*, 426, 542
- Kennicutt, R. C., Jr., Stetson, P. B., Saha, A., et al. 1998, *ApJ*, 498, 181
- Kochanek, C. S. 1997, *ApJ*, 491, 13
- Kudritzki, R.-P., Urbaneja, M. A., Gazak, Z., et al. 2012, *ApJ*, 747, 15
- Macri, L. M., Calzetti, D., Freedman, W. L., et al. 2001, *ApJ*, 549, 721
- Macri, L. M., & Riess, A. G. 2009, *American Institute of Physics Conference Series*, 1170, 23
- Macri, L. M., Stanek, K. Z., Bersier, D., Greenhill, L. J., & Reid, M. J. 2006, *ApJ*, 652, 1133
- Majaess, D., Turner, D., & Lane, D. 2009, *Acta A*, 59, 403
- Majaess, D., Turner, D., Moni Bidin, C., et al. 2011, *ApJ*, 741, L27
- Riess, A. G., Macri, L., Casertano, S., et al. 2009, *ApJ*, 699, 539
- Rizzi, L., Tully, R. B., Makarov, D., et al. 2007, *ApJ*, 661, 815
- Sakai, S., Ferrarese, L., Kennicutt, R. C., Jr., & Saha, A. 2004, *ApJ*, 608, 42
- Sandage, A., Tammann, G. A., & Reindl, B. 2004, *A&A*, 424, 43
- Scowcroft, V., Bersier, D., Mould, J. R., & Wood, P. R. 2009, *MNRAS*, 396, 1287
- Shappee, B. J., & Stanek, K. Z. 2011, *ApJ*, 733, 124
- Soderblom, D. R., Nelan, E., Benedict, G. F., et al. 2005, *AJ*, 129, 1616
- Turner, D. G. 1996, *JRASC*, 90, 82
- Turner, D. G. 2010, *Ap&SS*, 326, 219
- Turner, D. G., & Majaess, D. J. 2010, *Bulletin of the American Astronomical Society*, 42, 929
- van Leeuwen, F. 2009, *A&A*, 497, 209

CHAPTER 11

ACKNOWLEDGEMENTS

David Turner and Dave Lane were my mentors. They provided the education and inspiration needed to tackle all of the research. In addition, the following individuals provided pertinent advice and observations for the following chapters:

- Chapter 2: A. Henden, T. Krajci.
- Chapter 3: T. Krajci.
- Chapter 4: W. Gieren.
- Chapter 5: C. Moni Bidin, F. Mauro, D. Geisler, W. Gieren, D. Minniti, A-N. Chené, P. Lucas, J. Borissova, R. Kurtev, I. Dékány, R. Saito.
- Chapter 6: W. Gieren, D. Balam.
- Chapter 7: C. Moni Bidin, D. Geisler, J. Borissova, D. Minniti, C. Bonatto, W. Gieren, G. Carraro, R. Kurtev, F. Mauro, A-N. Chené, D. W. Forbes, P. Lucas, I. Dékány, R. K. Saito, M. Soto.
- Chapter 9: W. Gieren.